DEVELOPMENT OF AN INTERVERTEBRAL DISC MECHANOBIOLOGICAL SYSTEM

by

Robert Allen Hartman

Bachelor of Science, University of Pittsburgh, 2008

Submitted to the Graduate Faculty of

the Swanson School of Engineering in partial fulfillment

of the requirements for the degree of

Master of Science

University of Pittsburgh

2010

UNIVERSITY OF PITTSBURGH

SWANSON SCHOOL OF ENGINEERING

This thesis was presented

by

Robert Allen Hartman

It was defended on

November 16, 2010

and approved by

James D. Kang, MD, Department of Orthopaedic Surgery

Richard E. Debski, PhD, Department of Bioengineering

Thesis Advisor: Gwendolyn A. Sowa, MD, PhD, Department of Physical Medicine & Rehabilitation, Department of Bioengineering, and Department of Orthopaedic Surgery

DEVELOPMENT OF AN INTERVERTEBRAL DISC MECHANOBIOLOGICAL SYSTEM

Robert Allen Hartman, MS

University of Pittsburgh, 2010

Intervertebral disc degeneration is a leading cause of low back pain, a significant socioeconomic burden with a broad array of costly treatment options. Motion-based therapy has shown modest efficacy in treating back pain. Basic science research has begun to identify thresholds of beneficial and detrimental mechanical loading of the intervertebral disc. Ex-vivo mechanobiological systems are important experimental models for determining the effect of loading parameters on disc biology and matrix homeostasis. A novel experimental platform has been developed to facilitate in-situ loading of a rabbit functional spinal unit (FSU) with outcome measures relevant to disc matrix homeostasis and cell behavior. First, the system was designed for multi-axis motion outside of an incubator and validated for rigid fixation and stable, physiologic environmental conditions that maintained adequate cell viability. Following system development and validation, experimental testing on rabbit FSUs proceeded with cyclic compression and four-hour constant compression compared. Disc tissue was analyzed for cell viability using a colorimetric absorbance assay or relative gene expression. Conditioned media was assayed for matrix metalloproteinase activity, type-II collagen degradation fragments, prostaglandins, and an aggrecan epitope implicated in aggrecan synthesis. Cell viability remains high (>90%) regardless of loading. Relative gene expression shows small increases in anabolism and larger, variable increases in catabolic and inflammatory markers. These trends are more reliable in AF than NP. Interestingly, matrix metalloproteinase activity trends toward a decrease

in media in loaded specimen culture. Although type-II collagen fragment concentrations do not correlate with loading, the aggrecan synthesis marker concentrations do. Results indicate increased catabolism and aggrecan turnover in response to loading, though the net effect on matrix homeostasis at later time points is unclear. Future work will explore applying other loading patterns, performing bending and torsion, and coupling local inflammatory stimuli with loading. This novel experimental platform will explore the effect of physiologic motion simulations on disc homeostasis, helping to improve motion-based therapies.

TABLE OF CONTENTS

LIST OF TABLES

LIST OF FIGURES

PREFACE

The completion of the research project represents an important milestone in my life. As I reflect, I would like to extend my sincere gratitude to those who have helped and guided me on this way. First, I would like to thank Dr. Sowa for her patient and involved guidance in research and for cultivating a passion for the translational potential of this work. Kevin Bell has been a mentor to me in research since my undergraduate sophomore year, and I could never repay him for his professional help and personal friendship--for always being there to troubleshoot ideas, solve problems with me, and be a tremendous source of stability and levity in my life. I would also like to thank Dr. Kang who supported me in my early years of spine research and fostered a desire for excellence in research. My high school math and science teacher, Mrs. Huyett, played a formative role in encouraging discovery of God's wondrous creation and in demanding of me diligence, honesty, humility, and spontaneity. Without the support and unrelenting love of my parents and siblings, I would simply not have the capacity for the rigors of research. The many brothers and sisters in my church family have also been a tremendous support, and it was their bad backs that planted the desire in me to enter this field. My girlfriend has walked with me on this journey for the past year, and I am deeply grateful for her loving encouragement and understanding. Finally, I humbly acknowledge and thank my faithful Lord and Savior who anchors me with His loving call and has given me this amazing opportunity to appreciate His craftsmanship.

This work would not have been possible without the assistance and support of many people. Kevin Bell helped in general problem solving and theoretical and technical guidance in traditional engineering design and implementation. J. Paulo Coehlo and William Witt helped in rabbit surgery and RNA extraction troubleshooting; Mr. Coehlo conducted RT-PCR, and Mr. Witt spear-headed the fluorogenic MMP activity assay development. Wan Huang, Barrett Woods, and Nora Sherry helped in running the ELISAs for conditioned media analysis. James Iatridis and Sharan Ramaswamy were instrumental in shaping the conceptual development of the system. This work was supported by NIH/NIAMS (1R21 AR055681), Department of Physical Medicine & Rehabilitation, Department of Bioengineering, Department of Orthopaedic Surgery, and The Albert B. Ferguson, Jr. MD Orthopaedic Fund of The Pittsburgh Foundation.

1.0 INTRODUCTION

Low back pain (LBP) is the second most frequent reason for patients to visit a physician in the United States [1] with greater than a quarter of Americans experiencing LBP annually [2] and approximately 80% of the population experiencing LBP over their lifetimes [3]. Not only do individual patients experience dramatic reduction in quality of life, but direct medical and related monetary costs added to indirect costs associated with lost productivity sum to an annual, national economic burden that approaches $100B (Dagenias, 2008). Intervertebral disc (IVD) degeneration (IDD) is the leading etiology of LBP, accounting for more than 30% of non-idiopathic LBP [2]. It is a common degenerative disorder that is highly associated with age, genetic predisposition, metabolic disorder, and traumatic loading. IDD assaults spine function through changes to disc cell phenotypic behavior, biochemical tissue composition, and mechanical properties.

Diagnosis and treatment of IDD varies broadly on an international stage, ranging from cultures with little social awareness of back pain to those like the United States where back pain in general is the most expensive work-related disability [2]. Treatment of IDD spans a broad spectrum, including prescription of pharmocologics [4], physical manipulations, acupuncture, herbal therapies [8], steroid injections, exercise-based therapies [5-7], and surgery [9]. Moreover, treatment costs of LBP appear to be on the rise amidst the current climate of systematic attempts at health care cost reduction [10]. Deyo et al. illustrate profound increases in

diagnostic magnetic resonance imaging (307%) and common LBP management schemes: lumbosacral injections (629%), opoid analgesics (423%), and disc degeneration fusion surgeries (220%) from the mid-1990s to early 2000s [11]. Additionally, rates of surgery in the U.S. well surpass those of other industrialized nations [1] while long-term (>3 months) benefits from surgery relative to intensive rehabilitation are not demonstrable [9]. Despite these rising treatment rates, the incidence of back pain appears to have increased very little since 1990 [12], suggesting overtreatment or uncertainty regarding appropriate management.

Interestingly, recent observational studies note the moderate efficacy of exercise-based therapies in alleviating back pain [5-7, 13]. For years, immobilization and bed rest have been known to be ineffective and potentially deleterious [14], pointing to the importance of motion preservation in treatment. On the other hand, overloading can exacerbate symptoms and worsen underlying degeneration [15]. It seems clear then that thresholds of loading exist that can be beneficial or detrimental to disc health. Basic science studies have begun exploring regulation of matrix homeostasis of the IVD in response to varying magnitudes, frequencies, and modes of loading. Translation of basic science results to the clinic requires more refined characterization of how mechanical loading patterns influence the IVD and more physiologic modes of loading. Additionally, translating mechanobiological findings to clinical prescription of motion-based therapies with specificity to help prevent or retard symptoms of degeneration requires an improved understanding of subgroups of LBP [16]. Early and specific diagnosis of disc degeneration may be facilitated by disc-specific biomarkers—quantifiable biological outcomes that provide diagnostic utility for active changes to or processes in the IVD. Paralleling similar disease processes in articular cartilage, a useful biomarker profile will likely include serum concentrations of matrix fragments and inflammatory cytokines.

Translation of disc mechanobiology to the clinic requires improved understanding of beneficial and detrimental thresholds of loading in the IVD. Among the experimental platforms used for investigating loading effects on disc matrix homeostasis, ex-vivo organ culture models are important because they can maintain in-situ mechanical transduction mechanisms, permit control of environmental conditions, and facilitate variation of load magnitude, frequency, and duration. A range of biological outcomes including gene expression, matrix composition (proteoglycan or collagen content), matrix catabolism, matrix synthesis, hydration, cell viability, metabolic rates, and inflammatory markers have been used to evaluate the effect of loading on disc cells and tissue. By continuing to advance the modes and parameters of applied loading and to refine the characterization of the biological response, ex-vivo mechanobiological studies will facilitate improved understanding of the role of mechanics and other environmental variables in regulating disc health and will help to improve prescription of motion-based therapy.

2.0 BACKGROUND

2.1 THE INTERVERTEBRAL DISC

The intervertebral disc (IVD) is situated between vertebral bodies along the length of the spinal column, contributing to support of axial loads and to facilitation of multi-axis motion: flexion, extension, axial rotation, and lateral bending. A young, healthy IVD comprises two distinct tissue regions: the annulus fibrosus (AF) and nucleus pulposus (NP). The AF consists of concentric lamella composed of parallel collagenous fibers that are oriented ~30° from the axial plane at opposing directions in alternating sheets. This tough, fibrocartilaginous structure encapsulates the NP, a highly hydrated gel rich in proteoglycans and randomly oriented collagen fibers. The AF fibrous sheets connect adjacent vertebral bodies and constrain load-induced NP swelling. The AF experiences primarily tensile loading and the NP experiences primarily compression. Cartilaginous endplates border the subchondral bone at the edge of vertebral bodies, transmitting axial load to the disc and confining NP swelling inferiorly and superiorly.

Tissue composition complements IVD structure and mechanical function. The interaction of the NP and AF enables the disc to withstand high levels of compression and facilitate motion in six degrees-of-freedom (DOF). The IVD extracellular matrix (ECM) is composed of two phases: a solid, polymeric matrix and an interstitial fluid phase. The outer annulus fibrosus (OAF) is subjected to circumferential tension in compression, torsion, and

bending. While as many as ten forms of collagen have been identified in the disc [17], type I and type II collagen predominate in the AF. Type I is more abundant in the fibrous OAF, conveying high tensile strength. The ratio of type I to type II decreases radially inward, reflecting the changing mechanical environment of the AF, with the inner region experiencing more compression and less tension [18]. The role of the NP is primarily to resist high amounts of compression; its negatively charged matrix attracts high volumes of interstitial fluid and generates osmotic swelling pressure to counter compression in axial loading and bending. As a consequence, just as in hyaline articular cartilage, type II collagen dominates ECM composition in the inner annulus (IAF) and NP [19]. Although a variety of proteoglycans are present in disc tissue, aggrecan is functionally the most relevant in both the AF and NP. Negatively charged chondroitin- and keratin-sulfate glycosaminoglycan (GAG) sidechains bound to a protein core thant links to hylaronic acid to create the NP's high fixed charge density. Under compression, flow of interstitial fluid through the charged matrix creates electrokinetic effects [20]. The negatively charged aggrecan is primarily responsible for attracting large amounts of water, which increases the compressive modulus of the NP [15].

Cell phenotype varies depending on possible cell origin and regional location. AF cells are mesenchymal cells, typically fibroblastic, ellipsoidal, and oriented along collagen fibers in the direction of tensile strain [21]. Yet AF cells possess chondrocyte-like properties as well [22]; they synthesize large amounts of collagen to construct and remodel their fibrous ECM. The ratio of type I to type II collagen expression, over ten-fold higher than that in articular chondrocytes (ACs) [23], reflects the high degree of circumferential and radial tensile loading they experience. AF cells, also subjected to some compression, synthesize aggrecan [24]. Cells become more oval-shaped in the IAF, though they are mechanically very similar to OAF cells [21, 25]. The

NP has a dynamic cell population through development, maturity, and aging. The originators of the NP are notochordal cells; however, by early adolescence in humans, notochordal cells have nearly vanished and chondrocyte-like cells have populated the NP [26-28]. Similar to ACs, these cells are characterized by expression of Col-II, Sox-9, and aggrecan [22], yet the ECM they compose is distinctly different. The type II-to-type I collagen ratio is lower in NP cells than ACs, and its aggrecan-to-type II collagen ratio is much higher than ACs [23].

Disc cells, like ACs, exist within a pericellular matrix (PCM) that governs the cellular mechanical environment and cell-matrix interactions [21, 25, 29, 30]. Based on PCM studies in articular cartilage, cell surface–matrix interactions are governed by PCM components, soluble molecules like growth factors may be modified, incorporated, or restricted by the PCM [31], secreted cellular products like aggrecan may similarly be processed by the PCM [32], and cellular metabolism is dramatically altered by PCM retention in vitro [33]. The PCM has also been shown to modify the stress and strain experienced by the cell [34-37]. Microaspiration studies of chondrocytes and disc cells within their enclosing PCM demonstrate mechanical properties distinct from cells and ECM [36, 38]. Multi-phase models of ECM-PCM-cell interactions suggest that PCM geometry, modulus, and permeability directly influence strains experienced by chondrocytes [37] and disc cells [29]. Comparing healthy PCM to osteoarthritic PCM in a biphasic multi-scale model, Alexopoulos et al. demonstrate that cell strains are increased and fluid flows near cells are decreased in the diseased state [35]. Similarly, simulated degenerative changes to PCM properties lead to increased AC dynamic strains over a decade of loading frequencies: 0.01 – 0.1 Hz [37]. Thus, retention of the PCM preserves normal cellular metabolism and in-situ load transmission to cells, providing appropriate inputs for mechanobiological studies that seek to connect physiologic loading with cellular response.

2.2 INTERVERTEBRAL DISC DEGENERATION

2.2.1 Compositional Changes

In intervertebral disc degeneration (IDD), a proposed mechanism for degenerative changes is a shift in the balance of matrix synthesis and catabolism toward net matrix breakdown. If escalation of catabolic activity exceeds the rate of matrix repair and remodeling alters matrix composition, damage accumulates and disc structure is compromised. Early markers of degeneration, primarily evident in the NP, include loss of proteoglycans and dehydration. Degradation of aggrecan and loss of GAG side-chains occur via up-regulation of specific catabolic enzymes [39-42]. Reduced quantity and quality of aggrecan may also be associated with changes in biosynthesis of aggrecan components, foremost being GAGs [40, 43-45]. Degraded aggrecan fragments leach more readily from the matrix, reducing proteoglycan concentration and fixed charge density. As a result, NP tissue dehydrates and loses swelling pressure. The solid matrix bears more loading, prompting remodeling that makes the NP more fibrotic and elicits a dramatic increase in shear modulus [46]. Degenerative, fibrotic changes are manifested in an increased ratio of type I-to-type II collagen in the IAF and NP [23].

Concomitant changes in the AF are less severe, though the functional loss they impose is equivalent to that of the NP. As the NP fails to provide adequate fluid pressurization in compression and distribution of load to the surrounding AF, the annulus experiences higher levels of compression and greater tensile strains [15]. Altered stress distributions damage the AF and change matrix component synthesis [47], resulting in an increased compressive modulus in degeneration [48]. Delamination and disorganization of the collagen fibers are also hallmarks of IDD. Radial permeability decreases and axial and circumferential permeability increases,

reflecting delamination and altered fiber thickness [49]. Reduced radial permeability facilitates leaching of matrix fragments and reduces frictional drag of fluid through the matrix, altering viscoelastic behavior [50]. In general, the coupled mechanical interaction of the NP and AF erodes with degeneration, causing abnormal load distribution within the disc and to surrounding structures.

Degenerative changes are also observed in adjacent cartilaginous endplates, which may have profound effects on disc cell metabolism, viability, and synthetic capacity. Since the disc is largely avascular at skeletal maturity [51], nutrient access and waste removal occur by diffusion across the endplate capillary beds that terminate at the subchondral bone border [52]. In the human lumbar spine, diffusion distances to NP cells may be as large as 8 mm, and convective transport is shown to have little effect on the transport of small and/or charged molecules like O_2, glucose, and lactic acid [53]. In degeneration, endplate calcification and subchondral bone sclerosis pose a barrier to metabolic exchange, depriving disc cells of nutrients and oxygen and concentrating wastes and lactic acid within the disc [54]. Consequently, reduced cell density in the IAF and NP is often observed in degenerated discs [55]. Furthermore, nutrient deprivation studies that simulate this environment demonstrate reduced viability and altered synthesis [56-60]. Degeneration of the endplate also plays an indirect role in mechanically mediated degenerative changes within the disc; degenerated motion segments reveal altered thickness and local defects that reflect altered stress distributions within the endplate [61]. Changes in mechanical and structural properties of the endplate alter loading patterns within the disc that may mediate matrix damage and perturbed mechanical signaling [62]. MacLean et al. demonstrated the importance of the endplate in load transmission to the disc, underscoring how degenerative changes in the endplate may modulate the disc's mechanical environment [63]. In

summary, degenerative changes in the endplate deprive disc cells of viability and synthetic capacity and indirectly alter mechanical signaling.

2.2.2 Mechanical Signaling in Degeneration

Mechanical signaling changes with degeneration. Disc cells in a degenerated state likely exhibit altered mechanical properties as in degenerated articular chondrocytes [29, 35]. Similarly, degenerative changes are suspected in the composition and mechanical properties of their PCM [20, 30, 37, 64]. Altered cellular, pericellular matrix, and extracellular matrix properties imply that mechanical signaling, perceived to be instrumental in regulation of matrix homeostasis, must also be altered [35, 37]. Loads transmitted through the ECM are distributed differently throughout the disc in degeneration because of changes in matrix composition, fluid flow, fixed charge density, and swelling pressure [46, 48, 65, 66]. Altered loads are experienced by the PCM, which itself transduces mechanical signals differently when degenerated [37]. Cells respond to altered mechanical inputs with changed biological outputs that in turn modify pericellular and extracellular composition [45]. Thus, the disc may be in a deleterious cycle of altered loading patterns at a macroscopic scale (degenerated ECM) and altered cellular mechanical environments at a microscopic scale (degenerated PCM and cell).

The subsequent changes in the cellular mechanical environment influence cell activity and viability. Notably, cell density decreases with degeneration and aging [51]. Cell viability decreases in animal models of degeneration [67]; necrosis [27] and apoptosis [67, 68] reduce the number of viable, synthetic cells [69]. The fraction of senescent cells also increases with degeneration [70]. Disc cells increase production of enzymes that degrade the ECM and alter synthesis of ECM structural components [71-74]. Consequences of altered synthesis and

enzymatic activity re-characterize ECM composition and properties throughout degeneration and aging. Structural component synthesis lags catabolism, and aggrecan component and collagen type ratios change in degeneration [40, 43, 75, 76]. Increased catabolic signaling and enzymatic activity of matrix metalloproteinase (MMP) -1, -2, -3, -9, and -13 [72, 73, 77] and a disintegrin and metalloproteinase with thrombospondin motifs (ADAMTS) -4 and -5 [78, 79] are evident in degenerating discs. Similarly, degenerating disc cells secrete inflammatory signals—prostaglandins, nitrous oxide, tumor necrosis factor-alpha (TNFα), and various interleukins (IL-1, IL-6) [80, 81]. Finally, anti-catabolic proteins, like tissue inhibitor of matrix metalloproteinase (TIMP) -1 or -3, which counter the activity of MMPs, appear to be deregulated and less abundant than MMPs in IDD [82-84]. The level of production of enzymes and inflammatory signals varies with age and degree of degeneration, and it is presumed that these mediators are well-regulated in healthy discs, most elevated in actively degenerated specimens, and abated somewhat in severe degeneration [85]. Bearing in mind the temporal progression of IDD, changes in signaling and activity of structural, catabolic, inflammatory, and anti-catabolic proteins may be informative to the active disease process and as a marker of the effect of mechanical loading.

The connection between mechanics and biology is critical in the study of normo- and patho-physiology of the disc. Changes in cell-volume, fluid flow, pressures, osmolarity, electrokinetics, and cell deformation [20, 50] are theorized transducers of mechanical loading to intracellular signaling. Intracellular responses involve, at the least, cytoskeletal rearrangement [86] and Ca^{2+} transients [87] that mediate signaling pathways, which lead to changes in gene expression and protein synthesis and activity. These mechanically induced changes appear to be governed primarily by loading parameters: mode, magnitude, frequency, and duration. Court et

al. demonstrated how static bending of murine discs leads to increased cell death, reduced aggrecan expression, and increased disorganization of AF structure in the concave portion of the disc [88], illustrating how loading mode can influence disc biology. Cell culture studies have shown the effect of load magnitude. Low to moderate magnitudes (0.1-0.4 MPa) of static compression may be beneficial in terms of increases in proteoglycan and collagen gene expression [89] and protein synthesis [90]. Higher levels of compressive magnitude have been shown to down-regulate structural protein expression, up-regulate catabolic protein expression [91], and increase cell death [92], although thresholds are tissue region and species dependent [45]. Dynamic loading has proved, in general, to be healthier for the disc than static loading [15]. The NP appears to be more biologically responsive to frequency than the AF, with low to moderate frequencies (0.01-0.2 Hz) promoting structural gene expression and down-regulating catabolic gene expression [91]. In the same experiment, the AF at all frequencies and the NP at 1.0 Hz exhibited reduced structural and increased catabolic expression. Finally, studies illustrate the important regulator of duration on biologic outcomes [79, 93]. MacLean et al. witnessed gene expression of structural and catabolic genes increase with time (0.5-4 hrs) in the AF and structural expression decreases while catabolic expression is maintained in the NP at 4 hrs [79]. Although the exact mechanisms or cellular signaling pathways are not well characterized for IVD mechanical signaling, it is abundantly clear that mechanics helps to regulate cell behavior and matrix homeostasis.

2.3 DISC MECHANOBIOLOGY

As an important regulator of cell and matrix homeostasis, mechanobiology plays a prominent role in the initiation and mediation of degenerative changes in IDD. Mechanics may play a direct role in initiating changes to disc function through annular tears, nuclear herniations, end plate cracking, repetitive abnormal loading, or long-term hypomobility. Alternatively, genetically or biologically driven processes may provoke mechanical changes via altered biochemistry. In either case, the nature of and relationship between applied loading, ECM and interstitial fluid properties, and cellular micromechanical environment is altered in degeneration. Immobilization causes a general decrease in gene expression and leads to changes in cell viability and enzymatic activity associated with degeneration [94]. Moderate magnitudes of loading at moderate frequencies demonstrate matrix maintenance; other studies have shown anabolic and protective effects against degeneration based on loading thresholds [20, 90, 91]. High magnitudes of static loading, loading at frequencies above or below a threshold frequency, and long durations of loading seem to cause degenerative changes [15]. While these examples are not exhaustive, they illustrate what mechanobiological studies demonstrate—mechanical loading within acceptable thresholds has the capacity to facilitate matrix protection and repair, and loading outside these bounds mediates degenerative changes to cellular activity, phenotype, and viability in addition to matrix regulation and interstitial fluid.

Because of its salience in healthy disc tissue regulation and the progression of disc degeneration, IVD mechanobiology has become a rich research arena. Disc mechanobiology divides readily into three classifications based on model system: in-vitro cell culture, in-vivo milieu, and ex-vivo organ culture. In-vitro cell culture studies typically include cells plated in monolayer or seeded in 3D gels subjected to varied tensile stretch [24], compression [45],

hydrostatic pressure [95], osmotic pressure [96], and streaming potentials [50]. In-vivo studies have instrumented murine and lapine caudal and lumbar motion segments with controlled external fixators and subjected instrumented segments to various loading schemes. More recently, ex-vivo systems have been developed that isolate the disc and/or surrounding structures immediately post-mortem and simulate physiologic environmental conditions—mechanical loading, temperature, gas partial pressures, humidity, and nutrient supply. The outcomes tend to be similar across systems, including gene expression, protein synthesis, protein and proteoglycan content, enzymatic activity, and cell viability. Nevertheless, the model choice allows particular focus based on experimental question.

2.3.1 In-vitro Systems

Cell-level mechanobiology derives cell-type-specific forms of loading from disc-level strains. At a resting state of body weight support, during axial compression, and under bending conditions, cells in the AF are subjected to circumferential and axial tensile strain. To explore this loading mode, AF cells are cultured in monolayer and undergo strains of varying magnitudes and frequencies. Work by Sowa et al. has employed human and rabbit cells subjected to 3%, 6%, and 18% membrane strain at 0.1, 0.5, and 1 Hz [93]. Inflammatory stimuli (i.e. IL-1β) were also combined with mechanical loading. They examined gene expression of catabolic (MMP-1, MMP-3), anti-catabolic (TIMP-1), and inflammatory (iNOS, COX-2) genes and prostaglandin E2 (PGE2) production and identified beneficial levels of loading. Moderate strains at low frequencies (6% strain, 0.1 Hz) were most protective—i.e. down-regulation of catabolic and inflammatory and up-regulation of anti-catabolic genes.

Similar to appropriate tensile loading protocols developed for AF cell culture, NP cells are cultured in three dimensional explants or gels and loaded in compression or hydrostatic pressure. NP cells are frequently seeded in alginate beads that preserve appropriate cell phenotype [97]. Sowa et al. have developed a compression chamber that applies hydrostatic pressure to NP cells in alginate beads [98]. Gene expression (similar to that analyzed for stretched AF cells), enzymatic activity, cell viability, and matrix breakdown fragments (chondroitin sulfate-846 (CS-846), a putative marker of aggrecan synthesis) were assayed in response to differing magnitudes and durations of compression: 0.7, 2.0, and 4.0 MPa at 4 and 24 hours [98]. At 4 hours, increasing magnitudes of compression were anti-catabolic; however, all loading at 24 hours of loading was primarily catabolic. Other disc researchers have explored the effect of age in addition to loading magnitude, frequency, duration on NP cell culture [45]. Korecki et al. discovered that cell age, apart from age-related changes to the surrounding matrix, influenced cellular responses more than applied loading in alginate gels. Mature cells' gene expression profile was anabolic (increased aggrecan and type-I collagen) and anti-catabolic (reduced MMP-3), but less total GAG was secreted. Compressing young cells prompted no type-I collagen up-regulation, no change in aggrecan expression levels, and increases in MMP-3 levels. These NP cell compression studies are useful at a mechanistic level of mechanobiology.

Cell culture model systems generally permit probing of disc response to specific modes of mechanical transduction. Cellular responses are helpful in framing how well characterized loading patterns and tissue properties may influence cell behavior. However, replicating in-situ cell-matrix adhesions and cell-cell interactions is impossible, and simulating appropriate ECM and PCM presence and properties, electrokinetic and osmotic environments, and complex loading remains difficult. Translating in-vivo strains to mechanical inputs is daunting and

remains inaccurate despite the emergence of more refined models [29, 30]. Thus, translating cell-culture outcomes to the human situation is not tenable.

2.3.2 In-vivo Systems

In-vivo model systems demonstrate the role mechanics play in initiating and mediating loading-associated remodeling. For decades, IDD models were created by altering disc mechanics through imposed bipedalism [99], static compression [100], dynamic compression [91, 92] instability [101, 102], endplate perforation [103], and annular puncture [74, 104]. More recently, transcutaneous load applicators attached to adjacent vertebrae have explored controlled loading: static bending [88], static compression [105], dynamic compression [91], and torsion [106]. Previous description of loading parameters—mode, magnitude, frequency, and duration—relied nearly exclusively on in-vivo systems. The benefit of stable physiologic conditions—as opposed to achieving optimal, sterile culture conditions—makes in-vivo systems ideal for long-term studies, remodeling processes, and clinical interventions in combination with controlled loading. However, the costs and challenges of long-term animal research and difficulties in translating popular caudal disc models, lack of posterior structures and different matrix composition to human lumbar discs limit their application. Moreover, little is known about how physiologic loading is transmitted to cells, though modeling efforts have begun [29]. Finally, it is difficult to modify the local environment (e.g. add a local inflammatory stimulus) and to assess structural breakdown fragments and local responses (e.g. absence of conditioned media) to loading and/or coupled interventions.

2.3.3 Ex-vivo Systems

Ex-vivo organ culture systems represent a bridge between in-vitro and in-vivo model systems that fulfills an important role in disc mechanobiology. The past decade has witnessed the development of a range of disc organ culture systems [107-112]. Animal models include murine, lapine, ovine, and bovine discs with differences in size, geometry, loading, experimental duration, and endplate inclusion. Disc dimensions are salient parameters in disc organ culture because cell metabolism relies on diffusion for exchange; as a consequence, smaller animals have a relative advantage over larger ones because of smaller diffusion distances. Smaller animal models--murine and lapine--have demonstrated cell viability greater than 80% through four weeks of culture [108, 111]. In contrast, larger animal models generally remain viable for shorter durations; experimental time frames were six hours [112], one week [110], 5-8 days [109, 113], and three weeks [114]. Work by Lee et al. demonstrated the damaging effect of capillary bud clogging in the endplate at death on cell viability [110]. Researchers generally remove or shave the endplate to promote cell viability through improved metabolism [109]. In attempt to mimic the physiologic mechanical environment and explore the effect of loading parameters on system outcomes, researchers have applied static and dynamic compression [109, 110, 114, 115]. Table 1 summarizes the loading schemes used in these experiments.

Table 1. Compressive loading patterns used in ex-vivo mechanobiology studies

Researcher	Model	Frequency	Magnitude	Duration
Lee (2003)	bovine tail	static	0.25 MPa	1 hr - 1 wk
Wang (2006)	lapine lumbar	static	0.5, 1.0 MPa	6 hr
		0.1, 1.0 Hz	0.5, 1.0 MPa	
Gantenbein (2006)	ovine tail	static	0.2 MPa	4 d
		diurnal	0.2 / 0.8 MPa	
Korecki (2007)	bovine tail	static	0.2 MPa	4 - 8 d
		diurnal	0.1 / 0.3 MPa	
Korecki (2009)	bovine tail	static	0.2 MPa	1 hr / d, 5 d
		1.0 Hz	0.2 - 1.0 MPa	
		1.0 Hz	0.2 - 2.5 MPa	
Junger &	ovine tail	diurnal	0.2 / 0.6 Mpa	7 - 21 d
Gantenbein (2009)		0.2 Hz	0.4 / 0.8 MPa	4hr x 2 / d

Ex-vivo organ culture systems are critical tools for IVD mechanobiology in that in-situ cell-ECM and cell-cell interactions are preserved and environmental conditions (T, $[CO_2]$, $[O_2]$, pH, osmolarity) can be modulated. Researchers can intervene (e.g. inflammatory stimuli) locally and collect tissue and conditioned media to assess cellular response and matrix breakdown. Doing so connects loading and environmental conditions to the quest for disc-specific biomarkers of matrix breakdown (e.g. matrix fragments, inflammatory mediators). However, organ culture loading modes have historically been simple and limited by bioactive chamber design. All reviewed systems used uniaxial compressive loading exclusively because of the challenges of manipulating the disc without retaining bony vertebral bodies for attachment, which pose a significant barrier to disc nutrition in culture. Moreover, designing chambers to rigidly attach the specimen and accommodate multiple DOF is challenging. Importantly, maintaining tissue viability and phenotypic synthetic activity and preserving sterility over long periods limits experimental timeframes in ex-vivo systems. Nevertheless, ex-vivo disc culture

systems have helped to fulfill a vital role in characterizing loading parameters' effect on disc cell behavior and matrix homeostasis.

A number of these limitations of current ex-vivo systems can be improved by accepting a different set of advantages and disadvantages within a novel framework built to understand the effect of physiologic motions on disc biology. Adherence to the paradigm of endplate removal has limited investigations to uniaxial compression, but by accepting reduced experimental time frames, one can pursue more complex applied loading using the entire functional spinal unit. While removal of endplates or destruction of the FSU facilitates long term viability, it also limits the accuracy of "in-situ" as a descriptor of load distribution in disc organ culture models because of the role of the facets in supporting compression [116] and the action of the endplate in distributing loads to the underlying AF and NP [63, 117]. Moreover, Haschtmann et al. removed vertebral bodies but retained endplates in a lapine model with remarkable maintenance of disc viability [108]. It also has been suggested that administration of pre-mortem anti-coagulants could improve viability via enhanced metabolic exchange [109]. Including the entire FSU may facilitate in-situ loading, but incorporating and dissecting FSU bone and soft tissue contributes to the cytokines and matrix fragments found in the media. Consistent processing technique and adequate controls would allow for meaningful, disc-specific contributions to the media. In summary, attempts at non-axial, complex (i.e. physiologic) loading are precluded by destruction of posterior elements and bony vertebral bodies. It is reasonable to assume that viability may be maintained over shorter times with careful model selection and endplate treatment; thus, to pursue a system capable of multi-axis, more accurate simulation of in-vivo loading and preservation of the FSU—disc, endplates, facets, posterior ligaments, vertebral bodies—is both feasible and essential for better in-situ loading approximation.

Translating applied loading from an ex-vivo model to the clinical context may be achieved through measurement of intradiscal pressure (IDP) of the nucleus pulposus. IDP is time-varying; pressurization drops as applied loading remains constant and fluid exudes through the dense, charged matrix. Permeability of the AF and EP and fixed charge density of NP and AF are primary determinants of time-varying fluid flow [49]. IDP then varies with aging and degeneration because of the changes in tissue properties that occur in these processes. It stands to reason that attempts to relate applied loading to tissue changes and cellular response would be better served by comparison to IDP than to applied force or moment. As a result, disc researchers have developed a simplified relationship between applied force and IDP in axial compression experiments. Investigators customize the amount of applied axial force, F_a, based on each disc's area, A [63, 118, 119]:

$$IDP = \frac{F_a}{A}$$

Although this method accounts for inter-specimen variation, it does not consider inhomogeneity of disc tissue nor can it account for imperceptible variation in matrix composition and permeability that may be a function of species, degeneration, or age. More importantly, this method was not developed for FSUs; it does not account for the role of posterior structures in compression [116]. Good experimental practice, then, would explore the relationship between IDP and F_a in establishing a new model.

A review of the ex-vivo systems in use also reveals use of standard culture conditions (21% O_2) despite known hypoxia within the disc [107-114, 120]. Oxygen saturation has a strong effect on disc cell synthetic behavior and viability [58]. Urban et al. showed that ~5% O_2 is appropriate at disc margins [121]. Cell culture experiments seeking to replicate in-vivo hypoxia

have subjected cells to 1-3.5% O_2 [122-124]. Therefore, ex-vivo organ culture systems that aim at more physiologic conditions should incorporate hypoxia in culture conditions.

Another notable limitation of currents ex-vivo systems is the general lack of attention to identifying potential biomarkers. A biomarker may be defined as a quantifiable biological outcome that provides diagnostic and prognostic utility for active changes to or processes in the IVD. Useful biomarkers will be disc specific and more sensitive than current diagnostic tools like X-ray, computed tomography (CT), or magnetic resonance imaging (MRI), which reveal accumulated, anatomic changes rather than the active metabolic state. Borrowing from comparable disease processes like osteoarthritis, candidate disc biomarkers include synovial, serum, or urine concentrations of disc matrix fragments [125, 126] or inflammatory cytokines [127, 128]. It is likely that a combination or profile of biomarkers will be necessary for specific, sensitive detection, yet significant challenges exist in simply identifying and detecting candidate disc-specific biomarkers. If identified, a disc-specific biomarker profile would facilitate the goal of prescribed mechanical loading by providing measurable indications for treatment and therapeutic assessment.

Limited biomarker analysis has been performed in disc organ culture. Junger et al. assayed disc tissue for a neoeptitope of chondroitin sulfate, CS-846—a putative marker of aggrecan turnover [114]. However, analysis of conditioned media is likely more relevant to detecting fragments or molecules that will migrate to the serum. Korecki et al. examined conditioned media for released GAGs, but GAG size and structure make them unlikely systemic biomarkers [109]. Analysis of conditioned media for systemic biomarkers could include detection of a breakdown product of type-II collagen, C-telopeptide-II (CTX-II), a marker of aggrecan synthesis, CS-846, or an inflammatory marker, PGE2. Assaying for these proteins and

others could improve the understanding of mechanically-induced damage and remodeling. Detection of these markers and identification of disc-specific biomarkers of early degeneration or load-responsive biomarkers would be useful in guiding clinical treatment.

A comparison of existing ex-vivo mechanobiology systems and the current system proposed here are summarized in Table 2.

Table 2. A comparison of the advantages and disadvantages of disc mechanobiology systems

System	Advantages	Disadvantages
Cell culture	Mechanistic	Contrived loading Artificial cell-matrix & cell-cell adhesions Limited translation
In-vivo	Quasi-physiologic loading Physiologic environment Long experimental timeframes	Coupled interventions challenging Local matrix breakdown difficult to detect Cell mechanics unknown
Ex-vivo	Quasi-physiologic loading Matrix fragment detection Simulated physiologic environment Local, coupled interventions	Limited experimental timeframes Cell mechanics unknown Limited types of loading (axial only)
Current System	**Full-joint loading** **Capable of 6DOF loading** **Matrix fragment detection** **Simulated hypoxic environment**	**Short experimental timeframes** **Single outcome per test** **Cell mechanics unknown**

3.0 GOAL AND SPECIFIC AIMS

The goal of this project is the development of a novel ex-vivo intervertebral disc mechanobiological system that seeks physiologic loading capability and assessment of cellular and matrix responses using disc tissue and conditioned media. Design constraints and performance validation for the bioactive system are motivated by the goal of establishing a novel experimental platform with well-characterized mechanical inputs, controlled environmental parameters, and the capability of supporting an array of biological outcome measures that demonstrate baseline stability and responsiveness to mechanical loading.

3.1 SPECIFIC AIM 1

Design and validation of the proposed mechanobiological system stands as the first challenge to fulfilling this thesis' objective. Validation denotes testing of system performance against design constraints to demonstrate satisfaction of system claims. Explicitly, design constraints require that the bioactive chamber must (i) rigidly but nondestructively attach to adjacent vertebral bodies, (ii) be capable of six DOF motion, (iii) perform cyclic and static loading, (iv) maintain adequate IVD viability (>70%) in an FSU over 24 hours, (v) attain and preserve 37 °C (+/- 0.5 °C) and 5 % O2 (+/- 1% O_2) throughout experimentation, and (vi) enable analysis of conditioned media directly surrounding the disc. Desired outcomes after intervention (e.g. mechanical

loading) include, at a minimum, (a) region-specific cell viability/metabolic activity, (b) region-specific gene expression of catabolic (e.g. MMP-1, MMP-3), anti-catabolic (e.g. TIMP-1), inflammatory (e.g. COX-2, iNOS), and structural (aggrecan, collagen-II) genes, (c) matrix fragment (CTX-II, CS-846) detection from conditioned media, and (d) enzymatic activity of catabolic enzymes (MMP-1, MMP-3). A system attaining these design constraints would represent a novel ex-vivo experimental platform for future investigations of simulated exercise-based therapy on disc matrix homeostasis.

3.2 SPECIFIC AIM 2

To demonstrate system efficacy, biological outcomes must be able to detect effects of loading. Based on previous mechanobiological findings, magnitudes of static axial compression with estimated ~0.16 MPa and 1.0 MPa of intradiscal pressure (IDP) will be applied to rabbit FSUs for four hour durations. Pressures represent resting IDP and pressures experienced in mild exercise [129, 130]. It is hypothesized that 1.0 MPa/4 hour constant compression will have a beneficial effect on cell viability outcomes, though changes are expected to be minimal. Loading will increase anabolic and catabolic gene expression relative to unloaded and fresh controls. Enzymatic activity of MMP-1 and MMP-3 will also be increased in loaded samples relative to unloaded ones. Greater amounts of matrix fragments will be present in conditioned media from samples subjected to compressive loading relative to unloaded samples. Concentrations of prostaglandins will not be detectable in conditioned media because of their small size (< 2kDa).

4.0 EXPERIMENTAL METHODS

4.1 SYSTEM DESIGN CONCEPTION

Building 6 DOF loading capability into an ex-vivo mechanobiological system with stable environmental control and adequate cell viability (Specific Aim 1) requires innovation. Existing systems—mechanical actuators, load cells, bioreactors, tubing, and other system components—are typically designed to fit and operate within a standard laboratory incubator. Current ex-vivo systems have been limited to single DOF. Biomechanical spine testing systems that move spinal segments through physiologic rotations—flexion/extension (FE), lateral bending (LB), and axial rotation (AR)—tend to be complex, large devices that would not fit within a standard incubator [131, 132]. Their components would not be compatible with a warm, humid environment either. In the Ferguson Laboratory in the Department of Orthopaedic Surgery, researchers have developed a robot-based spine testing system composed of a serial-linkage robot (Staubli RX-90, Staubli, Inc., Duncan, SC) and an on-board universal force sensor (UFS Model 90M38A-150, JR3 Inc., Woodland, CA) [132]. This system has tested human and rabbit FSUs in FE, LB, and AR [133, 134]. Because of the open, flexible configuration of the serial-linkage robot and the precedent of physiologic FSU testing, compatibility with the robot-based spine testing system was imposed as a design constraint to meet the goal of 6 DOF compatibility.

Three basic design concepts were generated for attaining physiologic environmental conditions surrounding the FSU while achieving multi-axis loading. In reference to the bioreactor that houses the FSU, these concepts divide into (i) a design without an incubator, (ii) an intra-incubator design, and (iii) an extra-incubator design. The first design allows individual environmental parameter control and facilitates multi-axis motion. The challenge of maintaining sterility and controlling each parameter—temperature, O_2 concentration, CO_2 concentration, flow rate, media composition—was daunting and unnecessarily complex. The second design enjoys the advantages of controlled temperature, gas concentrations, and humidity in addition to ensured, long-term sterility. However, interfacing the robot with a bioactive chamber located within the incubator poses undesirable challenges. Any rigid connection from the robot to the chamber would pass through a flexible gasket in an incubator wall. Creating this elastomeric interface risks compromising incubator functional and mechanical integrity. The extra-incubator design places the bioactive chamber in the mechanical testing system in a closed flow loop with media housed within an incubator (see Figure 1). This design makes multi-axis motion more tenable, and closed loop flow with an incubator avoids the challenges of controlling temperature, dissolved oxygen, and carbon dioxide concentrations separately. However, preserving appropriate conditions in the bioactive chamber and avoiding increased risk of contamination pose challenges to this idea. The final design was selected, however, based on a cost-benefit analysis and general feasibility considerations. The advantages and disadvantages of each design concept are summarized in Table 3, and the elected design concept is illustrated in a schematic in Figure 1.

Table 3. Comparison of System Design Ideas

	No incubator	**Intra-incubator**	**Extra-incubator**
Summary:	Closed loop system with stations for gas exchange & fluid heating	End effector interfaces with flexible membrane in incubator wall to manipulate specimen within incubator	Gas & heat exchange in incubator, form closed loop with chamber
Advantages:	Robot interface possible: More physiologic loading possible Less control development for this loading Existing fixturing techniques & materials Could interface with ATM secondarily	Heat and gas exchange within incubator Axial, torsional, and bending loading Sterility challenges reduced O2 control possible	Robot interface possible (see before) Superior gas & heat exchange potential Sterility challenges reduced O2 control possible
Disadvantages:	Validation needed for each sub-system (probes) Large sterility challenges (obstructions) O2 control challenges	Bending may be limited Flexible membrane in incubator wall >limits bending range >risks incubator damage	Validation needed for intra-chamber conditions Sterility challenges

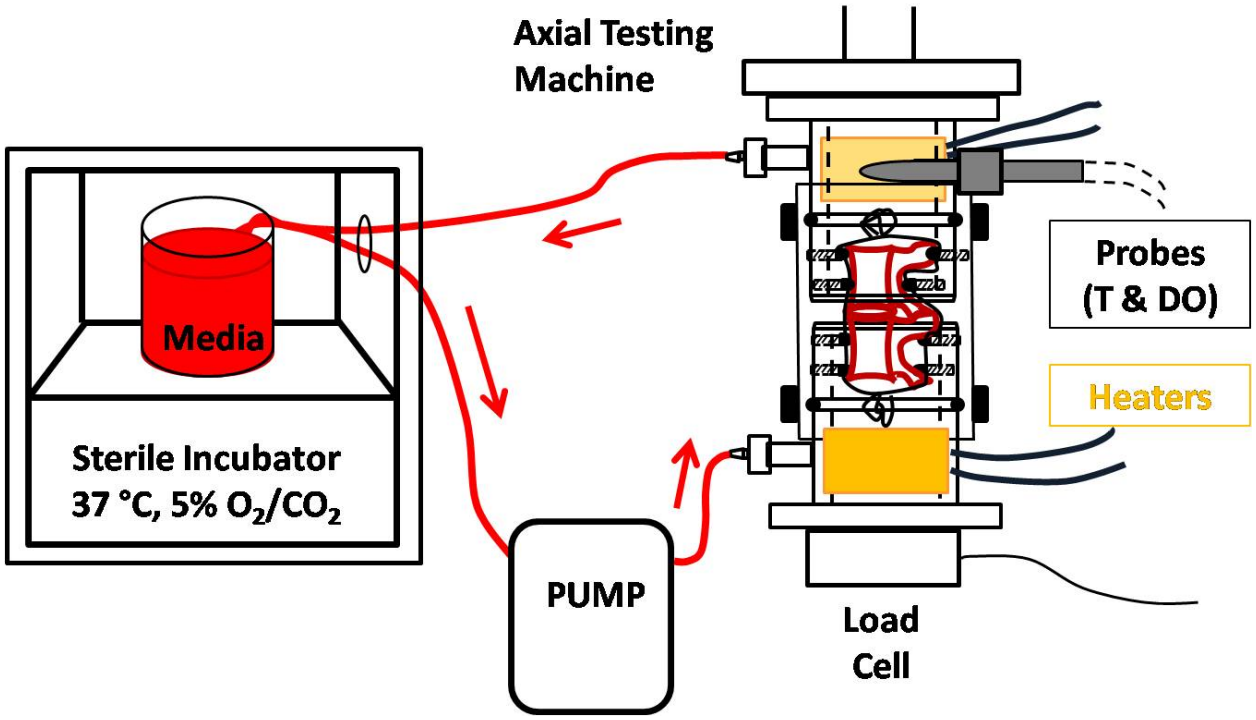

Figure 1. Schematic of chosen system design

4.2 APPLIED LOADING

While compatibility with a 6 DOF robot-based testing system informed decisions at each stage of device development, testing for this project focused on axial testing. Because of the emphasis on demonstrating concept feasibility and on maintaining biological stability and chamber conditions, testing for this thesis project utilized a self-made axial testing machine (ATM). A linear actuator with an optical encoder (D-B.125-HT23E10DIFF-4-1/4, Ultra Motion, Inc., Cutchogue, NY) placed in series with a 100 lb. load cell (MLP-100, Transducer Techniques, Inc., Temecula, CA) is controlled with a programmable motion controller (MicroLYNX-4, Intelligent Motion Systems, Inc., Marlborough, CT). Matlab (Matlab 2009R, The Mathworks, Inc., Natick, MA) integrates and controls the position information from the motion controller, read into a PC via RS-232 communication, with the load data, read into a PC via a 24-bit resolution data acquisition board (LabJack U6-Pro, LabJack Corp., Lakewood, CO), using a fuzzy logic control scheme. Load resolution was ~0.1 N. Displacement resolution was < 0.001 mm and accuracy was assessed with a linear-variable displacement transducer (Schaevitz LVDT, Measurement Specialties, Inc., Hampton, VA) connected to a signal conditioner (LVC-2400, Macro Sensors, Inc., Pennasuken, NJ). Load cell calibration was performed by weighing objects of known mass (20 – 3782 grams) and fitting voltage vs. weight data sets with linear relationships.

4.3 BIOACTIVE CHAMBER DEVELOPMENT

4.3.1 Design Alternatives

The bioactive chamber is central to meeting system design constraints. As previous mechanobiological systems have been designed (i) as disc only systems, (ii) for uniaxial compression and (iii) for incubator housing, a bioactive chamber intended for 6 DOF FSU manipulation and maintaining specimen viability, 37 °C (+/- 0.5 °C), 5% O_2 / 5% CO_2 (+/- 1%), and sterility outside an incubator must be novel. Additionally, the desire to collect conditioned media for matrix breakdown fragments influenced chamber development.

The first challenge of FSU testing is one of fixation: how to rigidly attach a specimen to the chamber. Traditional FSU or spinal segment testing involves bony bodies potted in epoxy resins (e.g. poly(methyl methacrylate)) (PMMA) and fixtures anchored to the resin blocks via screws or clamps [135, 136]. Potting FSUs in mechanobiological testing is undesirable due to detrimental effects on biologic processes and proteins from exothermic hardening. Additionally, coating the vertebra in resin would substantially hinder diffusion to and through the bone, limiting disc nutrition and waste exchange. Alternatives to traditional mechanical testing fixation, such as direct screw penetration of the bone [137], are challenging in the small, irregular anatomy and relatively delicate bone of rabbit or elderly human vertebrae.

The first attempt at non-destructive fixation borrowed heavily on a fixation scheme devised by Stokes et al. for use in rat tails in-vivo [138]. Parallel metal washers (1.5” O.D. / 1” I.D.) encircled the FSU. Two brad nails passed through the vertebral body and adhered to the washers using Loctite® (Product 4471, Loctite, Inc., Rocky Hill, CT) (see Figure 2). Each washer was attached to a parallel disk via 4-40 posts, which was in turn screwed to an end-

effector or platen (see Figure 3). A flexible membrane attached to each disc via pipe clamps. This design failed because of challenges in pin placement, pin-washer affixation, parallel construction, lack of side-wall ports for tubing and probes.

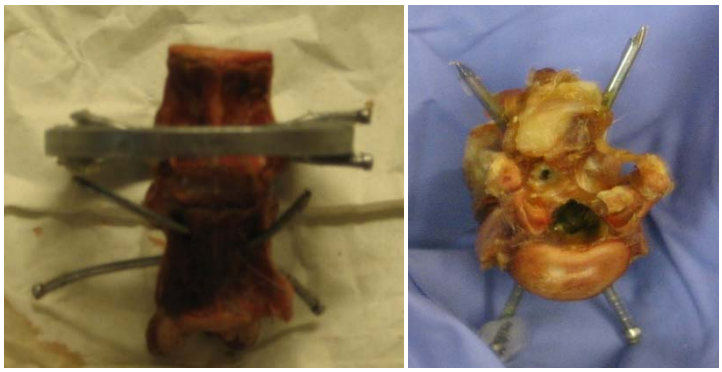

Figure 2. Ring attachment (left, coronal view) and pin placement in rabbit FSU (right, axial view)

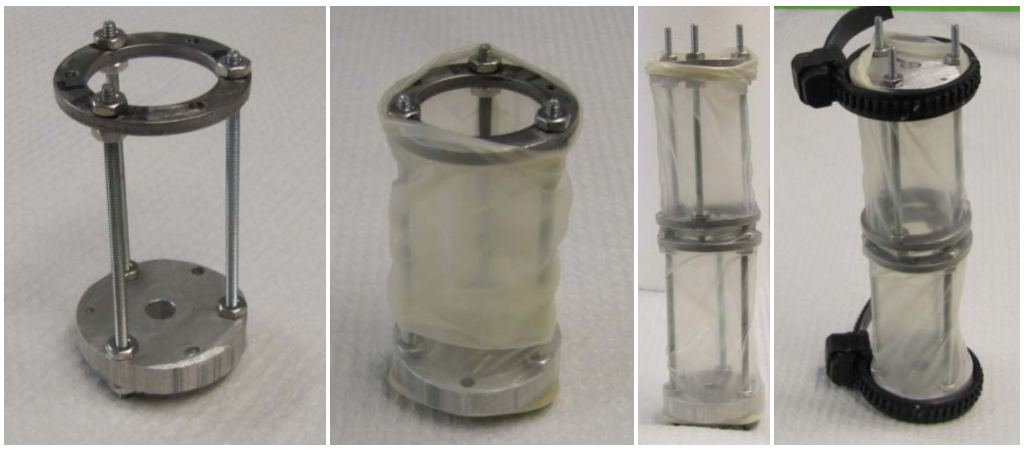

Figure 3. Ring-and-post design with flexible-walled membrane

A second attempt at a novel FSU attachment scheme placed each vertebra in a chuck. The simplicity and ease of use of this design was attractive, but it reduced fluid access to the bony surface—in particular that of the opposite, exposed subchondral bone. Also, future

applications in torsion seem unlikely to be rigid, and the chuck did not interface readily with a flexible walled chamber with side-wall ports.

4.3.2 Chamber Design

The final design for bioactive chamber fixtures is motivated by stated design constraints and the shortcomings of previous prototypes. Essentially, metal fixtures hold the adjacent vertebral bodies, and a flexible, rubber membrane seals against the metal fixtures. Fluid is pumped into the fixtures, fills the enclosed volume, and flows out in a closed flow loop. The fixtures were conceived in SolidWorks (SolidWorks 2005**,** Dassault Systèmes SolidWorks Corp., Concord, MA) as depicted in Figure 4. They were machined by the School of Medicine's Department of Cell and Physiology/Pharmocology Machine Shop out of 304 stainless-steel with bases compatible with both the ATM and the robot-based testing system. Figure 5 depicts the fixtures.

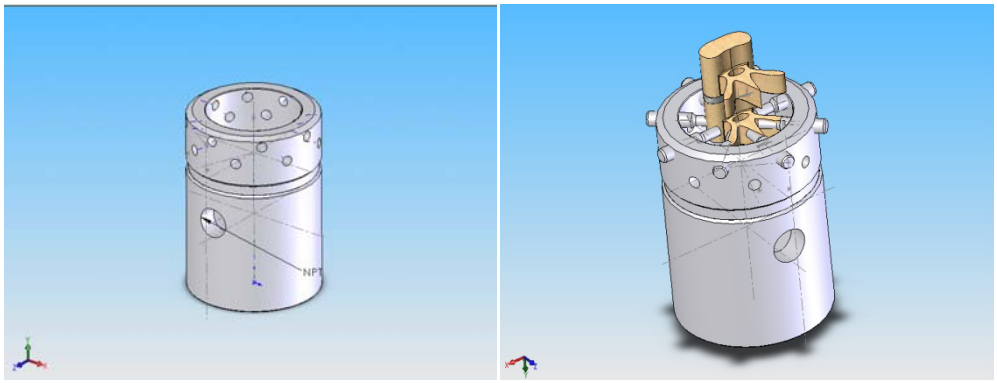

Figure 4. Fixture conceptualization in SolidWorks

Figure 5. Bioactive chamber lower fixture

To achieve rigid fixation, two rows of eight set screws (1/2”-3/4”L 6-32) can be tightened to variable depths and amounts of torsion to accommodate the irregular geometry of a vertebra. Media contact with the bony surface of the vertebra and opposite-side subchondral bone was increased with the small contact area afforded by screw-tips. To connect the chamber with the flow loop, rigid sidewalls were needed for media tubing influx/efflux and probe ports. Stainless-steel luer ports connected to male luer tubing couplings and custom-made brass fittings facilitated sealed probe access to the chamber. Figure 6 shows the upper fixture with tubing attached and temperature and dissolved oxygen probes inserted.

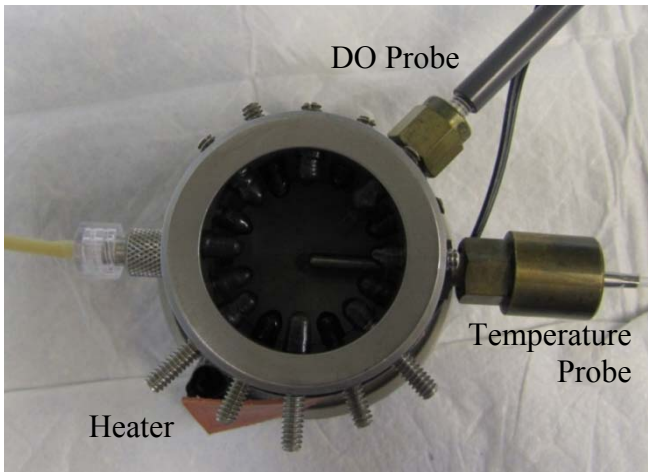

Figure 6. Bioactive chamber upper fixture with attached tubing and inserted probes

Fixture walls also accommodated rubber membrane attachment to allow media flow around the specimen. A groove was etched in fixture walls for an O-ring (1.5" O.D.). Pipe clamps can be tightened down on a thin, latex rubber membrane (Trojan Non-Lubricated Condom, Church & Dwight Co., Inc., Princeton, NJ) over the O-ring to seal the fluid portion of the chamber. The membrane flexibility allows 6 DOF motion while containing media. Plastic pipe clamps are necessary to avoid cutting the thin rubber membrane. Figure 7 shows the bioactive chamber; a specimen is mounted in the fixtures with a latex membrane clamped onto the chamber.

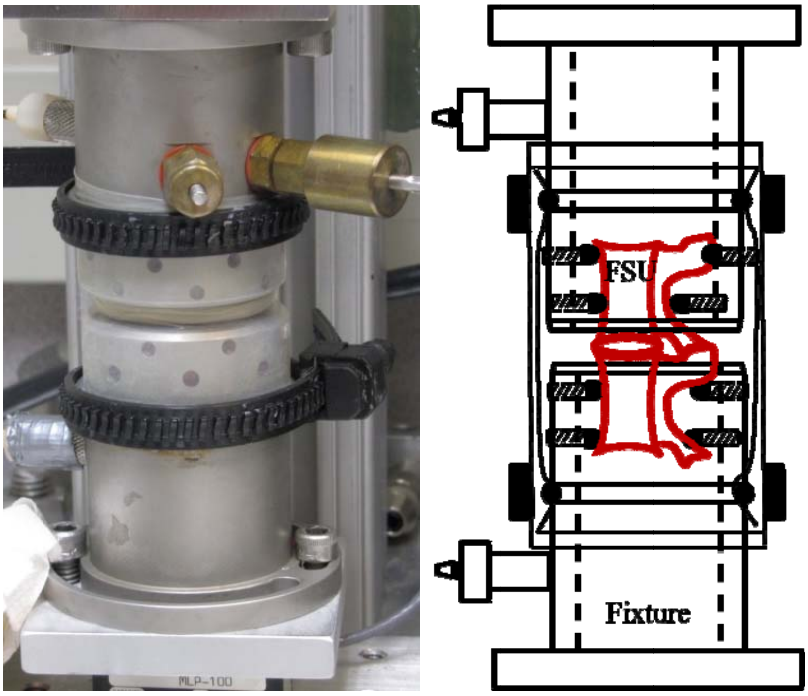

Figure 7. Bioactive chamber: fixtures securing FSU within latex membrane

To address the challenge of keeping conditioned media (i.e. media containing protein fragments and cytokines released from the specimen) volumes small, a segment of dialysis tubing (SpectraPor7, 2000 MWCO/24 mm diameter, Spectrum Laboratories, Inc., Ranch Dominguez, CA) surrounds the FSU. Because tri-folded tubing in SpectraPor closures (12 mm) leaked repeatedly, tubing is manually knotted (single knot) on the inferior and superior ends. Rubber push-on round caps (fit 1/16-1/8" O.D.) are threaded tightly onto screws to prevent perforation of the dialysis membrane (clearly shown in Figure5). Additionally, sharp points of the vertebra—at the disc border, at adjacent disc borders, and on superior facets—require surgical removal to avoid membrane tearing.

While dimensions of fixtures and accessories were selected for rabbit FSUs, the design could be scaled to human lumbar motion segments. This would require machining newly sized fixtures and sourcing appropriate screws, plates, dialysis membrane, rubber layers, O-rings, and

pipe clamps. These challenges are not conceptual; it is anticipated that the same methods of attachment could be applied to larger specimens.

4.3.3 Fixture Rigidity Testing

The rigidity of the fixture-specimen interface must be tested to demonstrate (1) that displacements of the specimen relative to the fixtures are small relative to measured joint displacements and (2) that the fixture-specimen interface has a stiffness of an order of magnitude greater than that of the joint. Obviously, the performance of the fixtures depends on the loading mode. For the initial testing presented here, fixtures were evaluated in uniaxial compression.

Rigidity of the fixturing system for rabbit FSU attachment was assessed in constant and cyclic compression using a Faro Arm digitizer (Titanium Series Faro Arm, FARO Technologies, Inc., Lake Mary, FL). A 3 mm ballpoint tip was placed on the end of the digitizer; its reported single pt. accuracy is +/- 0.025 mm. Hex-head screws (1.5" L, 6-32 HEX) with heads that fit the 3 mm ballpoint were set in the upper and lower fixtures. Three small machine screws (0.5" L, M1 HEX), also with heads that fit the digitizer tip, were placed in the body of the FSU such that the screw heads were close to the axial plane of the disc. To achieve this arrangement, tunnels were drilled in the vertebral body; freshly mixed PMMA was poured down the tunnels; screws were then threaded in; heads were positioned close to the joint line, and Bondo (Bondo Body Filler, 3M, Inc., Atlanta, GA) was placed topically around the screw heads for added support. The three larger screws were threaded in screw holes of the two rows in each fixture. Figure 8 illustrates the instrumented FSU alone and within fixtures attached to the ATM.

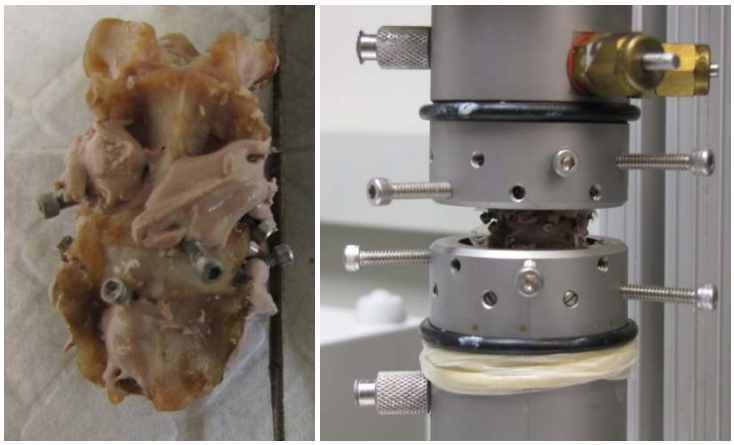

Figure 8. Screws as markers anchored to rabbit FSU (left); FSU mounted in fixtures (right)

L4-5 spines were chosen to best balance the trade-off between vertebral body length and disc volume, that is, between bone area for attachment strength and tissue for biological outcomes. L5-6 tends to be the largest disc, but L6 is considerably shorter than other lumbar vertebral bodies. While L3-4 vertebra are similar in size to L4-5, the disc tends to be marginally smaller. Thus, the L4-5 FSU was chosen for mechanical compression to compromise between surface area for improved fixation and tissue volume for anticipated biological outcomes.

The Faro Arm was used in conjunction with Rhinoceros software (Rhinoceros 3.0, McNeel North America, Seattle, WA) to collect points in space. Three screw head positions were recorded for each "body": upper fixture (UF), lower fixture (LF), superior vertebra (SV), and inferior vertebra (IV). Rigidity was assessed in three different conditions: (i) repeatability testing—collecting screw positions without displacing the UF (negative control), (ii) preconditioning—collecting screw positions at the 0 mm position before and after 5-15 cycles of load-target preconditioning, and (iii) creep—collecting screw positions at the 0 mm position before and after 1100 sec of constant-load loading. Repeatability testing included N=7 trials. Preconditioning tests (N=5) ranged from 5-15 cycles over a load-target range based on 0.5-1.0

MPa. Creep testing (N=3) was similarly performed over a load-target range based on 0.5-1.0 MPa. The repeatability group had the largest number of tests to best describe the limits of the method. Preconditioning trials seemed to be more variable than creep trials after N=3, so more trials were performed to better characterize stiffness in preconditioning.

The effect of frequency and displacement on fixture rigidity were also explored in N=1 specimen. Frequency testing consisted of collecting screw positions at the 0 mm position before and after cyclic loading at varying frequencies (0.4, 0.47, 0.63 Hz). Displacement testing entailed collecting screw positions at 0 mm displacement and some larger axial displacement (0-2 mm). Results are included in Appendix B.1.

Twelve screw positions (four bodies, three screws per body) were imported into Matlab and (a) screw displacements in the fixture reference frames were re-expressed in global reference frame components and (b) the temporal differences in angles and positions from transformations between vertebral body and fixture reference frames were used to analyze fixture rigidity. Global axes were manually aligned with the ATM such that the z-direction was positive in the direction of the linear actuator arm. For both methods, the three screw head points of each fixture were used to create orthonormal local coordinate systems (LCS): upper fixture coordinate system (UFCS) and lower fixture coordinate system (LFCS). In the first method, screw positions on vertebral bodies were collected in the global coordinate system (GCS), $P_G = (P_X, P_Y, P_Z)$, and transformed into the fixture LCS, P_L (P_x, P_y, P_z). Figure 9 shows the relationship of a general LCS with respect to a GCS, illustrating a traditional local-to-global transformation.

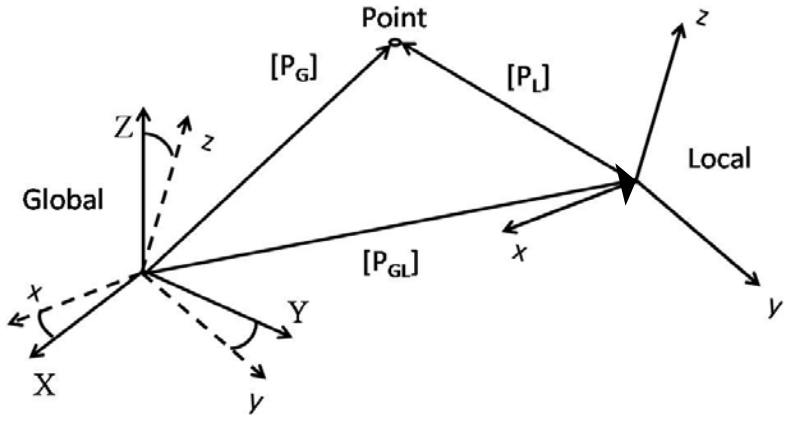

Figure 9. Basic depiction of local-to-global transformations

The transformation, from the local to the global reference frame, is given by

$$[T_{GL}] = \begin{bmatrix} \mathbf{R}_{GL} & P_{GL} \\ 0 \ldots & 1 \end{bmatrix}$$

$$\text{where } [R_{GL}] = \begin{bmatrix} \cos_{Xx} & \cos_{Xy} & \cos_{Xz} \\ \cos_{Yx} & \cos_{Yy} & \cos_{Yz} \\ \cos_{Zx} & \cos_{Zy} & \cos_{Zz} \end{bmatrix} \text{(direction cosines)}$$

$$\text{and } [P_{GL}] = \begin{bmatrix} L_X \\ L_Y \\ L_Z \end{bmatrix} \text{ is the vector pointing from the GCS to the LCS}$$

Inverting the rotation matrix and vector,

$$[T_{GL}]^{-1} = [T_{LG}]$$

forms the transformation from the global-to-local for definition of a point in the LCS:

$$[P_L] = [T_{LG}][P_G]$$

Method (a): Displacements measured in the GCS include error from the ATM, so simple subtraction of initial from final screw positions in the GCS was avoided. Moreover, while the GCS is manually aligned with ATM axes, LCSs are not aligned with global axes, so displacements in the LCS cannot be understood intuitively. Thus, changes in screw positions between initial and final states (final with respect to initial positions) were measured in the

fixture coordinate system and realigned with the GCS for more tractable vector components. This method is conservative and robust, but it does not contain rotational information

To summarize the procedure, global screw positions are transformed to the local fixture coordinate systems.

$$[P_L] = [T_{LG}][P_G]$$

Difference in screw position in the LCS, $P_{L\_f\text{-}i}$, between the initial, P_{Li}, and final position, P_{Lf}, was calculated.

$$[P_{L\_f\text{-}i}] = [P_{Lf}] - [P_{Li}]$$

$P_{L\_i\text{-}f}$ is realigned with the GCS at the starting point using $\mathbf{R}_{GL\_i}$.

$$P_{G_{i-f}} = [R_{GL_i}]\, P_{L_{i-f}}$$

Appendix B.2.1 contains the Matlab code that details this procedure.

Method (b): The second method compares changes in vertebral body position and orientation relative to the fixture coordinate system. This method creates an orthonormal LCS for the vertebral bodies in addition to fixture coordinate systems: superior vertebra coordinate system (SVCS) and inferior vertebra coordinate system (IVCS) as illustrated in Figure 10. Method (b) describes rotational rigidity, but results reflect an assumed order of rotations: $(R_x)(R_y)(R_z)$.

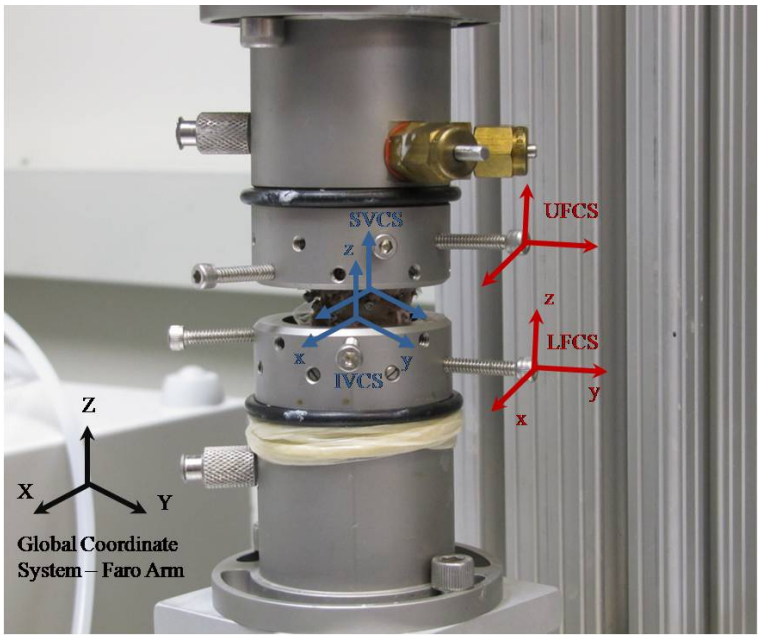

Figure 10. Global and local (fixture, specimen) coordinate systems defined from screw positions

The transformation matrices between UFCS-and-SVCS (T_{UF_SV}) and LFCS-and-IVCS (T_{LF_IV}),

$$[T_{UF\_SV}] = [T_{G\_UF}]^{-1} [T_{G\_SV}]$$

$$[T_{LF\_IV}] = [T_{G\_LF}]^{-1} [T_{G\_IV}]$$

were formed at initial and final positions. Displacements and Cardan angles (roll/pitch/yaw) were extracted from each spatial transformation. Appendix B.2.2 contains the Matlab code generated to make these calculations. Relative displacements and rotations were found by subtracting initial from final positions and rotations; these differences represent how much the vertebra moved with respect to the fixture subjected to given loading conditions (i-iii).

Stiffness: Finally, axial stiffness was calculated for the FSU and the fixture system. Differences in stiffness should be an order of magnitude apart for minimal contribution (~10%)

of fixation laxity to mechanical outcomes. The globally aligned z-displacement of each screw, $P_{G\_f\text{-}i,z}$, is averaged and used as a measure of vertebral body axial displacement relative to the fixture. The applied force is divided by this displacement to evaluate fixture-vertebra stiffness.

$$K_{\text{fixture\_vertebra}} = \frac{F_a}{\text{mean}(P_{G_{f-i,z}})}$$

Specimen stiffness is simply applied force divided by maximum displacement given by the optical encoder under that loading:

$$K_{\text{specimen}} = \frac{F_a}{\max(\Delta z_{ATM})}$$

Based on the criterion stated above, a rigid system should adhere to the following:

$$\frac{K_{\text{specimen}}}{K_{\text{fixture\_vertebra}}} < 0.10$$

4.4 VIABILITY ASSAY DEVELOPMENT

Cell viability is a critical outcome in organ culture because of the explicit goal of stable bioactivity during an intervention. As such, it is used to establish limits on experimental time frames and assess interventions' effects on cellular activity. A new spectrophotometric technique for disc tissue, adapted from an articular cartilage assay [139], was developed for simple quantification of cell viability.

A tetrazolium salt, MTT (3-(4,5-dimethylthiazol-2-yl)-2,5-diphnyltetrazolium bromide) (Thiazol blue tetrazolium bromide, Sigma-Alrich, Inc., St. Louis, MO), is reduced to formazan at metabolically active, viable mitochondria. Reduction causes a yellow-to-purple color shift; thus viable cells are purple in histological cross-sections. Tissue is embedded in O.C.T. compound,

frozen at -80 °C, sectioned with a cryostat into 5μm slices, and viewed under bright field microscopy. Images of rabbit AF at 20x in Figure 11 compare freshly harvested rabbit discs to desiccated negative controls. This technique was used by Korecki et al. in an ex-vivo bovine IVD culture, but difficulty in efficiently quantifying viability and obtaining repeatable sectioning of the highly hydrated rabbit NP motivated the development of a reliable, quantifiable method of MTT viability assessment.

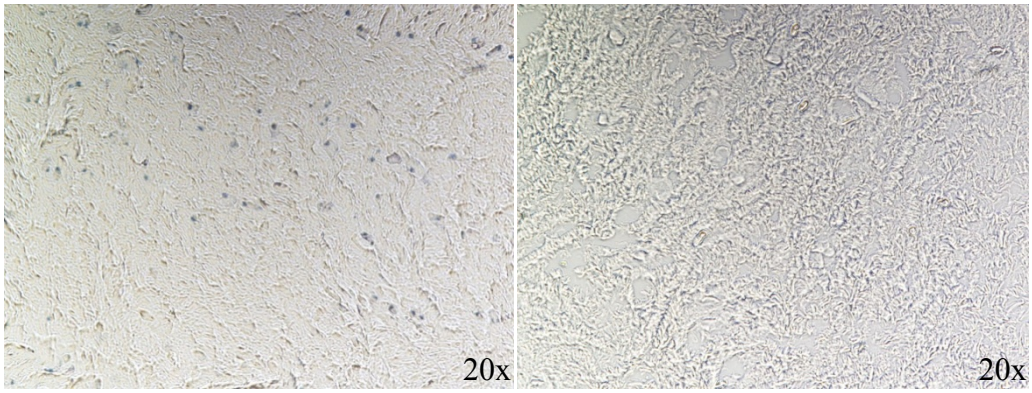

Figure 11. MTT staining of fresh (left) and desiccated (right) rabbit AF

Based on traditional tetrazolium salt reduction methodologies [112, 139], MTT staining is quantified using spectrophotometry. Basically, whole rabbit discs or wedges of human disc tissue are removed from an opened joint and placed in a 24-well plate. A volume of 1 ml of MTT (1 mg/ml) is added, and tissue incubates for two hours at standard laboratory conditions (37 °C, 5% CO_2). After incubation, tissue is rinsed in phosphate buffered saline (PBS), separated into AF and NP (if lapine), and cultured in 0.75 ml of 2-Methoxyethanol (CHROMASOLV® for HPLC, Sigma-Aldrich, Inc., St. Louis, MO) for 24 hours. Following organic extraction in the last step, 200 μl of extract from each sample is added to a 96-well plate. Samples are then placed in a spectrophotometer where absorbance is read at λ=570 nm for 1

second per well. Absorbance readings are normalized by tissue weight, which was determined per tissue region at the experimental end point. Positive controls are discs harvested at time, t=0; negative controls are desiccated for 48 hours at room temperature. Controls set the thresholds for viability for each test; typically, t=0 controls are set to one and all time points are normalized by the t=0 average weight-normalized value.

The validity of the absorbance-based method was demonstrated by comparing histological sections to absorbance readings of fresh, frozen, and desiccated FSUs. N=10 discs (L56, L34) were extracted from five rabbit lumbar spines. Four "fresh" discs were placed directly into MTT for two hours. Four discs were left to dehydrate for 48 hours before MTT incubation; they served as a negative control. Two discs were placed at -20 °C for 48 hours as for an additional negative control. Discs from each group were evenly divided for analysis: half to histology and half to colorimetric assay. While qualitative, the results of the two methods were compared for convergence to allow exclusive use of the colorimetric assay.

4.5 MODEL SELECTION

4.5.1 Rabbit Model

Use of New Zealand White (NZW) rabbits in IDD research is abundant in general and common in mechanobiological systems in each of the in-vitro, in-vivo, and ex-vivo niches. Researchers in the Department of Orthopaedic Surgery have advanced disc research using in-vivo studies of IDD, in-vitro 6 DOF mechanical testing (see Figure 12), and in vitro cell-level mechanobiology studies that employ rabbits. Additionally, NZW rabbit use is common at the University of

Pittsburgh, so frequent access to lumbar spines is available via tissue sharing. As a result, system design focused on the use of a rabbit FSU.

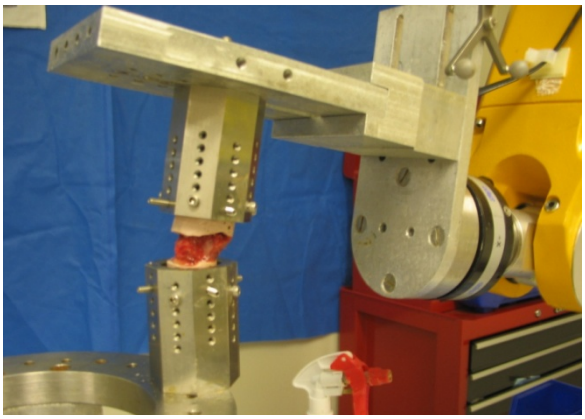

Figure 12. Biomechanical testing of rabbit FSU on robot-based spine testing system

Rabbit spines were obtained through several collaborations across the University of Pittsburgh. NZW rabbits aged 4-12 months old were included in this thesis project; the distribution of ages and grateful acknowledgement of support is listed in Appendix A1.

As a matter of process, thoracolumbar spines are aseptically removed from rabbits, placed in PBS, and transported back to the laboratory. Musculature surrounding the bones and neural tissue are removed, but ligamentous structures like facet capsules and interspinous ligaments are preserved to retain an intact FSU, which may then be used for mechanobiological testing (see Figure 13).

Figure 13. L2-L5 of rabbit lumbar spine (left) and single FSU (right)

Rabbit FSUs were tested for viability over experimental time frames up to 2 weeks. Initial experiments were performed in Dubelcco's Modified Eagle Medium (D-MEM) with 5-10% fetal bovine serum (FBS) and 1% penicillin/streptomycin (P/S) over a week at t=0, 1, 2, and 7 days. N=2 discs from separate rabbit lumbar FSUs were used for each time point. IVDs were not divided into regions; whole disc weight-normalized absorbance is reported at each time point. This experiment was repeated with N=2 discs divided into tissue region (AF vs. NP) at the similar time points: t=0, 1, 7 and 14 days. Based on these findings, a more detailed experiment was performed; viability was assessed from 0–30 hours at 0, 4, 8, 12, 22, and 30 hours. N=3 discs from separate rabbit lumbar FSUs were used at each time point. Weight-normalized absorbance readings at each time point are divided by t=0 values (set to 1).

4.5.2 Human Model

Initial intentions were to design a system for testing of bioactive human specimens. Collaboration with the Department of Pathology was established and a study investigating the viability of human lumbar motion segments was approved by the Committee for Oversight of

Research Involving the Dead (CORID)—CORID #221. Autopsy patients who (i) had consented to research, (ii) underwent a chest cavity examination, and (iii) had died in University of Pittsburgh Medical Center (UPMC) Presbyterian or UPMC Montefiore hospitals were included. Time after death was <12 hours if autopsies were performed on the day of death; if autopsies were performed the day after death, then bodies were stored overnight at ~4 ºC. Only patient age and sex were disclosed. Portions of the lumbar spine (typically T12-L3) were removed at the end of the autopsy. Specimens were placed in PBS with 2% penicillin/streptomycin (P/S) and 1% Fungizone™ (Amphotericin B, Sigma-Aldrich, St. Louis, MO) and transported immediately to the laboratory for dissection and viability analysis.

N=4 human lumbar spines were obtained between 11/08 and 08/09 for disc viability analysis (see Table 4). Using the MTT colorimetric viability assay developed for disc tissue, regional viability of human discs was measured over proposed testing time frames: 0, 4, 24, and 48 hours. One disc was used at each time point, so the number of extracted discs, which varied, determined the number of time points. Spines were divided into bone-disc-bone segments with muscle and adipose tissue removed at t=0. Segments were then cultured at 37 °C, 5% CO_2 in D-MEM with 5-10% FBS, 1% penicillin/streptomycin (P/S), and 1% Fungizone. At each time point, the joint was opened along the superior disc-endplate margin, and the disc was divided into wedges of the anterior OAF, lateral AF, posterior AF, and NP, which were sectioned into vertical thirds: low, middle, high. Viability analysis combined portions into two groups: AF and NP. Disc level was randomly assigned to each time point.

Table 4. Summary of human donor information

Age (yr)	Sex (M/F)
53	F
78	M
59	F
69	M

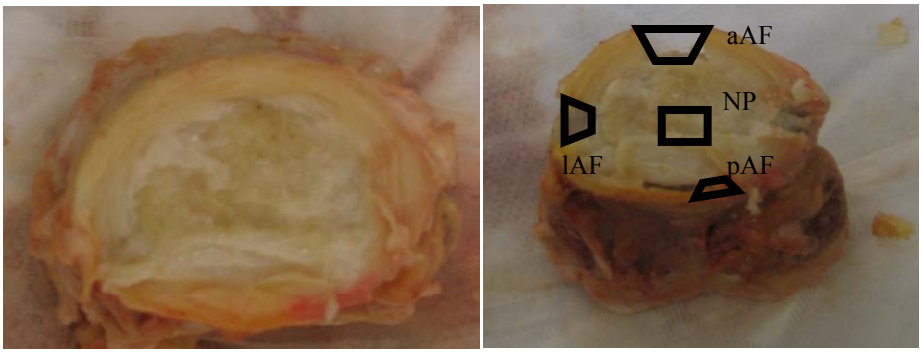

Figure 14. Human lumbar disc opened and intact (left) and removed wedges (right)

Results from human disc viability analysis are displayed in Figures 25 and 26 in Section 5.4.2; poor viability relative to desiccated controls is apparent. Changes in weight-normalized absorbance readings between t=0 and t=24 specimens and t=0 and desiccated negative controls were calculated for human and rabbit discs (Figure 27). No difference between fresh and desiccated controls for human specimens is evident, indicating unsuitability of the human model. Significant challenges exist in regards to the frequency of acceptable specimens; N=5 specimens met the inclusion criteria over a ten month window. Within the paradigm of 6 DOF motion, respectful removal of a lumbar spine from a human corpse involves cutting through the pedicles to avoid disfigurement, preventing retention of posterior structures. As a consequence, the human model was excluded from the project goals, which focused singularly on rabbit FSU model development.

4.6 INTRADISCAL PRESSURE

In addition to development of applied loading and assessment of fixture rigidity, measuring intradiscal pressure (IDP) during mechanical loading of rabbit FSUs is needed to validate the novel system. IDP validation is critical because it is clinically relevant and serves as primary means of relating mechanical inputs to biological changes. IDP was measured in discs subjected to a prescribed axial load using a commonly employed method in disc biomechanics (Johannessen, 2006; MacLean, 2007; Beckstein, 2008) to determine its suitability in rabbit FSU compression.

The goal of experimentation was to relate applied force to resultant IDP in the context of a rabbit FSU using the novel system. Disc researchers typically utilize the simple definition of pressure (force divided by area) to tailor applied loads to each disc. Using Vernier calipers, disc cross-sectional area is estimated using the following formula:

$$A = \frac{\pi}{4}(l_{AP})(l_{LAT})$$

where A is cross-sectional area, l_{AP} is the anterior-posterior measurement, and l_{LAT} is the lateral measurement. An applied compressive force in the ATM is calculated by multiplying the disc area by the target pressure. While moderate variability is expected based on inherent tissue variability between specimens and within experimental methods, it remains true that a sound mechanical system should elicit an IDP within ~20% of the target pressure based on an applied load.

N=5 L3-4 FSUs were dissected from 6-8 month-old, female NZW rabbits. FSUs were mounted in fixtures without a rubber membrane to allow for visual and tactile access to the disc. A 0.35mm fiber-optic pressure probe (Samba Preclin 360 MR, Samba Sensor, Goteborg,

Sweden) was inserted through a 20G needle antero-laterally into the putative NP center. NP center was estimated from l_{LAT} and l_{AP}. Figure 15 depicts the IDP testing configuration.

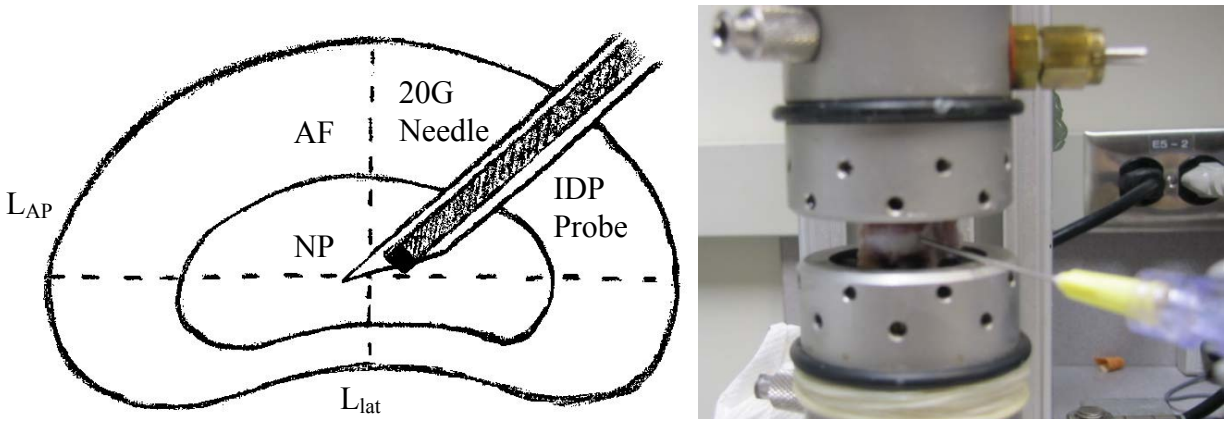

Figure 15. Intradiscal pressure probe inserted into the nucleus pulposus by antero-lateral approach

Each FSU was then subjected to ~10 cycles of preconditioning followed by 1100 seconds of constant axial compression while IDP and axial displacements were measured. Axial loads and displacements were collected in Matlab while IDP data were acquired simultaneously using Samba Sensor software (Samba Sensor 200, Samba Sensor, Goteborg, Sweden). After five minutes of recovery, the needle was withdrawn 2 mm in the needle track, and the loading paradigm was repeated.

Mean pressure was calculated over each peak, and an average of the mean peak pressures was calculated (see Appendix C.1 for Matlab code). It should be noted that in two of the trials, preconditioning did not reach 10 cycles. IDP during creep was measured continuously, but mean pressures were calculated over three windows of time: (1) early (0-1 min), (2) middle (8-10 min), and (3) late (16-18 min). Standard deviations were determined to quantify the variability across specimens at each time point. A Wilcoxon signed-rank test was performed to compare mean pressures between windows of time and between needle locations.

4.7 ENVIRONMENTAL CONDITIONS

Following fixture development and mechanical validation, attaining appropriate environmental conditions within the chamber is essential to fulfillment of design constraints. A HERACell CO_2/O_2 incubator (HERACell 150i, Thermo Scientific, Waltham, MA) maintains internal temperatures at 37 °C (+/- 0.5 °C), CO_2 air concentration at 5%, and internal O_2 air concentrations at targets within a range of 1-21% (+/- 0.5%) by displacing O_2 with N_2. Media housed in reservoirs within the incubator is circulated through PharMed tubing (I.D. 0.8 mm, W. T. 1.0 mm) (PharMed Tubing, Bio-Rad Laboratories, Inc., Hercules, CA) and the chamber using a peristaltic pump (Econo Pump, Bio-Rad Laboratories, Inc., Hercules, CA). Each component of the flow loop—media composition, heat source, tubing, connectors, etc.–was varied to achieve adequate viability, 37 °C (+/- 0.5 °C), and 5% O_2 (+/- 1%) within the chamber.

4.7.1 Culture conditions

Concentration of fetal bovine serum (FBS) varies across culture systems from 5-20% of media. In unloaded, standard incubator culture (37 °C, 21%/5% O_2/CO_2), the effect of %FBS on FSU disc viability was investigated. Rabbit lumbar FSUs were dissected and cleaned, placed in T-75 flasks, and immersed in D-MEM high glucose (4.5g/L D-glucose, 110 mg/L sodium pyruvate) (Gibco, Invitrogen Life Sciences, Carlsbad, CA) with 1% P/S. Three concentrations of FBS were compared: 5, 10, and 20%. N=3 FSUs were cultured at each concentration for 24 hours and viability was assessed using the MTT colorimetric assay. Based on the results of the first FBS concentration inquiry, the experiment was repeated for 10 and 20% FBS. Similarly,

N=3 FSUs were cultured in each condition for 24 hours and compared to fresh and desiccated controls.

Other culture conditions were explored in similar fashion. Removing adjacent endplates and boring 1/16" tunnels in the vertebral body was compared to retaining endplates after 24 hours. Hypoxic incubation (5% O_2) was compared to normoxic incubation at 24 hours; this experiment was performed twice. In each case, N=3 discs were regionally separated at each time point. Values at each time point were normalized to t=0 values.

4.7.2 Temperature

Because of the sensitivity of many proteins to elevated or depressed temperatures of even 1 °C, chamber temperature tolerances were set at +/- 0.5 °C. In order to control temperatures within the chamber to this accuracy, the bioactive system requires a highly accurate temperature probe. A 4-wire, platinum resistance temperature detector (RTD) probe (P-M-1/10-1/8-6-O-T-3, OMEGA Engineering, Inc., Stamford, CN), which correlates changes in metal resistance with temperature, was selected over a thermistor or thermocouple because of its touted stability (linearity), repeatability, and accuracy >0.08 °C. To preserve the accuracy of the probe, a pre-calibrated, data acquisition (DAQ) adjunct was acquired (PT-104, OMEGA Engineering, Inc., Stamford, CN). Temperature values were collected using OMEGA logging software (but can also be accomplished in Matlab).

Media temperature is controlled by the incubator, but heat is lost as media flows out of the incubator, through the pump, and across the chamber. Conceptual location of probes in the closed flow loop has varied through development. However, because conditions within the chamber are critical and creating chamber access ports was simpler than fabricating effective in-

flow probe adapters, customized brass ports were made for the RTD by the Department of Cell and Physiology/Pharmocology Machine Shop. Temperatures were recorded with the RTD inserted in a port in the upper fixture of the chamber with the tip of the RTD at the chamber center. The RTD is 2.5" long, with the first 5/8" containing the temperature sensing element—a wire wrapped ceramic core. Greater than 3/4" was within the chamber at all times, and the remaining length was contained within the brass port. The brass port contains two O-rings that seal the chamber from fluid leakage and temperature loss (see Figure 16). The chamber is readily invertible, which allowed temperature monitoring during development in the upper or lower fixture depending on configuration.

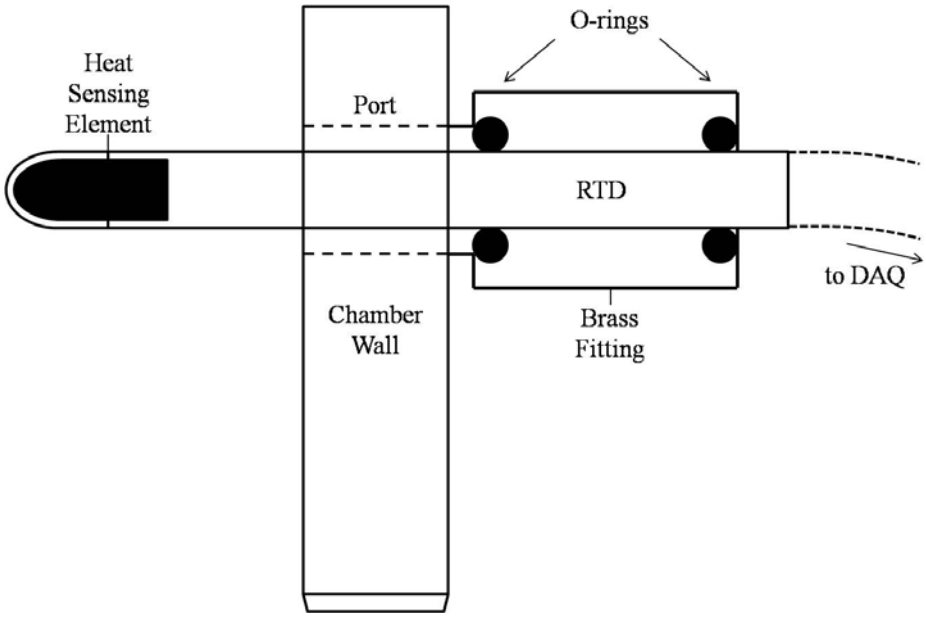

Figure 16. Schematic of RTD inserted through port in chamber wall

Design parameters were investigated using a simple model of fluid flow through rubber tubing that was constructed in Matlab (see Appendix D). It assumed steady-state, well-mixed water as the media and rubber walls for the tubing and chamber. Fluid temperatures started at 37

°C, and external temperatures were ≤ 25 °C. Fluid flow was varied to see its estimated effect on steady-state tubing and chamber temperatures. Increasing flow rate raised steady-state temperatures. Thermal conductivity of the tubing and wall thickness were varied to simulate the effect of insulation. Assuming thermal conductivity of cottonwool in an added tubing outer radius of 5 mm, temperatures could be preserved closer to 37 °C relative to un-insulated rubber tubing. Tubing diameter was varied to select the tubing that minimized heat loss before reaching the chamber. Smaller tubing inner diameters lost heat less readily. The assumed rubber walls for the chamber were an artifact of the original ring-structure fixture design, and so the model did not account for stainless steel fixture walls. While the accuracy of the early model is limited by simplifying assumptions and the iterative, evolutionary design process (it bears little resemblance to the final design), it did provide trends in varying design parameters to inform design choices.

Stable, appropriate temperatures in the chamber were pursued through modulation of system parameters, including (i) the addition of insulation, (ii) flow rate optimization, and (iii) ambient heat control. Developmental temperature experiments were conducted in one of two environments: (1) on a metal platform with ambient temperatures ~25 °C (+/- 1°C) or (2) atop a heated, metal surface connected with ambient temperatures ~29.5 °C (+/- 0.5°C). Fluid temperatures were recorded for 4-24 hours to compare steady-state temperature values and monitor long-term changes.

The temperature drop across the chamber was examined first. This was simply achieved by measuring temperatures at steady-state with the chamber upright and inverted so that the probe was on the top and bottom, respectively. Because of the slow movement of interstitial

fluid around the discs, high flow rates are considered non-physiological. Fluid was pumped at low flow rates to simulate anticipated testing rates: 0.75 – 1.5 ml/min [109].

Insulation: Attempts to use insulation began with a fiberglass insulation tube with silicone coating (1/2" I.D.) that flexibly surrounded the PharMed® tubing. Similar fiberglass insulation enclosed the chamber (4" I.D.) though it was cut with holes and tabs to leave access for tubing and probes. Fluid was pumped through the insulated system at low flow rates (<1.75 ml/min).

Flow rate: The effect of flow rate on temperature was also explored. Intra-incubator organ culture systems have flow rates between 0.12 – 1.1 ml/min [109, 114]. Fluid flows ranging from 0.05 ml/min to 1.75 ml/min were attainable with PharMed 0.8 mm I.D./1.0 mm W.T. tubing. It was anticipated that this extra-incubator design would require higher flow rates, though estimated in-vivo flow rates restrain large increases in fluid flow to achieve desired chamber temperatures. Initial intentions were to keep flows below 2.0 ml/min; however, because of unresponsive temperatures at low flow rates, 3.2 mm I.D./ 1.0 mm W.T. tubing was attached so that flow rates up to 40 ml/min became feasible. Fluid temperatures were recorded for each flow rate until temperature increases stopped.

Direct Heat: In response to the insufficient effectiveness of insulation and flow rate modulation of temperature and the apparent dominating contribution of ambient temperatures, applied heating was pursued as a direct means of attaining desirable temperatures within the chamber. Flexible silicone 10W heaters (1"x2" patches, 24V @ 0.8A, Electro Flex Heat, Inc., Bloomfield, CT) adhered to each stainless steel fixture. The heaters—flexible, silicone resistors—were connected to a 32V/0-3A programmable DC power supply (1786B, B.K. Precision Corp., Yorba Linda, CA) that could be controlled manually or in Matlab. Adjusting

voltage and current in response to RTD temperature values allowed for direct control of chamber fluid temperatures. Heat from the resistors is applied to stainless steel walls with good thermal conductivity. Adopting direct heating to control chamber temperatures removed the need for high flow rates and insulation, allowing more physiologic flow rates and greater access to and observation of the system (c.f. obfuscating insulation). Several proof-of-concept trials were performed to determine how quickly the heaters could increase chamber fluid temperature, how levels of current affected fluid temperature, and if the heaters could stably maintain 37 °C. Afterwards, heaters were used in all bioactive trials to attain and maintain 37 °C (+/- 0.5 °C).

4.7.3 Dissolved Oxygen

Simulation of the hypoxic IVD environment motivates the capability of controlling oxygen concentrations in culture media. The incubator maintains internal oxygen air concentrations at targets within a range of 1-21% (+/- 0.5%) by displacing O_2 with N_2 in attached cylinders. A small-diameter (<1/8" D) dissolved oxygen probe (MIL-70, Microelectrodes, Inc., Bedford, NH) was used to measure fluid oxygen concentrations by transducing oxygen concentration to an outputted voltage. The voltage, which has a range of ~0.25V, was read into Matlab by the LabJack U6-Pro with 24-bit resolution.

The DOP is calibrated by placing the probe in solutions of known oxygen concentration at a known temperature. Generally, deionized water equilibrated to 21% O_2 at room temperature is one calibration point, and the other is provided by a 0% oxygen solution (Zero Oxygen Solution, Oakton Instruments, Inc., Vernon Hills, IL), a reagent that actively removes oxygen from the solution. A simple linear model ($y = mx + b_0$), commonly employed for this application, is used to relate voltage to $\%O_2$. Initial tests were performed in water at room

temperature. However, transitioning to 37 °C from 25 °C and to D-MEM from water altered the temperature and salinity and thus the voltage outputs for known oxygen concentrations. Additionally, recording in the chamber was problematic because small forces applied to and twists of the acrylic housing during probe insertion apparently altered the Teflon membrane tension. Because oxygen permeability varies with membrane tension, these mechanical changes altered voltage-$\%O_2$ relationships.

In practice, then, the DOP was calibrated for each culture experiment. A small volume (1.5 ml) of culture media was set aside and placed in a 2 ml tube in a normoxic incubator to serve as a 21% O_2 calibration point. Warmed zero oxygen solution acted as the 0% O_2 point. The probe was inserted through a sealing, brass port similar to the temperature probe; the configuration is depicted in Figure 17. Samples were given more than 12 hours to equilibrate with ambient oxygen levels. A linear, two-point calibration method was assumed based on manufacturer recommendations (Microelectrodes, Inc.). The calibration procedure, performed in Matlab and given in Appendix E, simply calculated the slope

$$m = \frac{\%O2_{high} - \%O2_{low}}{V_{high} - V_{low}} = \frac{21\% - 0\%}{\Delta V}$$

and then used the y-intercept formula to find b_o in $y = mx + b_0$. Thus, voltages recorded in system validation and utilization were converted into $\%O_2$ using test-specific calibration.

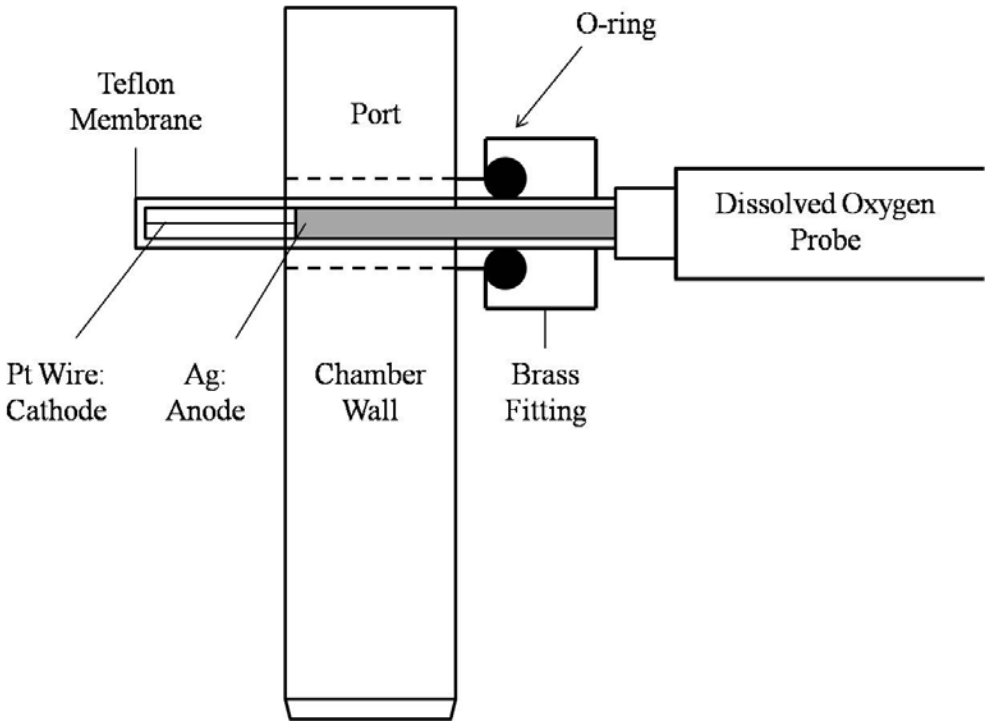

Figure 17. Schematic of DOP inserted through port in chamber wall

O_2 concentration estimations were used in development to iteratively test $\%O_2$ values and demonstrate the system's ability to maintain hypoxic conditions within the bioactive chamber. Developmental progressions were largely trial-and-error improvements in material selection; Table 5 summarizes the iterative development. PharMed® tubing was selected because of its low gas permeability (see Table 6), minimal leaching, and general biocompatibility. Initial testing demonstrated that O_2 levels were close to 21%, suggesting that one or more components in the flow loop were allowing oxygen exchange with surrounding air. Pump tubing was changed from silicone (Precut Silicone Tubing: 0.8 mm, Bio-Rad Laboratories, Inc., Hercules, CA), known to have high gas permeability, to Tygon (Tygon R-3603, Saint-Gobain Performance Plastics, Akron, OH), which has substantially lower permeability (see Table 6). Luer couplings were changed from nylon to polycarbonate for similar reduction of gas permeability (see Table

6). O_2 levels still failed to approach 5%, so the highly permeable component, the latex membrane, was doubled; one layer was placed under the O-ring and the other outside it. Then, a nitrile laboratory glove wrist (UltraSense Powder-Free Nitrile, MicroFlex Corporation, Reno, NV) was added as a third, outer layer. This configuration is illustrated in Figure 18. In experimentation, two layers of nitrile glove were attached for redundancy. In this configuration, depicted in Figure 19, O_2 levels in the chamber were maintained at 5 % O2.

Table 5. Summary of iterative trials of material selection changes for chamber hypoxia

Trial	External Tubing	Pump Tubing	Chamber	Connectors
1	PharMed®	Silicone	Latex-1	Nylon
2	PharMed®	Tygon	Latex-1	Polycarbonate
3	PharMed®	Tygon	Latex-2	Polycarbonate
4	PharMed®	Tygon	Latex-2 + Nitrile-1	Polycarbonate
5	PharMed®	Tygon	Latex-2 + Nitrile-2	Polycarbonate

Table 6. Gas permeability of tubing used in the flow loop

Gas	PharMed	Silicone	Viton ST	Polycarbonate	Permeability units
CO2	1200	25147	360	85	$\frac{\text{gas volume (cm}^3\text{) x wall thickness (mm)}}{\text{tubing ID (cm}^2\text{) x time (sec) x } \Delta\text{Pressure (cm Hg)}} \times 10^{-10}$
O2	200	4715	80	20	
N2	80	2284	40	3	

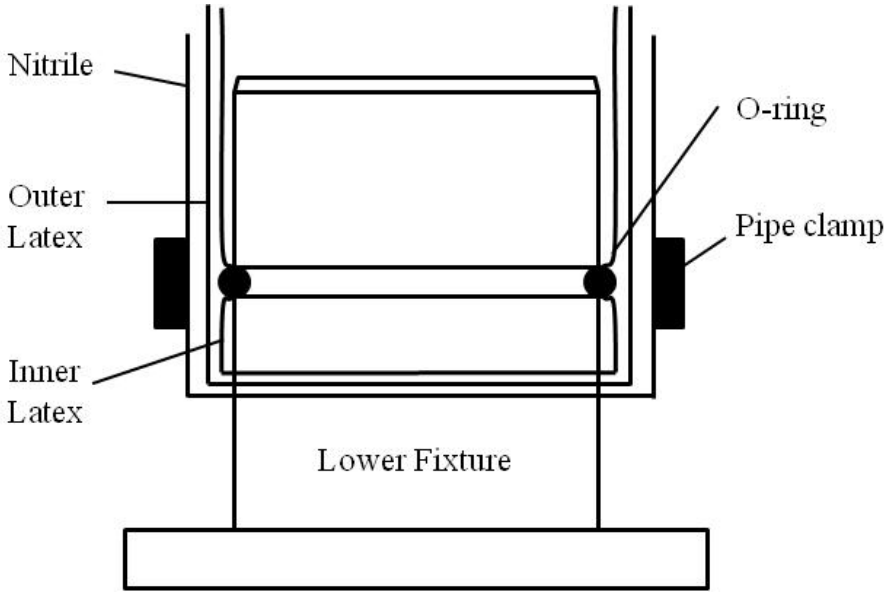

Figure 18. Lower fixture with rubber layers and clamps used to seal the chamber

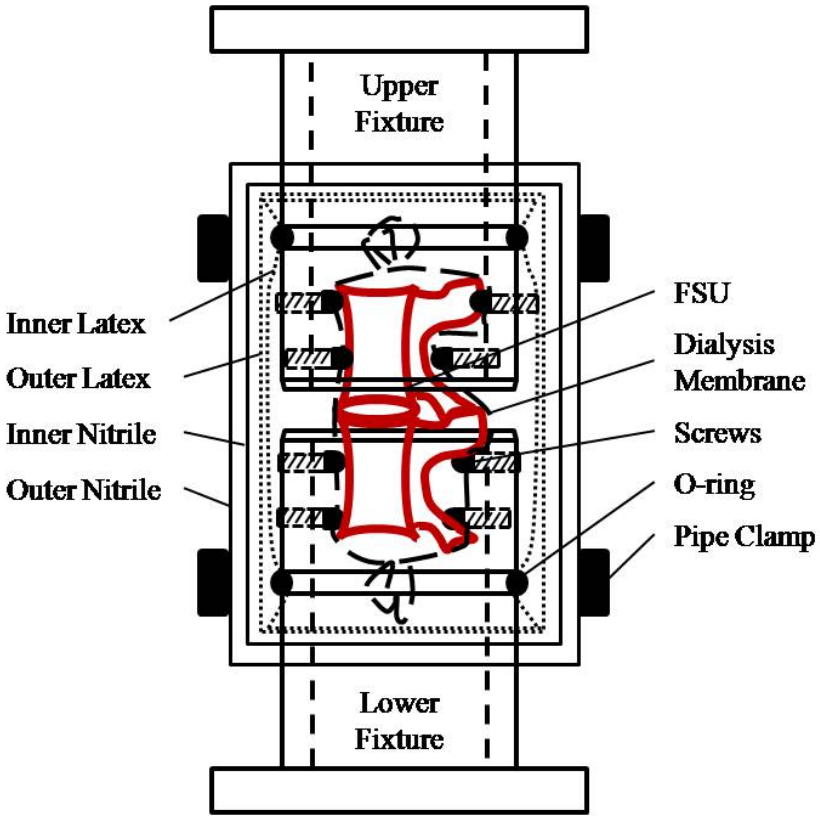

Figure 19. Bioactive chamber schematic

4.8 RNA ANALYSIS

4.8.1 RNA Extraction

Discs are separated into AF and NP, immediately flash-frozen in liquid nitrogen, and kept at -80 °C until RNA isolation. AF samples are stored in RNA Later solution (Bio-Rad) to improve yield; NP samples are not because of difficulties RNA Later storage cause in homogenization. Isolation begins with immersion of disc portions in Qiazol lysis reagent (Qiagen Inc., Valencia, CA) followed by mechanical homogenization of the NP with a micro-pestle and the AF with a rotator-stator homogenizer (TissueRuptor, Qiagen Inc., Valencia, CA). Chloroform is added to Qiazol to separate organic from aqueous cell and tissue components. Isopropanol is added to the resulting aqueous phase to precipitate nucleic acids, and the subsequent pellet is washed with 70% EtOH, dried, and suspended in nuclease-free water. DNA and GAGs are enzymatically cleaved with 0.39 Kunitz/ml DNAase I (Qiagen) and 1.25 Units/ml Chondroitinase ABC (Sigma-Aldrich). The addition of acidic phenol:chloroform (Ambion, Inc., Foster City, CA) traps DNA fragments in the acidic phenol allowing isolation of RNA. The sample is cleaned of residual contaminants with additional chloroform extractions. RNA is precipitated with 9.85 mg/ml, pH 5.2 sodium acetate (Sigma-Aldrich) in ethanol; pellets are washed and re-suspended in nuclease-free water. RNA from the sample is purified using RNAeasy Spin Minicolumns (Qiagen) and suspended in 42µl water. RNA yield is measured using 1.8µl of sample on a Nano Drop spectrophotometer (ND-1000, Nano Drop Technologies, Inc., Wilmington, DE) and stored at -80 ºC until gene expression analysis.

4.8.2 RT-PCR

Reverse transcription-polymerase chain reaction (RT-PCR) is used to analyze RNA. The ordering priority is catabolic (e.g. MMP-1, MMP-3), inflammatory (e.g. COX-2, iNOS), structural (e.g. aggrecan, collagen-II, collagen-I), and anti-catabolic genes (e. g. TIMP-1). Gene expression is quantified using previously validated primers [98, 140, 141] in rabbits and a Bio-Rad SYBR Green fluorescent reporter system (iQ5 Multi-color Real-time PCR Detection System, Bio-Rad). Primers are listed in Table 7. GAPDH acts as a housekeeping gene to normalize cycle threshold (C_t) values.

Table 7. Primer sequences used in RT-PCR

Gene	Sequence
GAPDH	Rev: 5'-GCTGAGATGATGACCCTTTTGG-3'
	For: 5'-GATGCTGGTGCCGAGTAC-3'
MMP-1	Rev: 5'-GCCTGTCACTCGCAAACC-3'
	For: 5'-GACCTACGCACCCACACAC-3'
MMP-3	Rev: 5'-CCAGTGGATAGGCTGAGCAAA-3'
	For: 5'-AGCCAATGGAAATGAAAACTCTTC-3'
COX-2	Rev: 5'-CAGGCACCAGACCAAACACTT-3'
	For: 5'-CACGCAGGTGGAGATGATCTAC-3'
Aggrecan	Rev: 5'-CGTAAAAGACCTCACCCTCCAT-3'
	For: 5'-GCTACGGAGACAAGGATGAGTTC-3'

The $2^{-\Delta\Delta Ct}$ method was used to evaluate changes in gene expression [142]. Transcript levels are compared first to GAPDH transcript levels, and then these normalized values are compared to appropriate controls: t=0 and unloaded disc samples. This method assumes similar amplification efficiencies between the housekeeping gene and the gene of interest, which was confirmed during validation. Explicitly, the amount of target gene is give by:

$$2^{-\Delta\Delta Ct}$$

where $\Delta\Delta C_t = \Delta C_{t,\ sample} - \Delta C_{t,\ control}$. $\Delta C_{t,\ sample} = C_{t,sample\ geneA} - C_{t,\ sample\ GAPDH}$ is the difference between the experimental sample's C_t for geneA and that sample's GAPDH C_t, and $\Delta C_{t,\ control} = C_{t,control\ geneA} - C_{t,\ control\ GAPDH}$ is the difference between a control (reference) sample's C_t for the same gene and the control sample's GAPDH C_t. Relative gene expression is presented as a fold change in gene expression due to loading relative to t=0 and unloaded control levels.

Initial experiments utilized 30 ng of RNA per well. However, because of challenges with stable GAPDH levels, 30-45 ng of RNA were used. Constant RNA amounts were used within samples for valid comparisons. T-score intervals are defined by

$$t_{value} = mean \pm (standard\ error * t_{crit})$$

where t_{crit} is the critical t_{value} derived from the t-distribution. A two-sided, 95% confidence interval was chosen; degrees of freedom depended on the number of tissue samples (n-1). They were used to determine if relative changes in gene expression were significant. If confidence intervals did not span a relative gene expression value of 1 (i.e. no change), then significance could be concluded. If intervals between samples did not overlap, then differences between conditions were considered to be significant.

4.9 CONDITIONED MEDIA ANALYSES

Conditioned media is collected and frozen after each experiment. Media from the dialysis membrane (2kDa MWCO) that surrounds the specimen is poured into a 15 ml tube. Final fluid volumes in the membrane are typically 1-2 ml.

Matrix Fragments: Analyses of conditioned media include ELISAs of CS-846 (CS-846 ELISA Kit, IBEX Pharmaceuticals Inc., Montreal, Canada) and CTX-II (Serum Pre-clinical CartiLaps® ELISA Kit, Immunodiagnostic Systems Inc., Fountain Hills, AZ). CS-846 samples were loaded undiluted at 50 µl/well; CTX-II samples were undiluted and loaded at 25 µl/well. ELISAs were performed according to instructions in the kits.

PGE2: PGE2 concentrations in conditioned media were quantified using a competitive enzyme immunoassay (Parameter^{TM}: PGE2 Assay, R & D Systems, Inc., Minneapolis, MN). Samples were loaded undiluted at 150 µl/well. The assay was performed according to kit instructions.

Zymography: Zymography utilized gelatin (10%) and casein (12%) gels (Ready Gel® Precast Gels, Bio-Rad). MMP-1 activity is expected on gelatin, and MMP-3 activity is anticipated on casein. Media samples were diluted 1/10 volume, and 20 µl were loaded in each lane. A power supply (Power Pac Basic, Bio-Rad) applied 100 V/40 mA across the gel for ~100 min. Gels were subsequently placed in a buffer (Zymogram Renaturation Buffer, Bio-Rad) for 30 min for protein renaturation and then agitated overnight at 37 ºC in a development buffer (Zymogram Development Buffer, Bio-Rad) that facilitates MMP cleavage of the substrate. On the following day, gels were stained with 0.5% Coomassie Blue in 40% methanol/10% acetic acid and destained with 40% methanol/10% acetic acid until clear bands indicating digested substrate became visually evident. Gels were immersed in distilled water until imaging using a

Versa Doc Imaging System (4000 MP, Bio-Rad). Resultant images were qualitatively assessed for differences.

Fluorogenic Substrate Assay: To improve sensitivity and specificity of MMP activity detection, a fluorogenic substrate assay was used. Simply, a protein sequence specific to MMP binding is bookended with a fluorophore and quencher. When active MMPs bind to the protein sequence, they cleave the substrate, separate the quencher from the fluorophore and allow uninhibited fluorescence. A spectrophotometer quantifies fluorescence over time using relative fluorescence units (RFUs). Because fluorescence is proportional to cleaved substrate, this method provides a basis for describing enzyme kinetics.

In practice, sample media is diluted in MMP activity buffer (200 mM NaCl, 50mM Tris-HCl (pH=7.5), 5 mM $CaCl_2$, 20 μM $ZnSO_4$, and 0.05% Brij 35) at desired ratios. In preliminary testing, dilutions of sample media to 1/10 for MMP-1 activity and 1/40 for MMP-3 were necessary to obtain linear fluorescence vs. time curves. Non-linearities indicate that the substrate (or non-enzyme reactant) is limiting the reaction. After dilution, 50 μl of sample are added to individual wells on an opaque, black 96-well plate. Fluorogenic substrate specific to MMP-1 (S1) (MMP-1 Substrate III Fluorogenic, EMD Biosciences, Inc., San Diego, CA) and specific to MMP-3 (S3) (MMP-3 Substrate II Fluorogenic, EMD Biosciences) are added to appropriate wells. A subset of wells is reserved as "non-substrate" controls to remove non-specific fluorescence inherent in the sample. Blank media also serves as a control; it receives S1, S3, and no substrate. RFUs are recorded for 1 second per well every 10 minutes over a 3 hour period.

Samples from experimentation were run in duplicate or triplicate. Average values were calculated at each time point for each set. Non-substrate specific fluorescence was subtracted at each time point using wells that contained sample but no substrate. The slope both before and

after correction were calculated as (i) average slope across the 3 hour period and (ii) maximum slope over every 40 min period (5 time points) during the 3 hour period. Identical samples were run in multiple trials; slopes for each sample were averaged across trials. N=5 loaded sample slopes were compared to N=3 average unloaded (chamber) sample slopes. Slopes describe relative enzyme activity. The negative control was blank culture media, and the positive control utilized purified MMP-3 (Sigma-Aldrich).

4.10 EXPERIMENTATION

After system validation studies were completed (Specific Aim 1), experimentation was performed to assess whether the system could detect biologically meaningful data (Specific Aim 2). Generous collaboration from University of Pittsburgh researchers provided rabbit spines to demonstrate system efficacy (Appendix A.1). The experimental process is presented in Figure 19. Spines are placed in PBS following extraction and returned immediately to the lab in a closed cooler. In a sterile tissue culture hood, spines are cleaned of musculature and segmented into L4-5 and L2-3 FSUs. First, the intervening L3-4 disc is set aside for a t=0 control for MTT viability analysis or RNA expression. The L4-5 disc is then measured with Vernier calipers and the FSU is allocated for loading in the chamber. L2-3 is placed in a 50 ml beaker of 5 % O2 media in the incubator to serve as an unloaded, time-matched control. In viability analysis, the L5-6 disc is removed and allowed to desiccate for 48 hours to serve as a negative control.

The L4-5 FSU is placed in a 38 mm diameter dialysis membrane (2 kDa MWCO) with a knotted inferior end and attached to the lower fixture. Screw tightening is progressive and careful ensuring axial alignment of the FSU. A volume of 2-3 ml of media is added to the

dialysis membrane to bathe the FSU; media is added so that it exceeds the height of the disc. The dialysis membrane is tied off on the superior end with room for fluid displacement when the upper fixture screws are tightened. The upper fixture is then similarly attached to the spine. The latex and nitrile layers, attached on the lower fixture, are pulled up the cylindrical chamber and attached with pipe clamps at the upper O-ring. The inner latex layer is placed under the O-ring; the outer latex layer is stretched over the O-rings. The unloaded control and loaded chamber are carried quickly to the incubator and ATM, respectively. A T-75 flask holding ~200 ml hypoxic culture media serves as the media reservoir. The unloaded control FSU floats in ~40 ml hypoxic culture media in a 50 ml beaker. Media is hypoxic through equilibration over 12 hours at 5% O_2 prior to experimentation.

The chamber is fastened to the ATM with two screws in each fixture, and tubing is connected at the incubator rear, the pump, and the chamber inlet/outlet. Pumping of media begins immediately at 1.4 ml/min; filling takes ~30 min. Meanwhile, DOP and temperature probes are inserted and data recording begins. Silicone heaters are attached to each fixture and the VDC is set to 20V/0.7A to ramp to 37 ºC and set to 0.43 (+/- 0.01) A to maintain 37 ºC. When DOP values drop sharply, fluid has reached the levels of the probes. With a full chamber of circulating fluid, fluid flow is set to 1.25 ml/min and 15 cycles of preconditioning commence at a target force to achieve initial 1.0 MPa IDP determined from measured disc area based on IDP testing methods described in section 3.6. Following preconditioning, the FSU is loaded for four hours of constant compression (i.e. creep). Force magnitudes from the load cell and displacement from the microcontroller are recorded along with chamber oxygen concentrations and temperatures from probes throughout mechanical testing.

Following mechanical testing, the specimen is unloaded and prepared for biological testing. The efflux tubing is disconnected at the rear of the incubator and media flow is reversed and set to 1.4 ml/min to drain the chamber. Temperature is maintained throughout chamber drainage. When flow from the chamber ceases, probes and heaters are removed, the chamber is disconnected from the ATM and returned to the tissue culture hood along with the unloaded control beaker from the incubator. In the sterile hood, the nitrile and latex membranes are removed, and fixtures are disconnected from the specimen. The upper knot of the dialysis membrane is undone, and a 1 ml pipette draws media within the membrane and discharges it in a 15 ml tube. The specimen is removed, the lower knot is undone, and the tubing is wrung out to maximize yield from the dialysis membrane. Conditioned media is prepared for analysis according to Section 4.9. The discs from the loaded and unloaded FSUs are extracted and allocated to either viability analysis or RNA isolation. In viability analysis, discs are placed immediately in MTT and methods described in Section 4.4 are followed. RNA isolation adheres to protocols described in Section 4.8. This method is pictorially summarized in Figure 20.

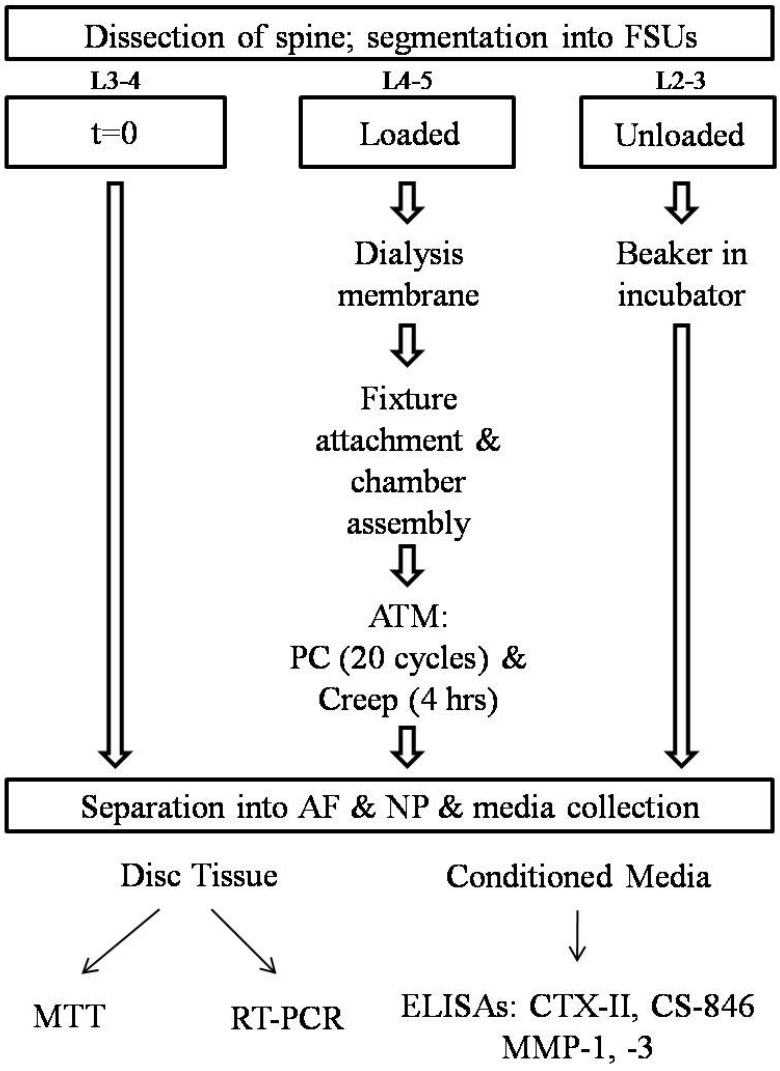

Figure 20. Flow chart of experimental process

5.0 RESULTS

5.1 APPLIED LOADING

Linear variable displacement transducer (LVDT) recordings validated the accuracy of axial testing machine (ATM) head motion for prescribed 2 mm displacements. Ten 2 mm displacements are illustrated in Figure 21. The mean displacement recorded by the LVDT was 1.971 (±0.0383) mm. This provides confidence that the recorded displacements, which were all <2mm, to be within <0.07mm.

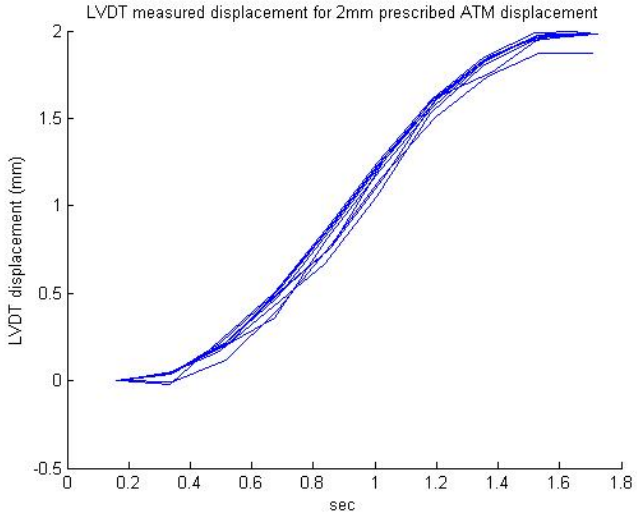

Figure 21. Validation of axial testing machine accuracy with LVDT

5.2 FIXTURE RIGIDITY

Screw Motion: Fixture rigidity in simulated testing protocols was assessed using two methods. Both methods relied on measurements before and after preconditioning (cyclic) and creep (constant load). Method (a) measured displacements of screw positions in the fixture frame aligned to the global coordinate system (GCS); Table 8 shows mean displacements with standard error. This analysis is a more conservative assessment of rigidity; it does not include rotational information. Repeatability bounds are between 0.08 and 0.16 mm. Mean axial displacements of FSUs in cyclic and constant load testing were 1.02 and 0.92 mm, respectively, so repeatability error was an order of magnitude smaller than relevant joint translations and similar to the accuracy of the digitizer. Cyclic preconditioning causes interface motion apparently larger than the repeatability measurement; it is larger in the x- (anterior-posterior) and z-direction (superior-inferior) of the upper fixture and largest in the x-direction in the lower fixture. Creep displacements are comparable to or less than repeatability measurements except for x-direction displacement in the lower fixture. Importantly, z-direction displacements in both fixtures tend to be similar to repeatability displacements, indicating little laxity in the axial direction.

Table 8. Displacements between initial and final positions of vertebral screws measured in the LCS and aligned with the GCS

Fixture	DOF	Repeatability	Preconditioning	Creep
UF-SV	x	0.08 (.02)	0.13 (.02)	0.07 (.03)
	y	0.13 (.06)	0.09 (.04)	0.06 (.04)
	z	0.09 (.04)	0.17 (.04)	0.05 (.02)
LF-IV	x	0.11 (.03)	0.25 (.07)	0.41 (.31)
	y	0.13 (.04)	0.11 (.05)	0.17 (.09)
	z	0.14 (.03)	0.16 (.10)	0.10 (.03)

Method (b) examines 6 DOF movement between the superior vertebral body and the upper fixture assessed in the upper fixture coordinate system (UFCS). It assumes a sequence of rotations between the specimen and fixture coordinate systems. Results listed in Table 9 show similar displacements (dx, dy, dz) to repeatability measurements; preconditioning and creep exceed repeatability displacements by 0.07 and 0.05 mm in the x-direction and 0.04 and 0.02 in the z-direction, respectively. These differences are small in the context created by ~1 mm joint displacements. Rotations about the x- and y-axis (rx, ry) appear larger in experimental simulation than repeatability rotations (up to 3x larger), but they are still relatively small (≤ 1.2 deg).

Table 9. Rotations and displacements between initial and final positions of superior vertebra relative to upper fixture

DOF	Repeatability	Preconditioning	Creep
rx °	0.33 (.13)	0.46 (.15)	0.56 (.17)
ry °	0.36 (.19)	0.30 (.12)	1.16 (.38)
rz °	1.14 (.40)	0.67 (.22)	0.93 (.28)
dx -mm	0.12 (.03)	0.19 (.05)	0.17 (.06)
dy -mm	0.14 (.04)	0.11 (.03)	0.10 (.05)
dz -mm	0.15 (.07)	0.19 (.06)	0.17 (.05)

The effect of frequency and displacement were also examined on N=1 rabbit FSUs. Results are included in Appendix B.1. Briefly, increasing frequencies from 0.4 to 0.63 Hz did not increase displacements or rotations, which were of similar magnitude to those listed in Table 9. Increasing displacement from 0 to 2 mm did increase rotations, but it did not influence displacements.

Stiffness: Stiffness of the fixture-vertebra interface is compared to stiffness of the joint in cyclic preconditioning and creep in Table 10. A joint-to-fixture stiffness ratio of 0.10, representing an order of magnitude difference, is desired; actual ratios approach this target.

Table 10. Axial stiffness of specimen joint and specimen-upper fixture interface

	Axial Stiffness (N/mm)		
Motion	**Fixture-Vertebra**	**FSU Stiffness**	**Ratio**
Cyclic	917.2 (606.9)	113.9 (38.3)	0.12
Creep	877.4 (171.4)	82.7 (0.97)	0.09

Thus, based on small screw position movement in the z-direction and fixture stiffness that approached the theoretical target, fixtures were found to be adequate for compression testing.

5.3 VIABILITY ASSAY DEVELOPMENT

The histological MTT method is compared to absorbance readings from the colorimetric method of fresh, frozen, and desiccated FSUs in Figure 22. Absorbance readings reflect the number of viable cells in representative histological sections, so higher absorbance denotes higher viability. Fresh histology samples manifest many positive cells; frozen sections showed few positive cells in lacunae, and desiccated showed disorganization of the matrix and no traces of viable cells with loss of most lacunae.

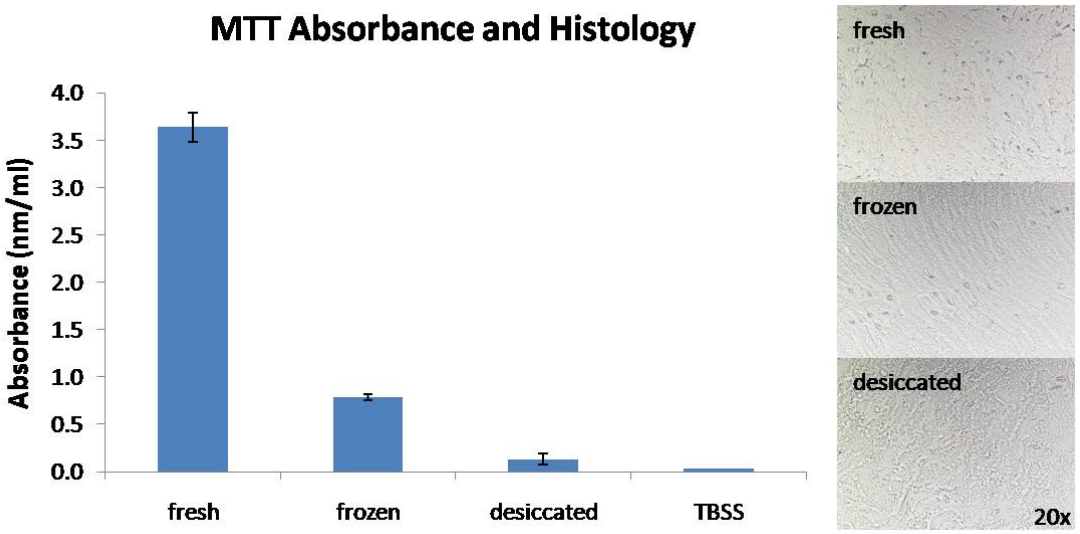

Figure 22. MTT absorbance values compared to histology

5.4 MODEL SELECTION

5.4.1 Rabbit Model

The first examination of rabbit FSU disc viability occurred at t=0, 1, 2, and 7 days; whole disc time-normalized viability is illustrated in Figure 23. A large drop in viability is observed at 24 hours (to 53.0%), and decreases continue, albeit much less steeply, across the week.

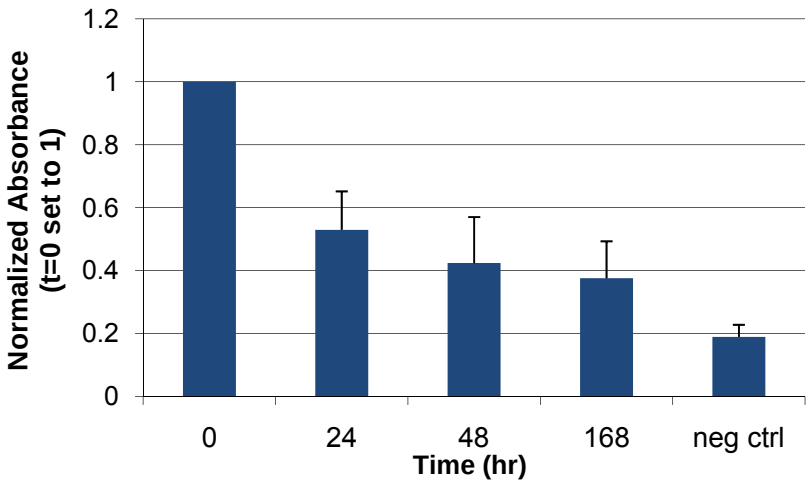

Figure 23. Whole disc viability over one week

The experiment was repeated over a longer time frame (t=0, 1, 7 and 14 days) assayed viability in the AF and NP separately (see Figure 24). AF viability generally remains high (>80%) but NP viability is near negative control values at each non-zero time point.

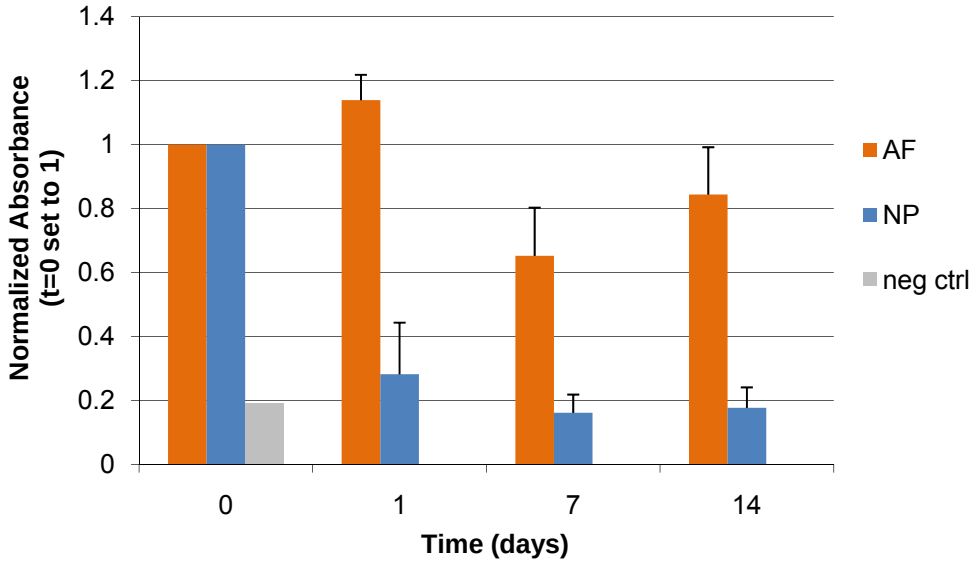

Figure 24. AF and NP viability over two weeks

The zoomed-in timescale of viability (0–30 hours), examining viability changes over the projected testing window, is given in Figure 25. Viability for both tissue regions tends to remain high through 12 hours, with only moderate decreases at 22 and 30 hours. Percent viability in the AF and NP at 30 hours is 67% and 70%, respectively, close to the imposed constraints of Specific Aim 1.

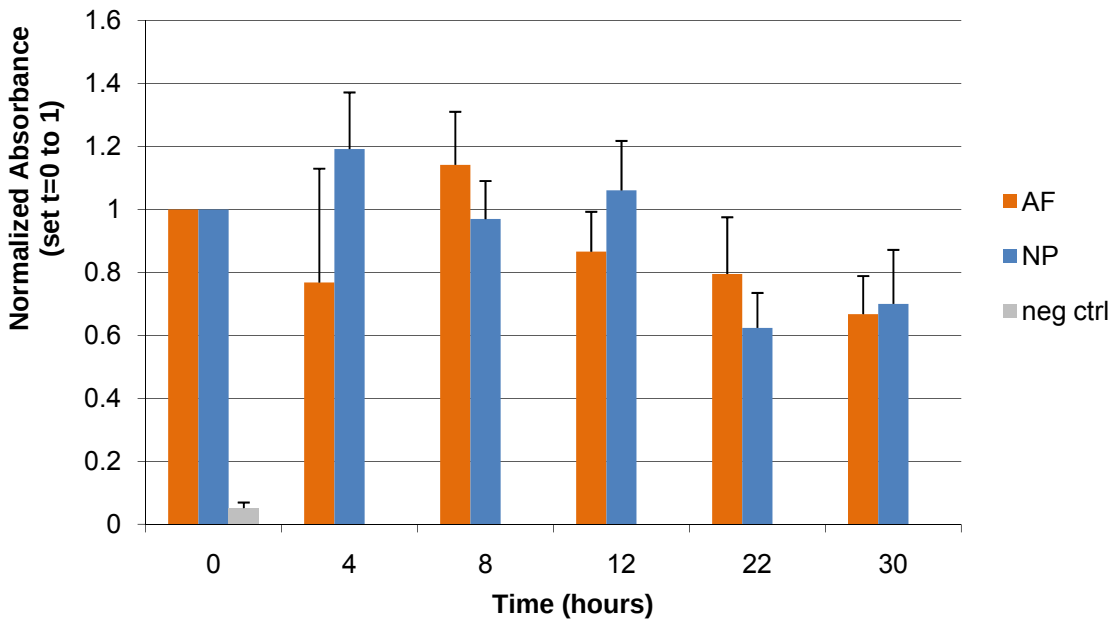

Figure 25. AF and NP viability over 30 hours

These results define a fairly stable 24 hour window for experimentation. Clearly, at early time points (<12 hours), discs in FSUs remain very viable, and a 4 hour mechanical intervention mirroring in-vitro cellular studies would occur well within that stable window.

5.4.2 Human Model

Human thoracolumbar disc portions were assessed for cell viability to determine the feasibility of using human motion segments for organ culture. Tissue-weight normalized absorbances (with t=0 values set to 1), are given for each cultured human specimen in Figures 26 and 27. Variability in temporal viability is high between the four samples. Most importantly, in each case, the negative control is near to or greater than the fresh (t=0) sample's normalized absorbance values. This clearly demonstrates the current deficiencies in human organ culture.

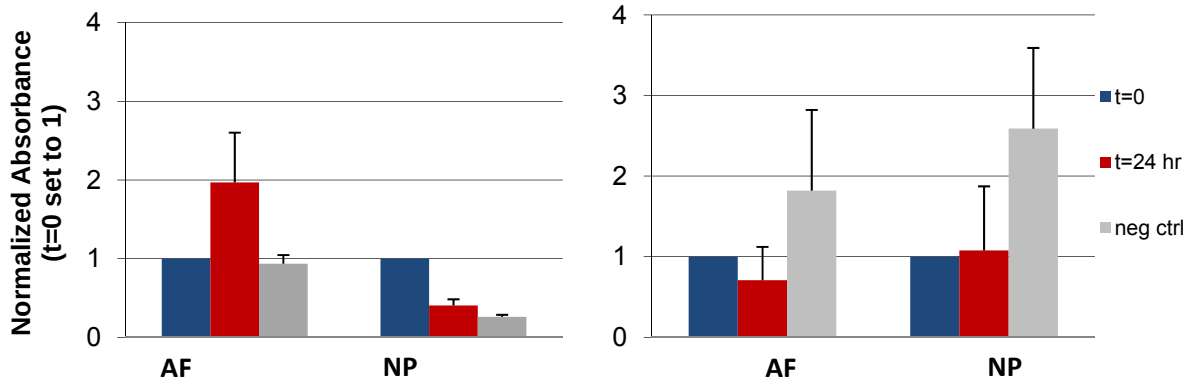

Figure 26. Cell viability in human disc culture of 59 y. o. female (left) and 78 y. o. male (right)

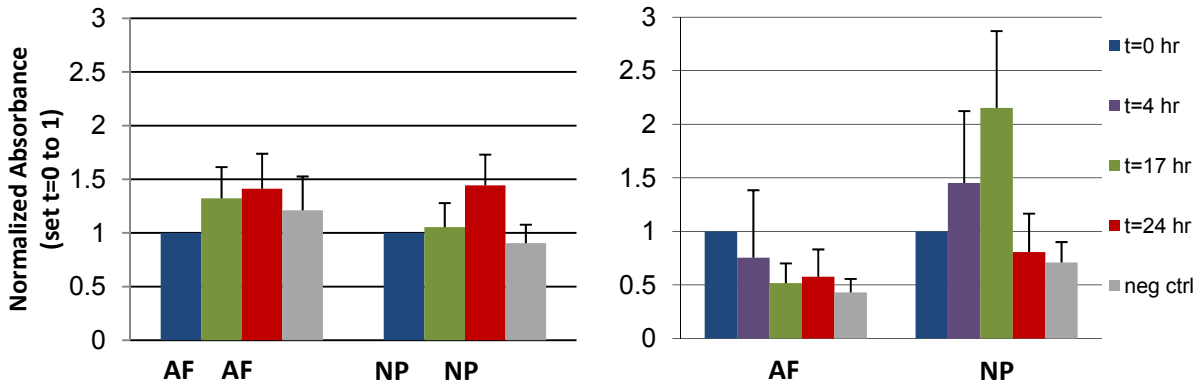

Figure 27. Cell viability in human disc culture of 69 y. o. male (left) and unknown female (right)

The differences between rabbit and human fresh discs and t=24 hour and desiccated discs are compared directly in Figure 28. Error bars represent standard deviations. Rabbit discs at t=24 hours show consistent ~30% decrease in viability. A consistent, large decrease (63% and 89% in AF and NP) in viability in desiccated controls demonstrates an effective assay; interventions' effects may be observed. In contrast, absorbance differences between conditions are small and highly variable in human culture. In particular, increases in desiccated controls relative to fresh discs preclude present use of the human model.

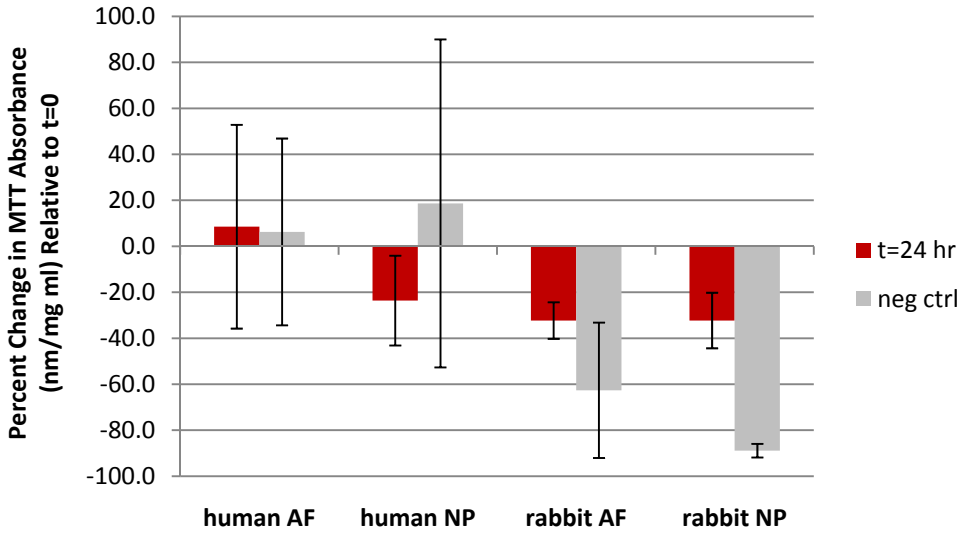

Figure 28. Human and rabbit viability of 24 hr & negative control relative to t=0

5.5 INTRADISCAL PRESSURE

Intradiscal pressure (IDP) was collected during cyclic and constant load-based compression with the probe at two different positions. A representative plot of cyclic preconditioning and creep testing forces (N) and IDP (MPa) with the IDP probe in the putative

NP center is provided in Figure 29. Forces and IDPs for the same specimen after a 5 minute recovery and needle repositioning (2 mm withdrawn) is illustrated in Figure 30. The target force, based on cross-sectional area of 57.1 mm^2 was 57 N. Left y-scales range from 0-100 N, and right y-scales range from 0-1.5 MPa. In this example, IDPs exceed the 1.0 MPa target. Pressure fluctuations match those of applied forces closely.

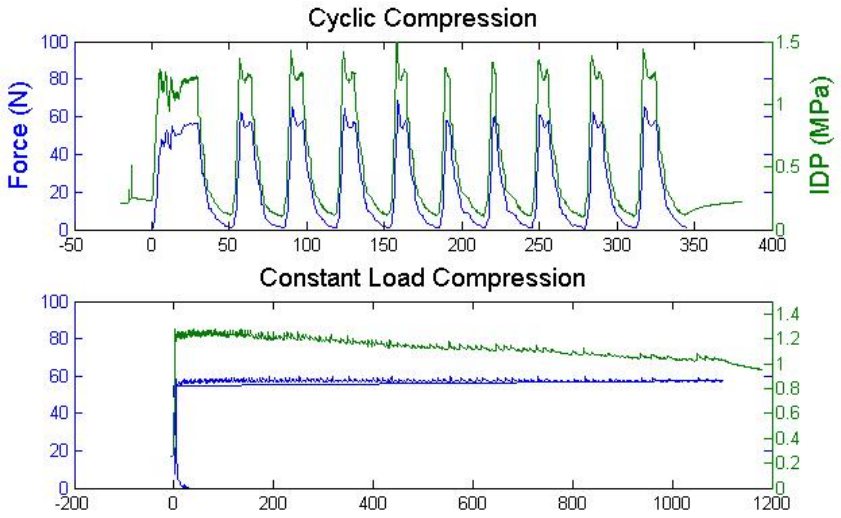

Figure 29. Force and IDP with probe at NP center for 10 cycles of preconditioning and constant compression

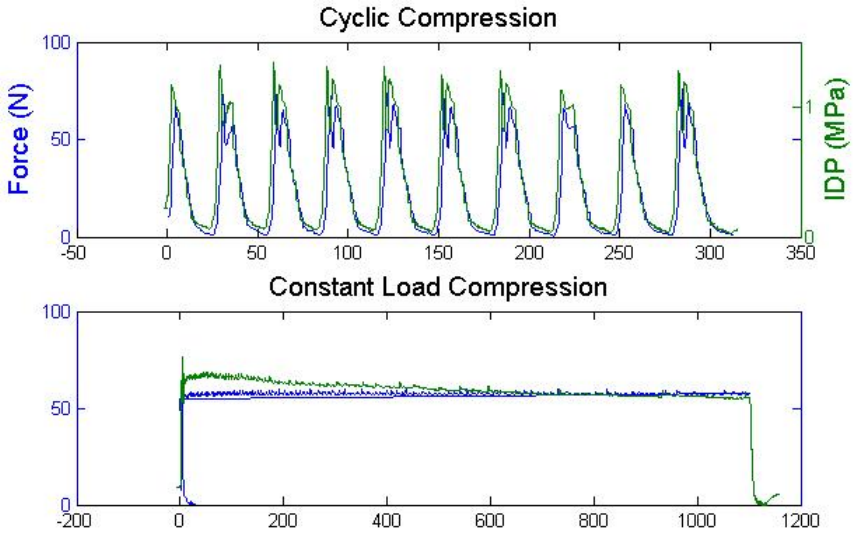

Figure 30. Force and IDP with probe at NP edge for 10 cycles of preconditioning and constant compression

Mean pressures for the two needle positions (NP center and lateral edge) over preconditioning peaks and during three phases of creep are illustrated in Figure 31. Differences between pressures read the NP center and edge were not significant, though a trend of initial, central pressures exceeding later, lateral pressures is evident. Center preconditioning pressures were 0.36 MPa greater than lateral position pressures, and differences during creep phases were 0.26, 0.14, and 0.09 MPa.

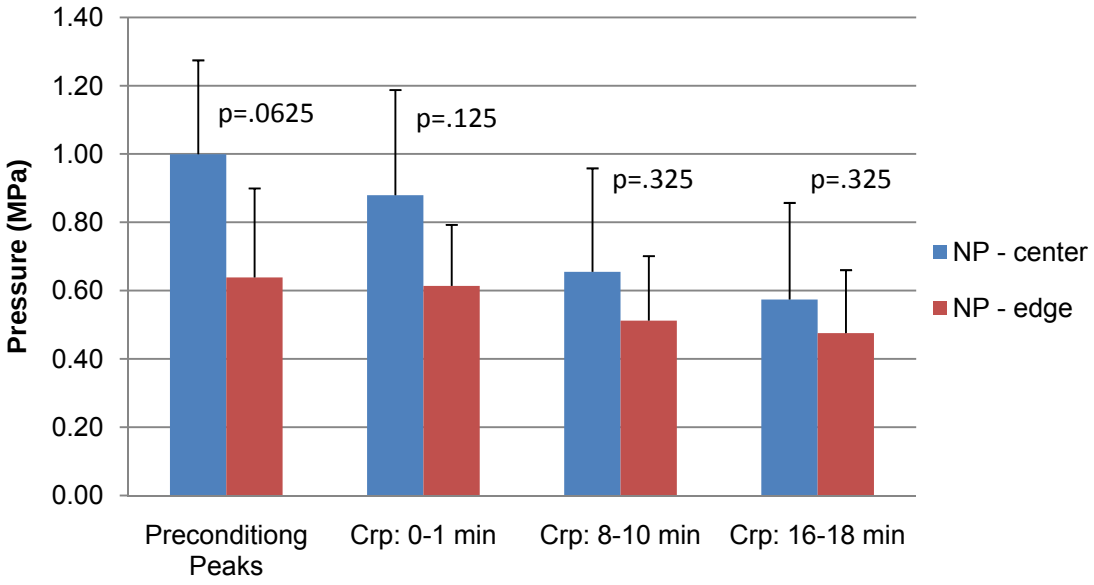

Figure 31. Mean pressures during preconditioning and three phases of creep at two IDP probe locations

A time-dependent trend of decreasing pressure is evident in IDP recordings during constant compression. Recorded pressures get progressively less than the target pressure (1.0 MPa) as the time of constant loading increases. Pressures at the NP center drop across creep phases: 0.96, 0.72, and 0.64 MPa; differences were not significant. Variability of pressure

recordings at the center of disc are quantified using the standard deviation of each phase: (i) Preconditiong—0.223 MPa, (ii) 0-1 min.—0.266 MPa, (iii) 8-10 min.—0.281 MPa, and (iv) 16-18 min.—0.268 MPa.

5.6 ENVIRONMENTAL CONDITIONS

5.6.1 Culture conditions

Organ culture variables were varied in FSUs immersed in DMEM to select optimal culture conditions for experimentation. Variations are listed in Table 11.

Table 11. Summary of culture media viability studies on immersed rabbit FSUs

Media Variable	States	Times
FBS concentration	5, 10, 20%	0, 24 h
FBS concentration	10, 20%	0, 24 h
Ascorbic acid	0, 2.5%	0, 24 h
Endplate/bone treatment	un-, perforated	0, 24 h
%O2	5%, 20%	0, 4, 24 h
%O2	5%, 20%	0, 4, 24, 48 h

FBS Concentration: Two experiments exploring the effect of FBS concentration in culture media on cell viability after 24 hours are depicted in Figure 32. Comparing across concentrations in the AF suggests improved viability with increasing %FBS, but results from the NP are mixed. Because both 10% and 20% FBS facilitate sufficient AF viability, 10% FBS appears best in the NP in Figure 31, and 10% FBS in the NP in the second trial facilitated 80% viability (not shown), organ culture experimentation was set to 10% FBS.

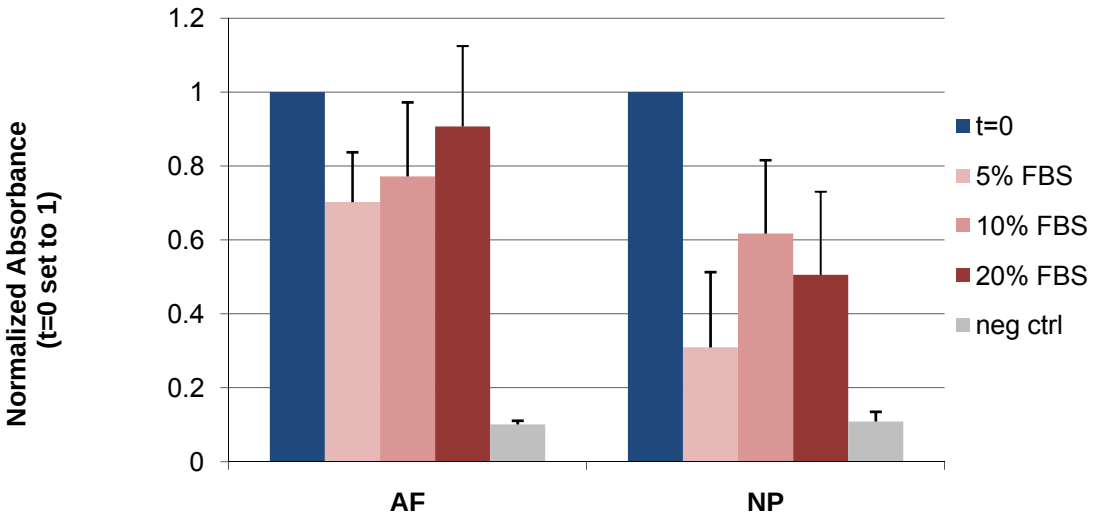

Figure 32. Effect of FBS concentration (5, 10, 20%) in media on disc viability

Adding 2.5% ascorbic acid to the culture media had minimal effect on viability at 24 hours (results not shown). Similarly, removing endplates and making ~1/16 in. tunnels through the cancellous bone between endplates had little effect on viability at t=24 hours; if anything, endplate treatment trended to reduce viability in the NP (see Figure 33).

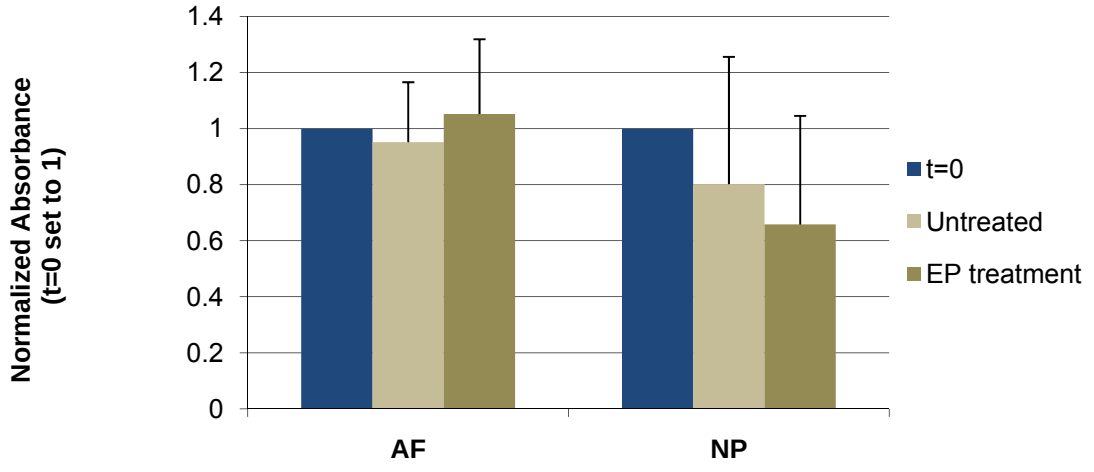

Figure 33. Effect of endplate treatment on disc viability at t=24 hrs

Hypoxia vs. normoxia: Finally, hypoxic culture (5 % O2) was compared to normoxic culture (21 % O2). This experiment was performed twice. In the first experiment (Figure 34), oxygen tension is compared at t=4 and t=24 hours. There is no apparent effect of oxygen tension on disc viability.

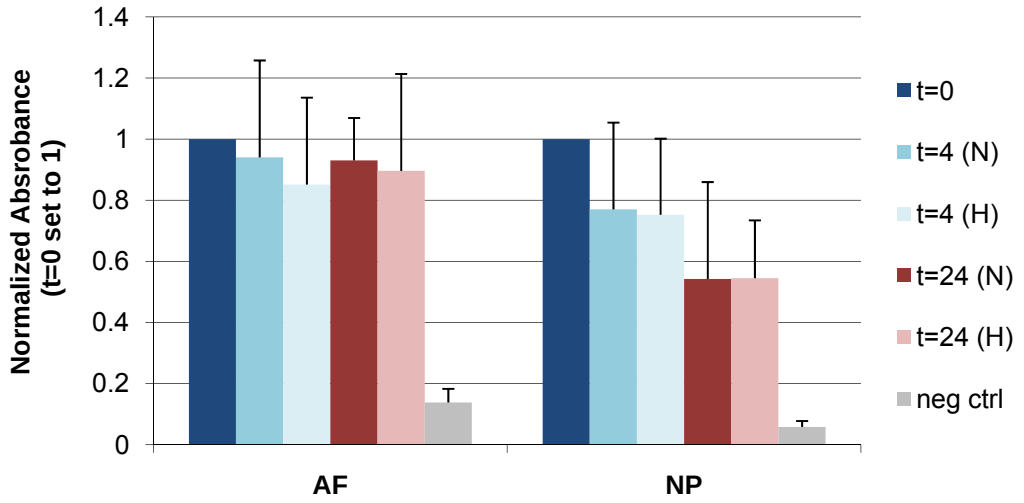

Figure 34. Normoxic (N) and hypoxic (H) culture are compared at t=4 and 24 hr

The second time it was performed, this experiment included a t=48 hour time point. Aside from the apparent anomaly at hypoxic t=4 hr, results in the NP trend toward improvement in viability with hypoxia. There is no consistent trend in the AF.

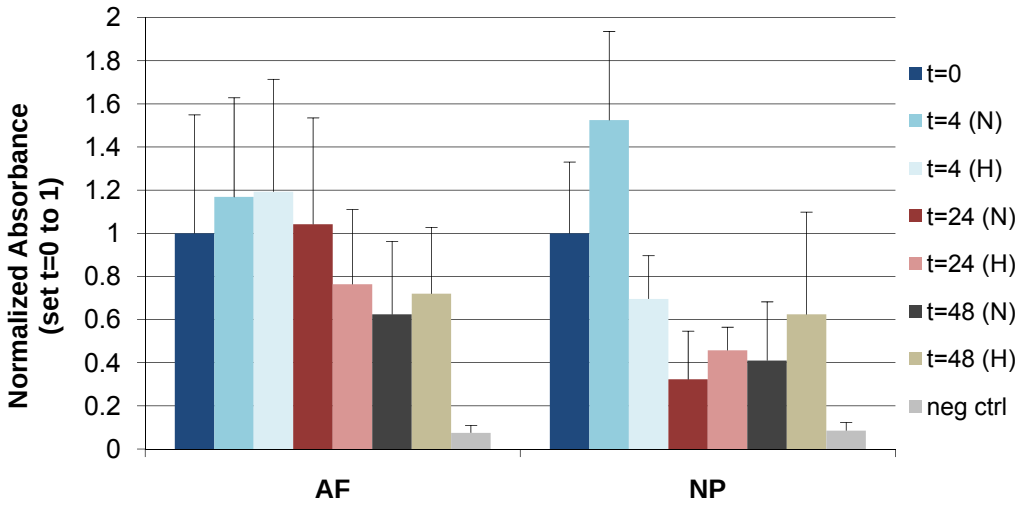

Figure 35. Normoxic (N) and hypoxic (H) culture compared at t=4, 24, and 48 hr

Finally, the effect of culturing FSUs (unloaded) in the bioactive chamber at t=4 hours under hypoxic conditions was assessed. Results are displayed in Figure 36. Chamber culture seems to reduce viability slightly relative to incubator-housed, unloaded FSUs, but chamber viability is greater than or equal to fresh disc viability. This supports use of the chamber for 4 hour studies.

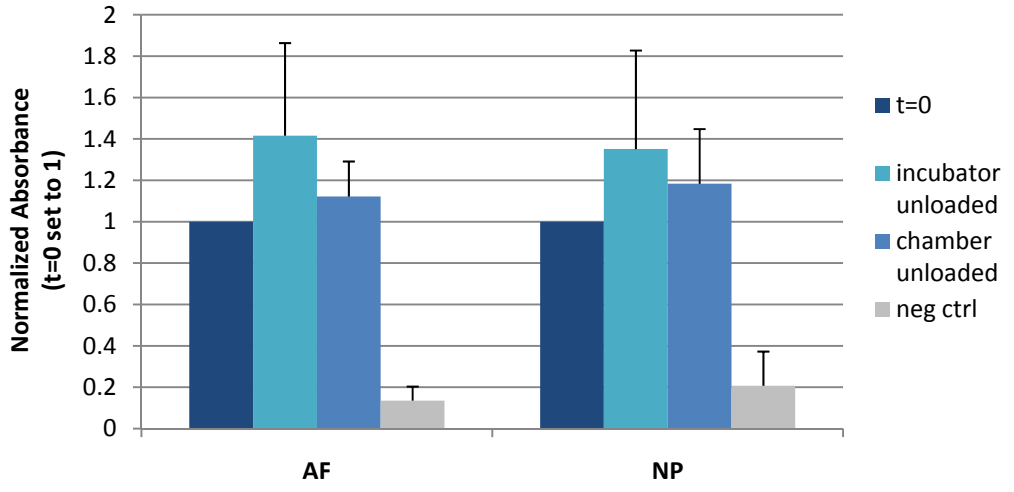

Figure 36. Effect of chamber culture on disc viability

5.6.2 Temperature

Temperature drop across the chamber (inflow vs. outflow) after ~8000 seconds of testing were <1 °C at 1.5 ml/min (illustrated by Figures D.1.2.1 and D.1.2.2 in Appendix D.1.2). The heat gradient across the chamber at experimental flow rates is not problematic.

Insulation: Insulating tubing and the chamber in silicone-capped fiberglass was largely ineffective at preserving heat in the tubing. Figures 37 illustrates the probe in the incubator (37 ºC) through ~12,000 seconds and then inserted in the insulated chamber. Chamber temperature plummeted to the ambient temperature (~29 °C) quickly; steady state chamber temperatures were ≤ 30°C.

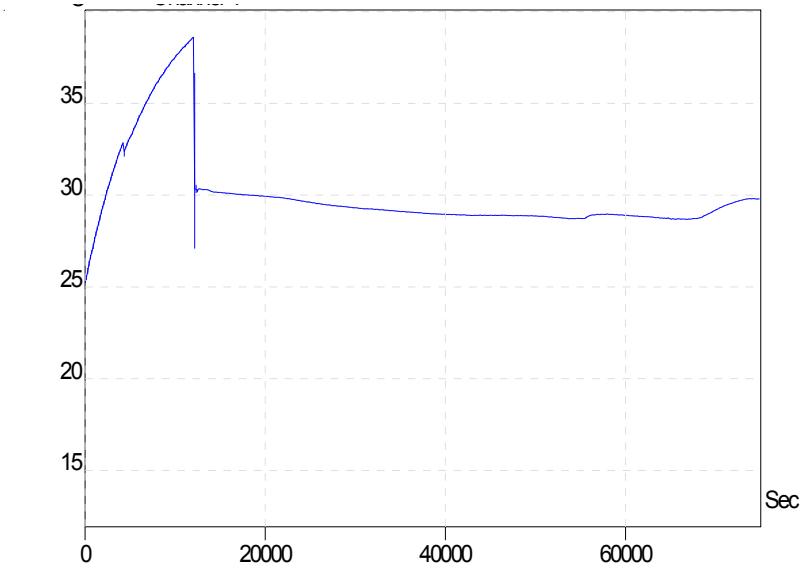

Figure 37. Temperature (C °) recording of RTD inside incubator (<12,000 s) and insulated chamber & tubing

A separate experiment explored the effect of insulation and the ambient environment. The insulated chamber was moved from a heated surface (ambient air ~29 °C) to a typical room temperature (~25 °C) bench top. Insulation did not maintain heat in the chamber; rather,

chamber temperature dropped ~3 ºC (29.5 ºC to 26.5 ºC) in ~100 seconds. Results are shown in Appendix D.1.3.

Flow rate: Flow rate had a small, inadequate effect on steady state temperatures within the chamber. Table 12 shows the effect of increasing flow rate on fluid temperatures; increases are relative to ambient air temperature. Graphical data is recorded in Appendix D.1.3. Increasing flow rates incrementally up to 35 ml/min over ~24 hours had a small impact on temperature (~3 °C increase in temperature). Thus, together with estimated physiologic range of in-vivo flows in the disc (0.15-0.3 ml/min), using flow rate to control temperature was technically and theoretically untenable.

Table 12. Effect of increasing flow rate on chamber temperatures relative to ambient air temperature

Flow Rate	Temperature Increase
1 ml/min	< 1 °C
5 ml/min	~1.3 °C
10 ml/min	~2 °C
30 ml/min	~2.4 °C
35 ml/min	~3 °C

Ambient effect: It was observed that the ambient temperature seemed to dominate chamber fluid temperatures as diurnal variations in temperature recordings were often similar to or greater than the intervention. Temperature dips overnight are evident in Figure 37 (~25,000seconds- 63,000) and Figure D.1.4.2 (~20,000 – 70,000). Evidently, the system was not robust to changes in its environment. This observation inspired a design to control the local chamber thermal environment with direct heat application.

Direct heat: Heat was applied directly to the chamber using flexible silicone resistors (one 1 in. x 2 in. pad per fixture). The recorded chamber fluid temperatures from the proof-of-

concept trial are displayed in Figure 38. Fluid temperatures were responsive to current changes (ramping at 20V/0.36A) and were slow enough to respond to change that minimal current changes could tune into a target value (settling toward 36°C at 17.5V/0.31A to 17V/0.3A). Following this trial, heat could be controlled easily by adjusting VDC current values to tune into a steady temperature between 36.5 and 37 ºC (evident in Figures 38-40). This method of thermal control was used throughout experimentation with relative ease.

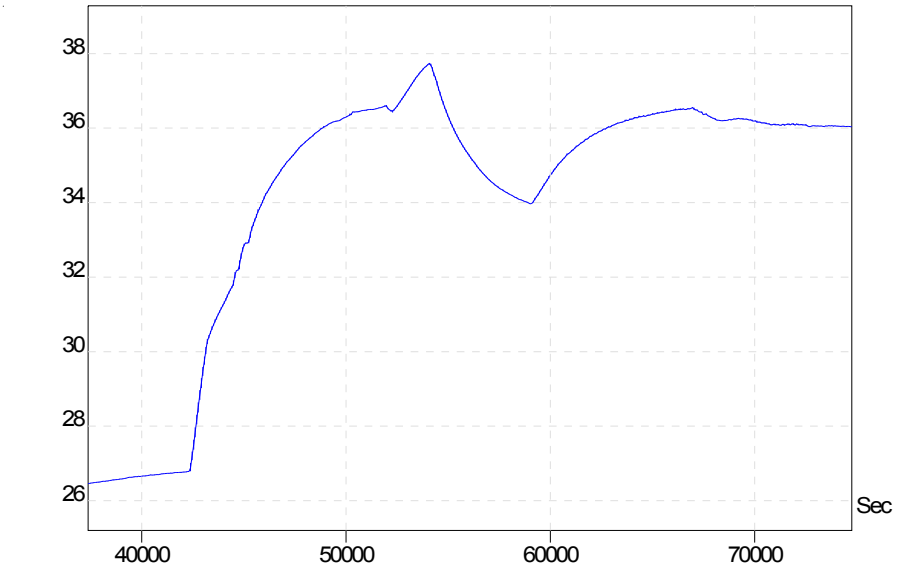

Figure 38. Effect of adherent silicone resistor current variation on chamber fluid heat

5.6.3 Dissolved Oxygen

Initial %O_2 readings with initial configuration—silicone tubing in the pump, nylon connectors, and a single latex layer connecting the fixtures—are recorded in Figure E.2. of Appendix E.2.2. Levels remained near 20 % O2 over 4 hours. To ensure that readings from the DOP were accurate and apparent decreases were drift, a negative control experiment was performed where the upper fixture was filled with culture media and left open to the room (ambient air: ~20 %

O2). Temperature and $\%O_2$ were recorded (Figure 39). Some reduction in $\%O_2$ is apparent, but this seems to level off after four hours.

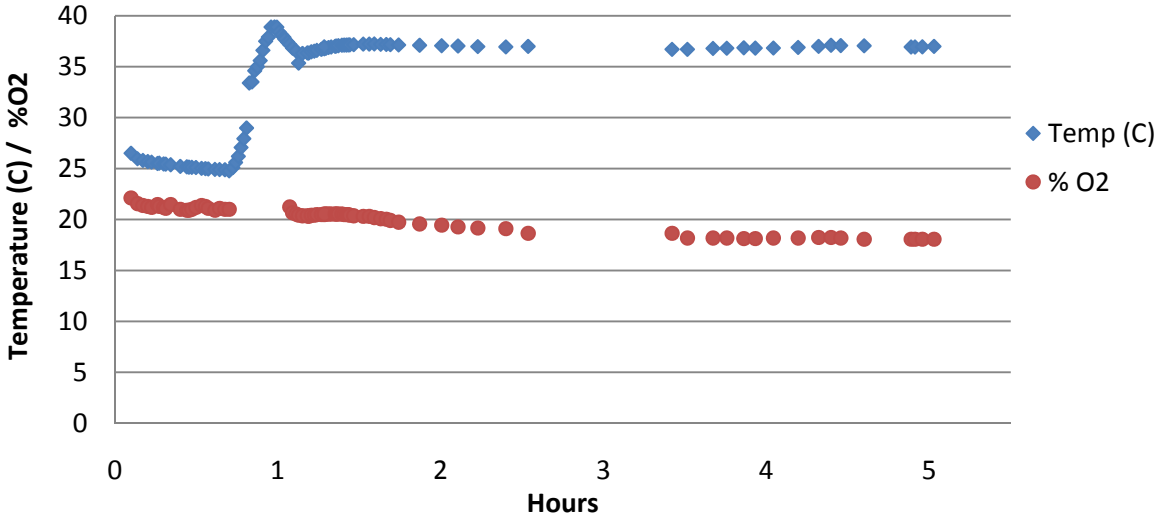

Figure 39. Dissolved oxygen probe $\%O_2$ readings (and temperature) in heated media open to room air

Changing pump tubing from silicone to Tygon, swapping nylon tubing connectors for polycarbonate ones, and adding a second latex layer did not lower $\%O_2$ readings in the chamber (results not shown). However, adding a nitrile rubber layer did alter the $\%O_2$ readings, as illustrated in a combined temperature-%O2 graph in Figure 40. Dissolved oxygen appeared to reach target levels within 5 hours.

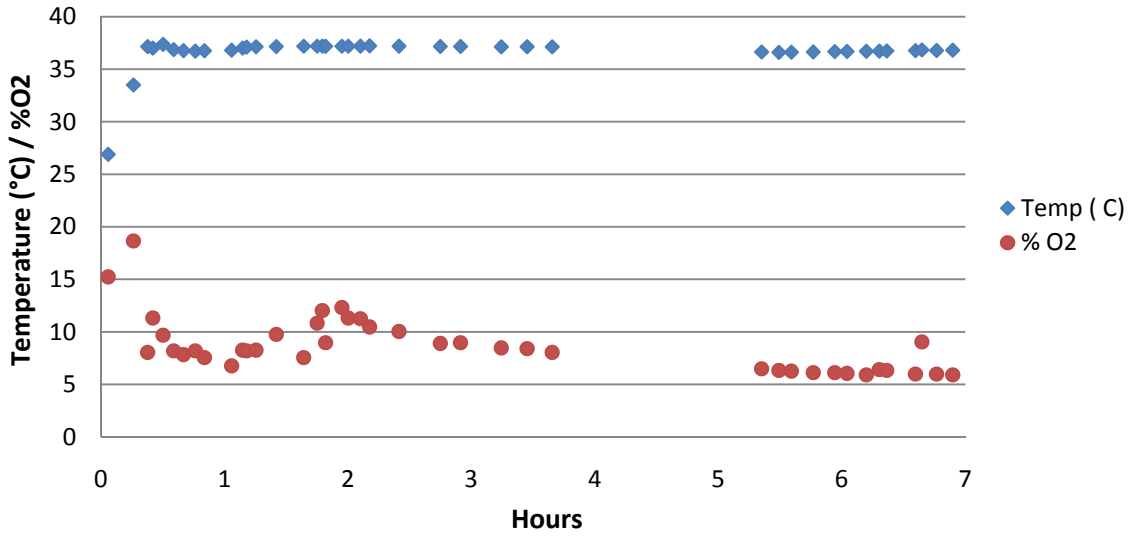

Figure 40. Dissolved oxygen probe $\%O_2$ readings (and temperature) in chamber fluid with outer nitrile layer

The final flexible membrane configuration—two latex and two nitrile layers—yielded a $\%O_2$ profile illustrated in Figure 41. Again, temperature and dissolved oxygen are reported over a simulated four hour compression test. In the equilibration phase (i), oxygen concentrations dropped to ~5% O_2. Throughout testing (ii), oxygen concentration stayed within +/- 1 % of 5 $\%O_2$. When the system drained and room air was pumped into the chamber (iii), oxygen levels rose.

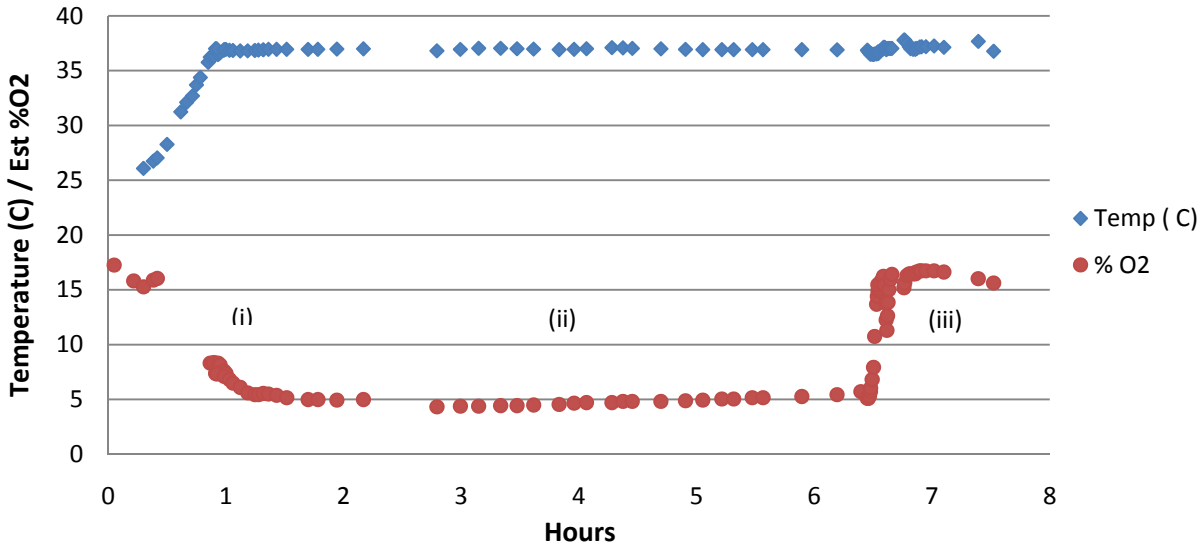

Figure 41. Dissolved oxygen probe $\%O_2$ readings (and temperature) in chamber during FSU compression

Repeated early trials of bioactive testing confirm the chamber's ability to maintain 5 $\%O_2$ with a configuration of two latex layers and two nitrile layers. The first latex layer is placed inside the O-ring; the second is outside it. This configuration is used in all experimental testing. Culture media is placed in incubator the night before testing for equilibration. Dissolved oxygen is recorded in all trials (not presented) and demonstrates repeatable media hypoxia.

5.7 EXPERIMENTAL VIABILITY

Four rabbit specimens were allocated to ascertain the effect of loading on disc viability over experimental timeframes (preparation + 4 hr loading). The specimens allocated for viability are displayed in Table 13 and viability results are depicted in Figure 42. Loading had little effect on viability in the AF, but it trended toward lower NP viability. Viability in culture increased relative to fresh controls (t=0) in all conditions except the loaded NP.

Table 13. Description of rabbit specimens used for viability assessment

Rabbit Age	Date	Type
~10 mo.	05/24/2010	Unloaded
~6 mo.	05/25/2010	Unloaded
~10 mo.	06/09/2010	Loaded
~6 mo.	07/06/2010	Loaded

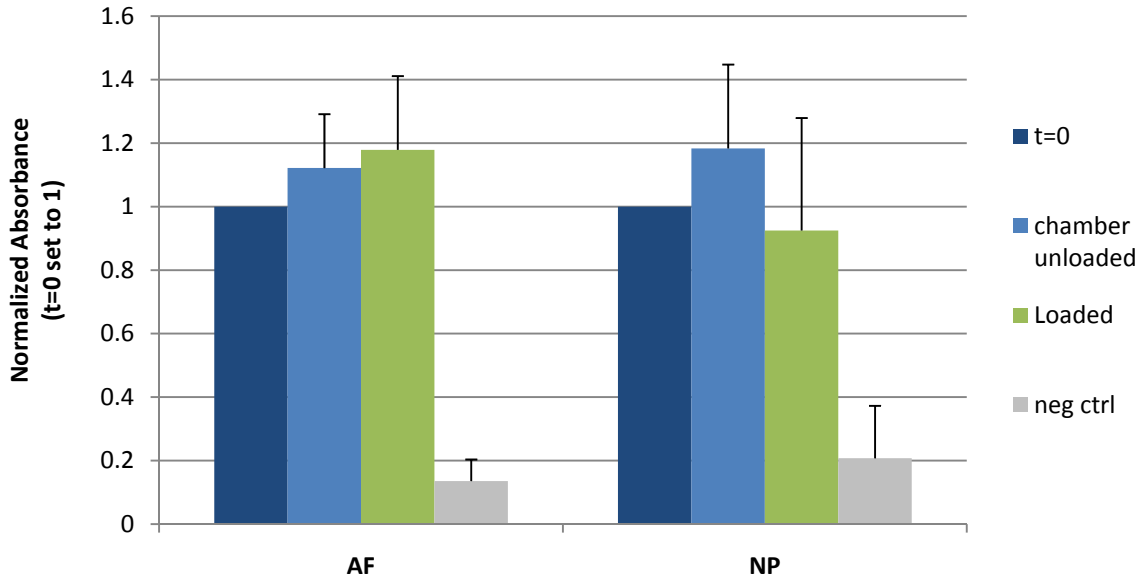

Figure 42. Effect of loading (1.0 MPa/4 hr) on disc viability

5.8 RNA ANALYSIS

5.8.1 RNA Extraction

N=10 rabbit spines were allocated for a loading regimen of 1.0 MPa. Yield from RNA isolation procedures are listed in Table 14. Highlighted samples were not included in PCR because of low yield or poor quality.

Table 14. RNA yield from fresh control, unloaded control, and loaded AF and NP

Yield: ng/ul							
Rabbit Age	**Date**	**AF: t=0**	**AF: U**	**AF: L**	**NP: t=0**	**NP: U**	**NP: L**
6-8 mo.	06/16/2010	4.34	7.65	16.95	-0.49	-1.05	-0.18
~4 mo.	06/18/2010	103.61	91.11	101.5	22.93	12.79	17.97
~10 mo.	06/21/2010	1.44	1.85	2.62	5	6.23	5.68
~6 mo.	06/23/2010	13.39	5.78	10.27	2.58	2.32	2.16
~12 mo.	06/28/2010	3.56	12.21	8.32	8.92	5.31	8.04
~10 mo.	07/07/2010	9.17	9.89	10.11	6.72	5.42	6.3
~10 mo.	07/13/2010	9.4	8.2	11.4	3.9	11.1	12.4
6-8 mo.	07/22/2010	3.58	5.22	8.94	11.79	11.87	10.23
6-8 mo.	08/04/2010	16.06	9.27	17.01	3.95	4.4	4.42
6-8 mo.	08/24/2010	8.79	15.09	35.3	6.54	3.96	5.3

5.8.2 RT-PCR

In NP samples from 06/21/2010 and 07/13/2010 and AF samples from 06/23/2010 and 07/13/2010, GAPDH Ct values differed between samples by more than 1.0 Ct. In these cases, the assumptions of the $2^{-\Delta\Delta Ct}$ method were not considered to be met, and those samples were not included in analysis. Remaining samples' relative gene expression was calculated for each tissue region. Table 15 summarizes the relative gene expression in each tissue region with respect to both controls; numbers in parentheses are standard errors. Figure 43 depicts the relative gene expression data with standard error.

Table 15. Relative gene expression of loaded in reference to t=0 and unloaded (U) controls

Gene	AF (t=0)	N	AF (U)	N	NP (t=0)	N	NP (U)	N
MMP-1	1.35 (0.46)	3	2.41 (1.66)	6	1.18 (0.83)	4	2.19 (1.21)	3
MMP-3	56.77 (4.98)	3	28.09 (40.30)	6	1.89 (1.17)	4	7.76 (12.27)	3
Agg	1.47 (0.67)	2	1.85 (0.70)	3	0.54 (0.04)	2	1.99 (2.01)	2
COX-2	51.09 (61.75)	3	1.88 (0.44)	4				

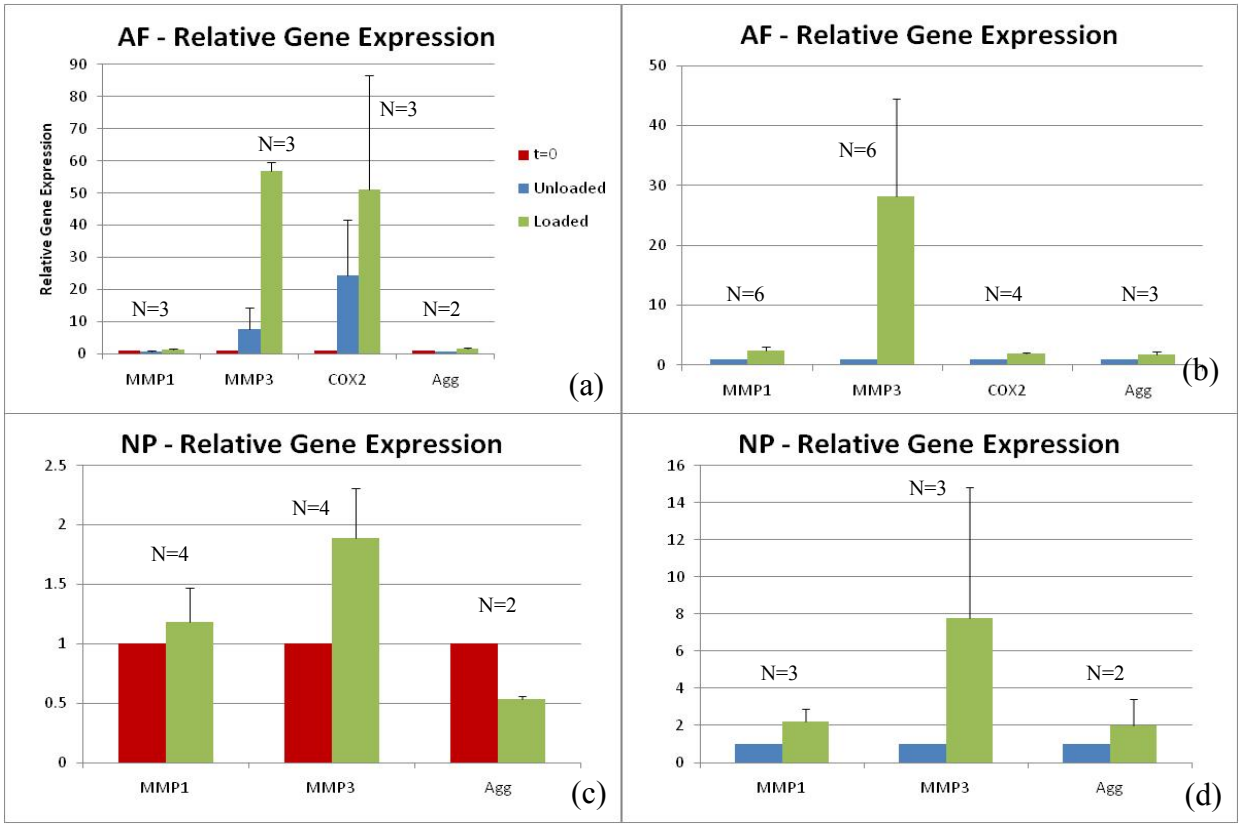

Figure 43. Relative gene expression in AF and NP relative to t=0 and unloaded disc controls: (a) AF expression relative to t=0, (b) AF expression relative to unloaded, (c) NP expression relative to t=0, and (d) NP expression relative to unloaded.

In the AF, MMP-1 and aggrecan increase by less than 50% with respect to fresh samples, and MMP-3 and COX-2 increase by more than fifty times. Use of t-score intervals shows that the effect of loading on MMP-3 was significant and that changes in loading were significantly higher than those in the unloaded state. Changes relative to unloaded samples show similar trends for MMP-1 and aggrecan with slightly larger up-regulation. COX-2 expression changes less dramatically with respect to an unloaded reference, explained in part by the large up-regulation of COX-2 in unloaded culture relative to fresh discs evident in Figure 43 (a). This difference; however, is significant. MMP-3 up-regulation is also dampened relative to fresh

controls (see Figure 43 (b)); however, load-specific up-regulation is large. Interestingly, the variability increases in this comparison. Transcriptional changes are generally less dramatic in the NP, and none reached significance (see Figure 43 (c) & (d)). Expression of MMP-3 relative to fresh samples is nearly doubled, MMP-1 seems unchanged, and aggrecan appears to be down-regulated. In contrast, relative to unloaded controls, MMP-1 and aggrecan expression are similarly up-regulated by twofold, and MMP-3 is increased only eightfold with sizable variability. No changes in the NP were significant.

5.9 CONDITIONED MEDIA ANALYSES

5.9.1 MMP Activity

Zymography: Zymography appeared to be insensitive to differences between samples' MMP activity; specifically, no qualitative difference was evident between blank media and conditioned media. Undiluted media left obfuscating protein smears; a range of dilutions revealed that 1/10 dilutions were necessary for clean lanes on the gels. MMP-1 activity, purported to appear as bands around 54 kDa on gelatin, is evidently similar for each condition on the gel in Figure 44. MMP-3 activity on casein gels is equally inconclusive as no activity bands in ex-vivo samples are evident in Figure 45. Positive controls for MMP-3 included loading the enzymatic portion of the protein directly on to the gel and IL-1β-stimulated cell culture. As a consequence of its insensitivity, zymography is not a conclusive measure of 1.0 MPa/4 hr loading effects on MMP activity.

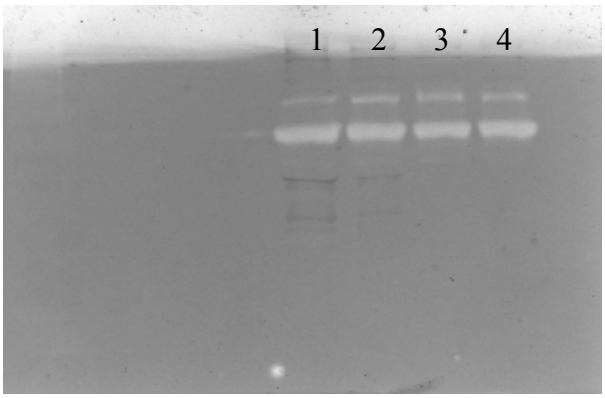

Figure 44. Gelatin zymogram detecting MMP-1 activity at ~54kDa (lower, larger band). Media 1-1.0 MPa loaded, 2-unloaded chamber, 3-incubator unloaded, 4-blank media.

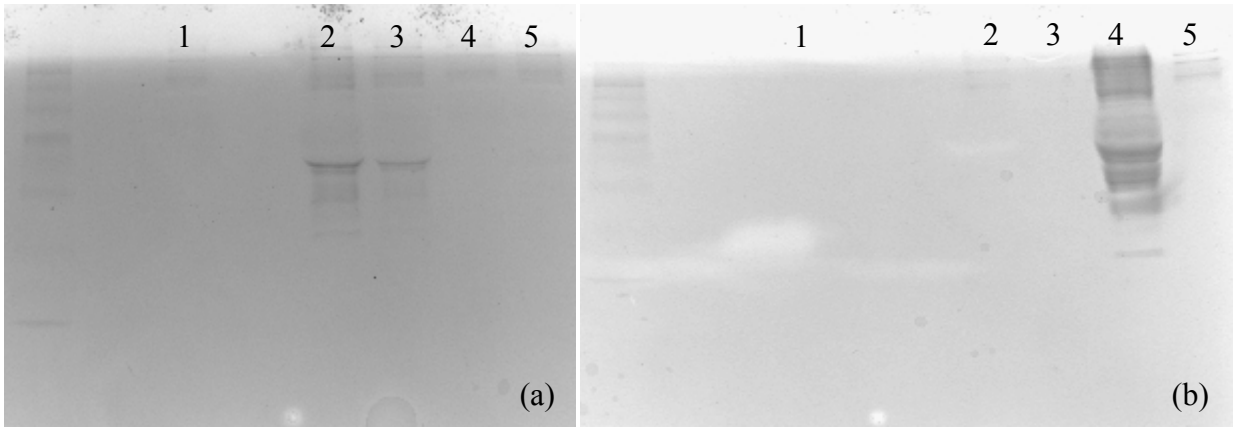

Figure 45. Casein zymogram detecting MMP-3 activity at ~45 kDa. Gel (a): Sample 1-MMP-3 control at 100 ng/µl, 2-loaded chamber, 3-unloaded chamber, 4-unloaded incubator, 5-blank media. Gel (b): Sample 1-MMP-3 control at 25 µg/µl, 2-AF cell culture stimulated with IL-1β, 3-unstimulated AF cell culture, 4-loaded chamber media at 10x dilution, 5-blank media.

Fluorogenic substrate assay: The fluorogenic substrate assay proved to be more sensitive to differences in conditioned media than zymography. Similar to zymography, the first task was to obtain proper dilutions of samples because undiluted media yielded highly non-linear enzyme activity (fluorescence) curves. Based on running a number of sample concentrations with 50 µl of substrate, a 1/10 dilution was sufficient for MMP-1 activity detection and 1/40 dilution was necessary for MMP-3. See Figure 46 for linear relative fluorescence units (RFUs) vs. time curves at these dilutions.

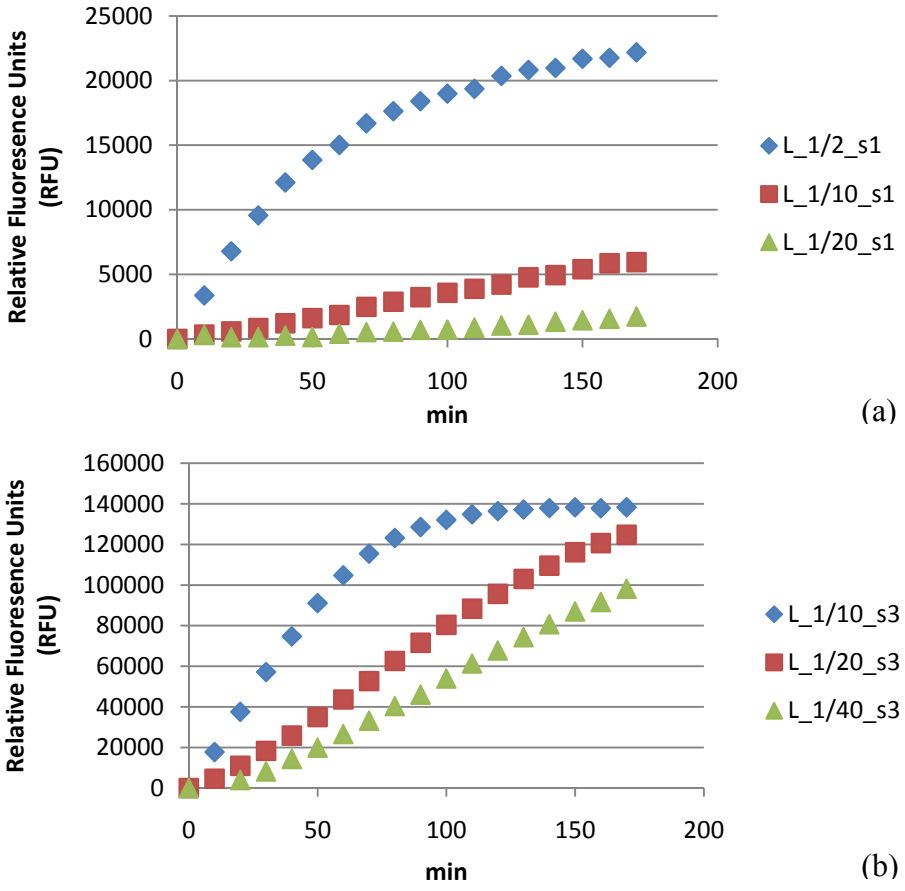

Figure 46. Enzymatic curves in fluorescence (RFU) vs. time (min). (a) MMP-1 activity in loaded sample 7/13/2010 at 1/2, 1/10, and 1/20 dilutions in MMP buffer. (b) MMP-3 activity in same sample at 1/10, 1/20, and 1/40 dilutions.

Dilutions were 1/10 and 1/40 dilutions for MMP-1 and MMP-3. Separate aliquots of N=3 unloaded and N=5 loaded samples for MMP-1 and N=2 unloaded and N=5 loaded samples for MMP 3 were run on multiple days. Maximum slopes of the individual trials are recorded in Table 16 and Table 17, and average maximum slopes for each condition are reported in Figure 47. Slopes for unloaded samples trended to be higher than loaded sample slopes, though differences were not significant for MMP-1 or MMP-3 ($p=0.57$ and $p=0.38$, respectively).

Table 16. Maximum slope of MMP-1 activity curves in conditioned media

Sample	Type	Run 1	Run 2	Run 3	Run 4	Avg
05/25/10	Unloaded	0.72353	0.70023			**0.71188**
06/25/10	Unloaded	0.72811	0.41717	0.28867	0.66017	**0.45533**
09/03/10	Unloaded	0.64424	0.63496	0.96829		**0.80162**
06/28/10	Loaded	0.47919	0.85255	0.24877		**0.55066**
07/06/10	Loaded	0.89114	0.47825	0.25132		**0.36478**
07/07/10	Loaded	0.79441	0.37242	0.25145		**0.31193**
07/13/10	Loaded	0.5155	1.22699	1.01731	0.2828	**0.76065**
07/22/10	Loaded	0.81195	0.14387			**0.14387**

Table 17. Maximum slope of MMP-3 activity curves in conditioned media

Sample	Type	Run 1	Run 2	Run 3	Avg
06/25/10	Unloaded	9.09277	5.11656	1.35436	**5.187897**
09/03/10	Unloaded	8.8656	6.88393	1.72049	**5.82334**
06/28/10	Loaded	15.4941	2.45741	4.76554	**7.57235**
07/06/10	Loaded	9.66464	1.87105	1.69772	**4.411137**
07/07/10	Loaded	5.7965	5.06895	1.63603	**4.16716**
07/13/10	Loaded	9.56261	6.27415	2.03791	**5.121835**
07/22/10	Loaded	4.71123	3.45569	1.41103	**3.19265**

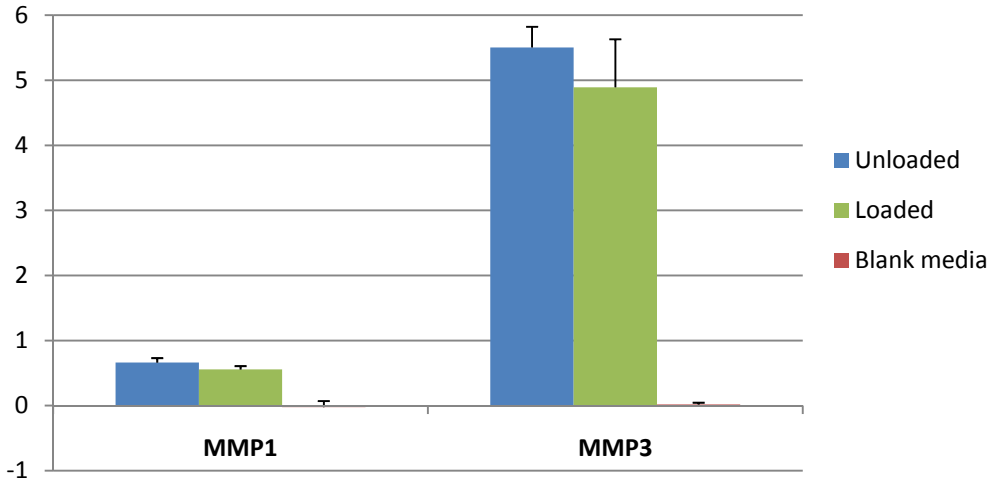

Figure 47. Average maximum slope for MMP-1 and MMP-3 enzymatic activity from loaded and unloaded conditioned media

5.9.2 Matrix Fragments

Conditioned media within the dialysis membrane (2 kDa MWCO) was analyzed using serum CTX-II and CS-846 ELISAs. All samples were ran undiluted and fell well within the linear range of the standard curves. CTX-II concentrations do not appear to be related to loading in the pilot data set (n=2 for each condition). In contrast, CS-846 concentration increased nearly twofold in loaded samples (n=2 per condition). Actual values and standard deviations are reported in Table 18 and average values are depicted in Figure 48.

Table 18. CTX-II and CS-846 concentrations measured in conditioned media

Loading	Age	CTX-II (pg/ml)	CS-846 (ng/ml)
Unloaded	6 mo.	119.535	319.249
Unloaded	10 mo.	475.912	266.105
Loaded	4 mo.	513.648	509.142
Loaded	10 mo.	84.5598	623.221

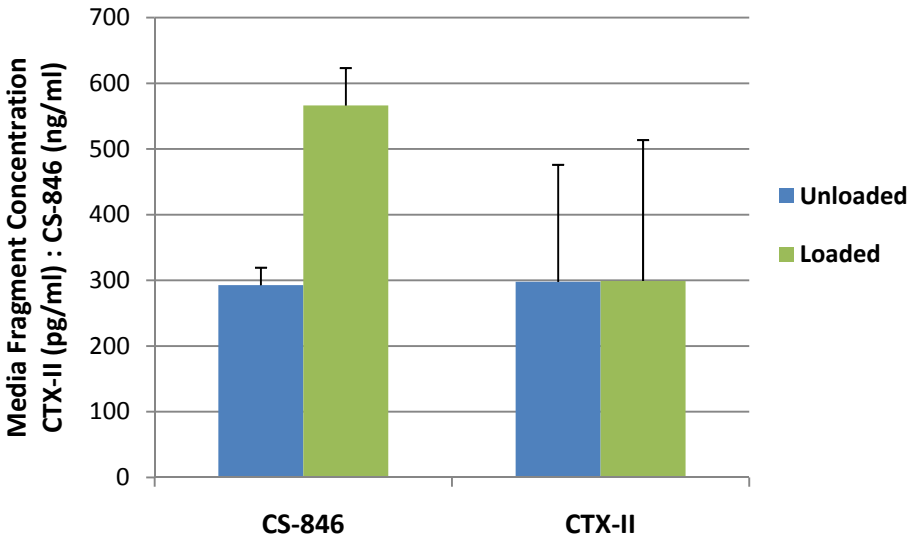

Figure 48. CS-846 and CTX-II concentrations in conditioned media of chamber unloaded and loaded samples.

5.9.3 PGE2

Conditioned media within the dialysis membrane was also analyzed with a PGE2 competitive enzyme immunoassay. Concentrations do not appear to be related to loading (n=3 loaded and n=2 unloaded).

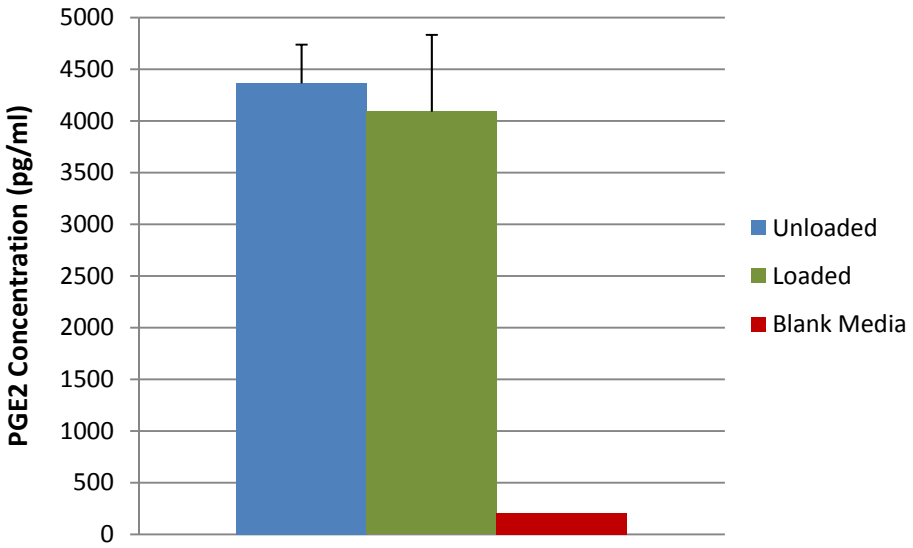

Figure 49. PGE2 concentrations in conditioned media of chamber unloaded and loaded samples

6.0 DISCUSSION

6.1 DEVELOPMENT & VALIDATION

In the novel design central to this thesis, the functional spinal unit (FSU)—adjacent endplates, vertebral bodies, and posterior structure—is preserved in organ culture to facilitate in-situ load transmission to the disc and enable physiologic, six degrees-of-freedom (DOF) motion. The design simulates in-vivo physiology by placing a bioactive testing chamber that houses the FSU in a monitored flow loop of hypoxic, temperature-controlled media. Intervertebral disc (IVD) tissue may be analyzed readily (e.g. gene expression), and the surrounding media volume is minimized with an inner dialysis membrane for detection of released matrix fragments, catabolic and anti-catabolic enzymes, and inflammatory mediators. The system will help (1) to advance characterization of loading effects on disc biology and (2) to narrow the search for disc-specific, load-responsive biomarkers. Both aims are essential to prescription of motion-based therapy treatment for intervertebral disc degeneration (IDD).

To properly perform mechanobiological research, mechanical inputs should be thoroughly characterized so that connections between applied loading and biological response are sound. A custom-built axial testing machine (ATM) was used for establishing the system, though development decisions were made at each step considering future robotic, 6 DOF applications. To avoid interruption of biological processes and diffusive metabolic exchange,

traditional joint-testing potting methods of fixation were eschewed. Two rings of eight rubber-tipped screws tighten against each vertebral body, and rigidity was assessed in uniaxial compression. Future work on the serial-linkage robot will need to quantify rigidity in each DOF.

Fixture rigidity approached or met theoretical targets set a priori. Based on a model of two springs in series, fixture stiffness should be ten times higher than joint stiffness so that fixture laxity contributes less than 10% error to recorded displacements. Rigidity testing showed joint stiffness to come close to 10% of fixture stiffness; preconditioning and creep testing demonstrated joint stiffness 12% and 9% of fixture stiffness, respectively. Screw displacements were also measured to quantify the motion of the specimen relative to fixtures, and screw head displacements were similar to or less than 0.07 mm larger than repeatability measurements. In the context of joint displacements of ~1 mm and digitizer repeatability ~0.1 mm, these screw displacements are acceptably small. Creep tests tended to be more rigid than preconditioning tests; greater specimen-fixture motion in preconditioning is expected because cyclic loading and unloading is more likely to loosen the bone-screw interface. Variability, especially in fixture stiffness, was high in preconditioning trials, indicating the need for careful attention to fixation methods and improved pre-test assessment of fixation rigidity.

Intradiscal pressure (IDP) measurements were made in the nucleus pulposus (NP) of rabbit FSUs using the novel fixtures in order to (1) determine the appropriateness of a commonly used method to assign axial force magnitude aimed to generate a target IDP, (2) provide indirect evidence of rigid attachment, and (3) relate findings to the in-vivo environment. The common method employed by disc biomechanists to attain a target pressure does not account for time-varying IDP. In compression, the negatively charged glycosaminoglycans (GAGs) of the aggrecan-rich NP matrix attract water, causing nuclear swelling and annular circumferential

tensile strain. Sustained loading drives the fluid from the disc, yet the fixed charge density of the GAGs and the low permeability of the disc matrix elicit frictional drag from the fluid movement through the solid matrix. This phenomenon accounts for much of the viscoelastic (time-varying) behavior of the disc and is important in energy dissipation of applied loading. IDP in the NP depends on the interaction of the fluid and solid matrix, and as a consequence, is also a time-varying property.

Results from preconditioning and creep demonstrate the accuracy of the accepted method of prescribing specimen-specific loading in rabbit FSUs in preconditioning but not in creep. In preconditioning where target loads are held for short times, the average pressure at the center of the NP was 1.0 MPa. Attainment of target pressures in preconditioning supports this method's application in cyclic loading of rabbit FSUs. Additionally, this method is unlikely to underestimate the applied force needed to generate the target pressure because the role of the facets, other posterior structures, and potential fixture laxity would act to reduce IDP. Thus, attainment of target pressures indirectly supports fixture adequacy in preconditioning. In creep, the temporal decrease in IDP suggests this method overestimates the steady-state pressure within the NP by at least 40%. Strong rigidity data in creep support the explanation that decreasing pressures can be attributed to reduced swelling pressure under constant compression and not to weakened force transmission. Thus, in making clinically relevant connections between applied loading and observed biological changes over 4 hours of constant compression, a temporal drop in pressure should be considered. However, the magnitude and rate of IDP decrease likely differ between IDP testing and experimentation not only because of different durations (20 minutes vs. 4 hours) but also because of different boundary conditions (exposed to air vs. fluid-bathed).

Needle positions at the center and edge of the NP show decreasing IDP means under constant loading. IDPs with the needle in the withdrawn position trended toward lower IDPs than with the probe at the NP center. While this may demonstrate spatial variation in NP pressure, this is likely an effect of a short recovery time (5 min) between tests and depressurization of the NP. This effect is probably accentuated in this study because of the absence of a surrounding fluid bath. The short recovery choice and short experimental duration was deliberate to avoid tissue dehydration, which would undoubtedly alter fluid interactions with the disc matrix. However, the needle was retracted between tests, and the order of needle positions was not varied, so the reduced IDP observed at the putative edge of the NP is strongly influenced by other experimental variables.

Viability studies were conducted to optimize FSU culture conditions. MTT assays are often interpreted not simply as a measure of viability, but also as an indication of intracellular metabolic activity [139]. The experimentation window set by viability >70% seems to be closed by NP viability after 24 hours. In contrast, AF viability remains fairly high even after one and two weeks of culture. This regional difference may be explained by the fact that FSU culture imposes barriers (bony vertebrae and endplates) to nutrient and metabolite diffusion to and from the disc. NP cells are known to be sensitive to nutrient and oxygen deprivation [122, 123]. Because NP cells are subjected to greater diffusion distances than cells in the AF, inner cells are deprived of nutrition and subjected to a build-up of acidic metabolites. In response, culture conditions (i.e. serum concentration, endplate perforation, ascorbic acid addition) were varied in attempts to maximize NP cell viability within 24 hour periods. Extending this window of stable cellular viability may be achieved with pre-mortem anti-coagulant administration to reduce capillary bud clogging in subchondral bone, a known challenge to long-term viability in IVD

organ culture. Finally, bioactive chamber culture maintained high viability in both tissue regions over >4 hours, establishing a stable basis for comparisons based on loading.

In defining environmental conditions in the bioactive chamber, temperatures of 37 °C and hypoxia are clearly indicated by in-vivo conditions. Attempts to control the fluid temperature without control of stainless-steel chamber walls were futile; the metal chamber acted as a heat sink. However, the thermal conductivity of the fixtures was exploited with the application of heaters directly to the metal surface. Connecting the heaters to a programmable power supply enabled fast heating and facile control.

Hypoxia has been ignored in other organ culture studies, yet cellular studies demonstrate its importance in regulating cell viability and synthetic activity [122, 123]. Here, trends in 5% vs. 21% O_2 incubation suggest hypoxia improves metabolic activity (Figure 34). Surrounding tissues of the FSU consume oxygen and nutrients from media in addition to imposing longer diffusing distances for gases, nutrients, and waste products. Thus, $\%O_2$ in the center of NP is likely well below 5%, which is in agreement with models of disc oxygen concentrations [54]. It is also unlikely that oxygen deprivation explains reduced viability in the NP because lower NP viability was evident in both 21% and 5% culture. Regardless, accurate, appropriate temperatures and oxygen concentrations surrounding the disc are important because of disc cell sensitivity to changes in these variables.

Finally, while performing viability assays and isolating RNA from disc tissue for RT-PCR is widespread, analysis of conditioned media from disc organ culture is often difficult in other ex-vivo systems because of large media volumes. Adding a sealed dialysis membrane around the FSU with a low MWCO reduces the media volume in which matrix fragments may exist. High concentrations of CS-846 and CTX-II after only four hours illustrate this advantage.

However, all the tissues that compose the FSU contribute to molecules in the media. Uniaxial compression is borne primarily by the disc, so differences observed in conditioned media between loaded and unloaded samples stem largely from the disc. However, motions in 6 DOF recruit ligaments and increase the role of the facets, so interpretations of conditioned media must then consider the entire joint complex.

In summary, the completion of Specific Aim 1 allows for interventions of mechanical loading and utilization of biological assays within a well-characterized experimental platform.

6.2 MECHANOBIOLOGICAL EXPERIMENTATION

Experimentation using the novel system sought to demonstrate biological changes in response to loading with an initial target pressure of 1.0 MPa. It was hypothesized that loading would have a minimal but positive effect on viability. Results comparing unloaded and loaded discs in the bioactive chamber show minimal changes in the AF but a slight decrease (~10%) in NP viability.

Relative gene expression illustrated effects of culture and loading. All genes increased relative expression after culture (i.e. relative to t=0 fresh controls) except aggrecan in the NP. Comparisons between MTT results from cultured discs and fresh discs may reflect general metabolic increases as chamber cultured disc were increased by ~20% relative to fresh discs (Figure 36). Both catabolic (MMP-1, -3) and anabolic (aggrecan) gene expression were hypothesized to increase in response to loading. While not all comparisons reached statistical significance, all genes were up-regulated in response to loading. This increase in loaded discs' gene expression relative to unloaded discs may not be attributed soley to increased metabolism because MTT results show minimal or negative changes in metabolism between loaded and

unloaded discs (Figure 42). This reinforces the expectation that observed changes in gene expression are mechanically mediated. MMP-3 was most responsive to loading, increasing by 28 and 7.8 in the AF and NP, respectively. This corroborates findings in-vitro and in-vivo that MMP-3 is inducible in response to loading [79, 98]. By contrast, MMP-1, COX-2, and aggrecan uniformly increased by approximately only twofold in response to loading in both AF and NP. These results reinforce the idea that MMP-1 and MMP-3 are regulated separately, and that MMP-3 is a more sensitive marker of load-responsive changes. While sensitive, the increase in response to loading was highly variable. It is also apparent and expected from COX-2 expression (increased by 24.4 relative to t=0) that specimen isolation and preparation was inflammatory. COX-2 was significantly up-regulated in response to loading, which may be important clinically. Changes in aggrecan expression were inconclusive, especially in the NP where decreases are evident relative to fresh discs. Interestingly, changes in gene expression in the AF tended to be larger than changes in the NP. This is expected given different cell types, different mechanical environments of the tissues, and different cellular stresses, strains, and PCM modulation between the two regions [29]. These data are important in beginning to understand mechanisms for load-responsive remodeling in the disc, and given the relatively short window for experimentation, changes in gene expression are likely to be the most salient outcome.

However, gene expression data must be combined with protein assays, which are closer to actual changes to cellular and matrix homeostasis. Connections between MMP-1 gene expression and MMP-1 activity data are apparent. MMP-1 was not load responsive at the gene level, and little difference was detectable in MMP-1 activity through zymography or the fluorogenic enzymatic activity assay. In contrast, MMP-3 activity does not increase as

expectations based on gene expression would indicate; instead, activity seemed to be lower in loaded specimens. However, it is reasonable that layers of regulation in translation, post-translational modification, and activation of the pro-enzyme modulate the transcriptional response. Also, four hours may be insufficient to observe this effect, particularly in comparing gene expression to conditioned media concentrations of a large enzyme like MMP-3 that would not diffuse rapidly into the media. These results counter the hypothesis that MMP enzyme activity increases with four hours of compression, underscoring the importance of end-product analysis and pointing to the need for longer culture durations.

A touted advantage of the system is detection of structural breakdown fragments and inflammatory mediators in conditioned media. Screening and analysis of matrix fragments may help in the search for disc specific, load-responsive biomarkers. It was hypothesized that both C-telopeptide-II (CTX-II) and chondroitin sulfate-846 would increase in response to loading. However, CTX-II media concentrations did not correlate with loading. CTX-II levels in serum of rabbits with induced disc degeneration have been shown to be sensitive markers of IDD [143]; however, this was the first time that CTX-II has been examined as a biomarker in ex-vivo conditioned media. Longer constant loading, known to be detrimental to the collagenous matrix of the AF, might demonstrate load-responsiveness in conditioned media. In contrast to CTX-II, CS-846 concentrations appeared to correlate with loading, suggesting increased aggrecan synthesis. CS-846 results are surprising based on findings by Junger et al. who did not observe changes in CS-846 in the AF or NP after 7 days in culture and only slight changes after 21 days [114]. Junger et al. examined tissue, while this project assayed conditioned media surrounding the entire joint. Nevertheless, aggrecan gene expression in this study was elevated slightly

(twofold) in loaded AF relative to unloaded, which supports a finding of increased aggrecan synthesis.

PGE2 results are also surprising. Because of the small size of PGE2, it was anticipated that concentrations would be too low to detect. Moreover, increases in COX-2, and upstream enzyme that facilitates production of PGE2, predict load-responsive increases in PGE2. Yet this was not observed at 4 hours. This may illustrate the temporal and regulatory gap between transcriptional and translational and signaling changes. It may also point to the importance of other regulators of PGE2 production.

While not conclusive assessments, ELISA results provide interesting pilot data and demonstrate the utility of the system, namely, detection of leached macromolecules in small media volumes. Experimentation in general shows the capability of the system (1) to support biological assays and (2) to identify load sensitive outcomes.

6.3 CAVEATS

Continued use and advancement of the bioactive testing systems relies in part on documentation of practical advice regarding system usage. Subtleties in chamber assembly and experimental protocol are described below.

6.3.1 Preparation

The day prior to experimentation requires preparation of system components. All tubing, connectors, fixtures, screws, O-rings, and surgical tools (for spine extraction) must be autoclaved. The tissue culture hood should also be prepared with a diaper pad, screw drivers, pipe clamps, Vernier calipers, and 1 mL pipette subjected to EtOH and UV light. On the day of experimentation, rubber membranes should be prepared. A non-lubricated latex Trojan condom is folded in half length-wise and cut to form two long, open-ended cylindrical membranes. Nitrile layers are formed from the wrist portion of rubber gloves of different colors. Rubber membranes should be rinsed with EtOH and subjected to UV light. Repeated autoclaving and specimen attachment may damage rubber tips, so sterile, rubber-tipped screws of ½ in. and ¾ in. should be kept in the tissue culture hood to replace screws that may have a split rubber cap. In general, ¾ in. screws are placed holes that contact the most posterior portion of the FSU; all other screw holes contain ½ in. screws.

6.3.2 Dissection

First, muscle on the anterior portion of the spine is removed to expose the discs and identify the levels of interest. Bulk muscle and fascia can be removed with a scalpel, but finer removal of muscle is better accomplished with small rongeurs. Care must be taken in the posterior to preserve the facet capsule and the interspinous ligaments. To open the L3-4 disc, use rongeurs to break the facets and slowly cut from anterior-to-posterior along the superior border between the AF and the endplate with a scalpel. Too much pressure or speed can cause the NP to eject because of the pressure of the extending joint. Scoop the NP into a waiting 1.5 ml tube. Cut the along the inferior AF-endplate margin to dislodge the AF and similarly place it in a 1.5 ml tube. The L5-6 and L1-2 discs that border the L4-5 and L2-3 FSUs may be carefully removed and stored as back-up tissue or simply cut through to isolate the FSUs of interest. Endplates on the resulting FSUs are best removed with rongeurs; clamping the endplate and twisting about the medial-lateral axis should result in the endplate cleanly "popping" off. Finally, the spinal cord and nerve roots are removed. The specimen is then rinsed in PBS.

6.3.3 Chamber Assembly

An excess of 2 in. beyond the FSU must be left on either end of the dialysis membrane to provide enough material for an adequate knot. Latex membranes should be applied first; the inner membrane fits under the O-ring and the outer membrane stretches over it. When attaching the rabbit with screws, bring opposing points of contact up against the FSU serially paying close attention to the axial alignment. When all screws are up against the vertebra, three or four rounds of iterative tightening should ensue, all the while maintaining axial alignment of the

specimen (especially avoiding anterior rotation of the FSU). Avoid over-tightening single screws as this may lead to damage of the underlying dialysis membrane. A similar process is used for attaching the upper fixture, though it is more challenging to maintain axial alignment. It is helpful to tighten a screw in the upper row to gauge the height of the vertebral body so that adequate distance (> 5mm) between fixtures can be achieved. Once both fixtures are securely attached to the FSU, then the latex layers are pulled up; the inner followed by the outer. The latex can stretch over protruding screws without tearing. Once the nitrile layers have been set overtop the latex ones and pipe clamps are tightened against the underlying O-ring, clamps have a tendency to slip off the O-ring. Extra care needs to be paid to avoid this condition, which can lead to leaks.

6.3.4 System Assembly

During chamber filling, it is helpful to monitor the dissolved oxygen readings to describe what is going on within the chamber. Voltages from the probe rapidly become positive when warm, hypoxic media reaches the level of the probe. Also, if voltages drop during testing, this is typically an indication of a leak in the chamber. Similarly, if the rubber layers swell and bulging is evident with palpation of the chamber wall, this is indicative of blocked tubing or connectors. Typically, a connector is at fault (at the chamber outlet or rear of incubator) and needs to be replaced.

6.3.5 Maintenance

Several components of the chamber require attention and maintenance. The O-rings degrade after repeated autoclaving (~8-10 runs). Similarly, the rubber tips on screws require replacement periodically (~10-12 runs). Dissolved oxygen and temperature probes should be cleaned in tergazyme and rinsed in deionized water after testing. They are then suspended in 15 ml tubes to minimize risk of contamination. EtOH treatment of the temperature probe is acceptable; EtOH should not be applied to the Teflon membrane of the dissolved oxygen probe.

6.4 LIMITATIONS

While the rabbit FSU model presented here offers the unique advantages of in-situ loading and multi-DOF motion in a controllable environment, there are noteworthy limitations to the model. Most notably, disc viability is not robust over long time frames ($t > 24$ hours). Initial attempts to improve viability with bone tunnels were not successful, though modified attempts may increase perfusion of media to the disc and improve viability. Alternatively, rabbits can be treated with heparin prior to death to prevent clogging of the capillary buds in the subchondral bone; this is thought to improve nutrition of disc cells in the NP and inner AF.

Fixture rigidity results demonstrated an order of magnitude difference between fixture-specimen interface stiffness and FSU stiffness in static and dynamic stiffness. However, variability was high in cyclic compression, suggesting inconsistencies in the attachment of FSUs to the chambers. This reinforces the need for attentive fixation and axial specimen alignment and points to potential for improvements in fixation methods. These may include measurement

of the torque applied to screws for more repeatable secure attachment. A fully automated process is not advisable because of the potential for tearing the dialysis membrane. Nonetheless, physiologic IDP near expected magnitudes for prescribed forces reinforces the conclusion of adequate fixture stiffness.

As noted, temporal and positional changes in IDP must be understood as trends. A temporal decrease in NP swelling pressure under constant load is expected, but the nature of the decrease is a function of the boundary conditions and duration of compression. In this experimentation, the short term, open-air testing arrangement certainly differs from the closed-loop testing configuration and from in-vivo conditions. Moreover, the positional variation is likely dominated by incomplete recovery between the two needle positions. It is difficult to conclude that pressure varies spatially within the NP based on this data.

Analysis of conditioned media must be understood in the context of the tissues composing the entire FSU. While treatments for disc degeneration seek disc-specific biomarkers, media analyses actually measure and identify load-responsive markers from disc, endplate, facet joints, bone, ligaments, and residual muscle. The time-matched control allows for isolation of fixation and loading, but no control permits disc-specific analysis in conditioned media. MMPs and prostaglandins may be released from all of the tissues composing the FSU. Moreover, because of the size of MMPs, CS-846, and CTX-II, it is unlikely that they diffuse from the center of the disc (NP, inner AF) over four hours to enter the surrounding media. This underscores the need to perform longer periods of testing (e.g. 24 hour testing) with two protocols: (1) 24 hours of compression and (2) 4 hours of compression followed by 20 hours of recovery. The former allows for analyses of changes in gene expression relative to 4 hour data, and the latter allows for

diffusion of proteins and end products through the disc and into the matrix. Similar concerns about large protein diffusion and effects on multiple tissues must inform future studies that include inflammatory cytokines for coupled (i.e. mechanical loading + inflammatory stimulus) interventions.

6.5 FUTURE STUDIES

All mechanical testing in this study was limited to uniaxial compression with cyclic preconditioning. Since completion of development, duration of experimentation (e.g. 4 hours loading followed by 20 hours recovery or 24 hours loading), frequency, and magnitude of loading can be varied using the ATM. However, utilizing the flexible chamber with a serial-linkage robot in 6 DOF represents a novel advancement in ex-vivo disc mechanobiology and is the most exciting future application.

Mechanical inputs may also be coupled with biological interventions. Mirroring work by Sowa et al. in cell culture, an inflammatory mediator (e.g. IL-1β) may be introduced in the small dialysis membrane media. This coupled intervention of loading and inflammation is derived from disc pathologies like IDD where inflammatory mediators are increased locally. Combining the two interventions allows for detection of additive or synergistic interactions, which is clinically relevant. Similarly, this system is poised to study simulation of a traumatic injury like NP herniation where the local milieu and its interaction with loading are of clinical interest.

This system could also be used as an outcome test for in-vivo animal studies. Specimens with varying age, injury, and therapeutic interventions could simultaneously be mechanically and mechanobiologically evaluated. Traditional mechanical properties derived from viscoelastic or

flexibility tests would describe in-vivo remodeling effects on tissue composition, and biological outcomes would describe load-responsive characteristic markers (e.g. changes in MMP activity). Thus, this experimental platform may be further developed to test and characterize a broad array of unexplored, clinically relevant questions in disc mechanobiology.

A touted advantage of the system is the ability to aid in the identification of biomarkers related to changes in disc biology. To achieve this goal, media from the dialysis membrane could be used in two-dimensional gel electrophoresis. By comparing blots from loaded and unloaded FSUs and running mass spectroscopy on proteins uniquely present in loaded blots, this method could identify load-responsive markers. These proteins could then serve as outcomes in ex-vivo and in-vivo mechanobiological studies to determine their candidacy as serum biomarkers of beneficial or detrimental loading.

The possibility of an ex-vivo human model elicits much clinical interest; thus, future work may include further attempts to develop a viable human disc organ culture. To overcome the challenges associated with a human model, a number of steps could be taken. Stricter inclusion criteria that exclude older patients and collaboration with the Department of Pathology to minimize time after death could raise initial viability. Nutrition and waste exchange within the disc might be improved with endplate treatment and bone mass minimization. Improved frequency might occur at larger hospital centers or through better communication mechanisms between the Department of Pathology and researchers. Clearly, further development would be needed for human disc organ culture, but the clinical upside remains attractive.

6.6 CONCLUSIONS

The development of an ex-vivo IVD mechanobiological system that preserves the full functional spinal unit with the capacity for six degree-of-freedom motion represents a novel experimental advancement. This system also enables analysis of small conditioned media volumes for detection of released matrix fragments or inflammatory mediators. Development of the system included validation of rigid fixation and stable temperature and dissolved oxygen surrounding the specimen. Initial experimental testing illustrates the ability of the novel platform to explore thresholds of loading in regulation of disc matrix homeostasis. This system will play an important role in the bench-to-bedside research paradigm by bridging a gap between in-vitro cell and in-vivo animal or human studies of disc mechanobiology in simulating complex, physiologic loading and measuring relevant biological responses.

APPENDIX A

RABBIT TISSUE SHARING

A.1 COLLABORATORS & DEPARTMENTS

This work owes an enormous debt of gratitude to the collaborators listed below who generously allowed tissue sharing of New Zealand White rabbit lumbar spines.

Table A.1. Rabbit spine age distribution and tissue sharing acknowledgement

Age	N	Department	PI
~4 mo.	1	Children's Hospital	Mooney
5-6 mo.	5	Oral Biology	Sfeir
6-8 mo.	28	Ophthamology	Gordon
~11.5 mo.	5	Oral Biology	Almarza
~12 mo.	3	Bioengineering & Oral Biology	Little & Almarza

APPENDIX B

RIGIDITY ANALYSIS

B.1 FURTHER FIXTURE RIGIDITY TESTING

Frequency: Rotations and displacements of the vertebral reference frames relative to the fixture reference frames before and after testing (method (b)) at different frequencies of loading are illustrated in Figures B.1.1. This testing was performed on N=1 FSU.

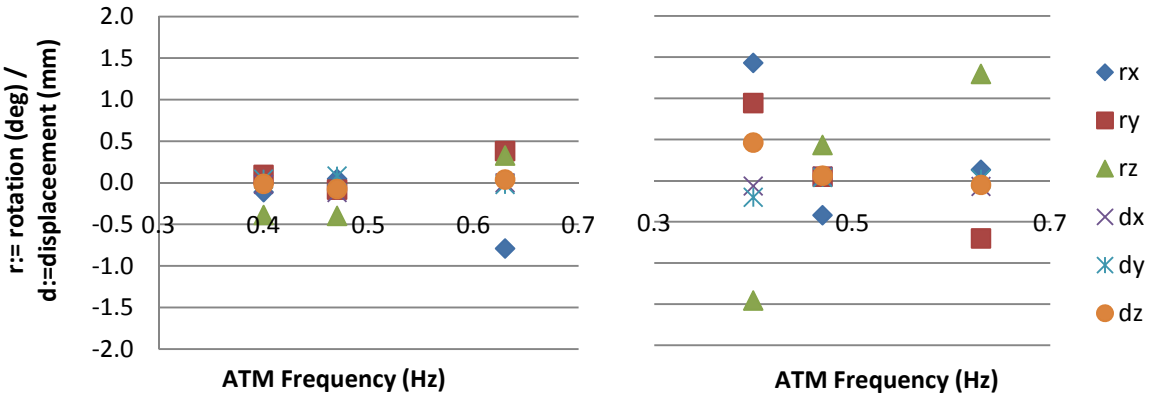

Figure B.1.1. Differences in initial and final vertebra-fixture transformations at 0 mm displacement for three frequencies (+.25 to -.75 mm compression) in the upper (left) and lower (right) fixtures

Displacement: Similar analysis was performed on the same FSU as a function of displacement from 0 mm; rotations and angles between the two LCS (method (b)) at 0 mm and x mm are depicted in Figure B.1.2. Because of experimental challenges in accessing screws in the inferior vertebra during higher levels of displacement, only the SVCS-UFCS relation is analyzed.

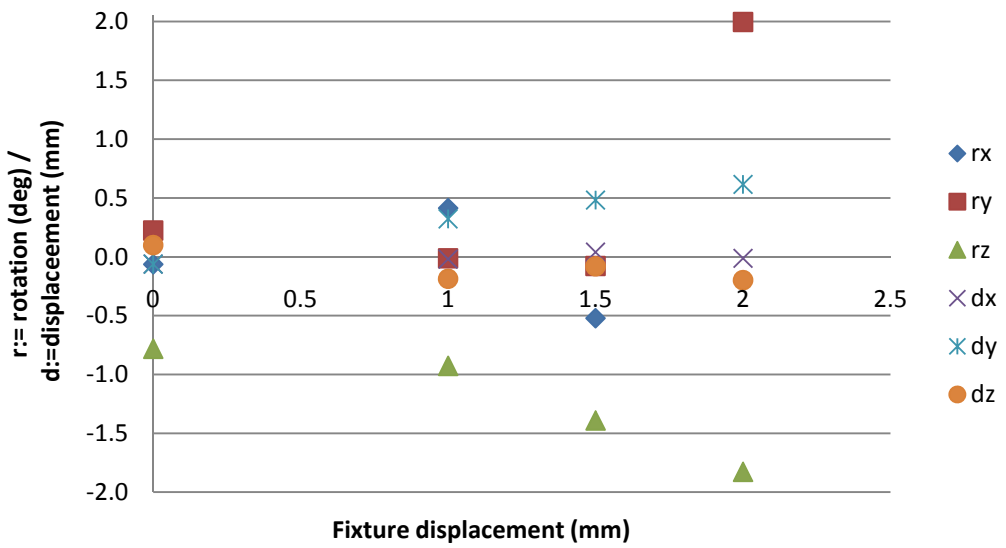

Figure B.1.2. Differences in initial and final UFCS-SVCS between 0 mm and x mm axial displacement

B.2 MATLAB CODE FOR RIGIDITY ANALYSIS

B.2.1 Method (a)

This code (1) loads screw-position files before and after a motion captured by the Faro Arm using Rhinocerous 3D, (2) creates local fixture coordinate systems, (3) forms local-to-global transformations for the fixture coordinate systems, (4) determines screw positions in the fixture coordinate system (5) subtracts initial screw position from final screw position based on fixture coordinates, (6) aligns these difference vectors in the global coordinate system to lend meaning to components, and (7) prints the results to a text file.

```
%analyzes .txt files generated from Rhino program using FARO ARM postCrp
date = '022610';
```

```
state = 'CrpX';

%need to modify file name as necessary
faroPre = load('z:\Ortho Research 3\FergusonLab\Students\Hartman, Robert\ATM
Development\Attachment\022610\FARO_postPC3_022610.txt');
faroPost = load('z:\Ortho Research 3\FergusonLab\Students\Hartman, Robert\ATM
Development\Attachment\022610\FARO_postCrp_022610.txt');

for k = 1:2
    if k == 1
        faro = faroPre;
    elseif k == 2
        faro = faroPost;
    end

    %2/16/10 - order of digitizing: UF>SV>LF>IV
    %2/17 & 2/18 - " : UF>LF>SV>IV
    %teasing out the three points per item
    UF = faro(10:12,:); %upper fixture
    LF = faro(7:9,:); %superior vertebra
    SV = faro(4:6,:); %lower fixture - x,y,z in rows
    IV = faro(1:3,:); %inferior vertebra

%% superior screw positions
    %form coordinate systems for each item (not aligned w/ GCS)
    %formed 1, 2, 3 in CCW manner
    UF1 = UF(3,:) - UF(2,:);
    UF2 = UF(1,:) - UF(2,:);
    UF3 = cross(UF1,UF2);   %z+ is up (cranial)

    %normalize vectors to form transformation matrix
    UFx = UF1 / norm(UF1);
    UFy = UF2 / norm(UF2);
    UFz = UF3 / norm(UF3);

    %upper fixture in global RF; origin set at middle screw (2)
    T_G_UF = [UFx(1), UFy(1), UFz(1), UF(2,1);...
        UFx(2), UFy(2), UFz(2), UF(2,2);...
        UFx(3), UFy(3), UFz(3), UF(2,3);...
        0, 0, 0, 1];

    %P_L = T_LG * P_G (screws in LCS of upper fixture)
    sUF = zeros(4,3);
    sUF(1:4,1) = inv(T_G_UF) * [SV(1,1); SV(1,2); SV(1,3); 1]; %x,y,z in
columns
    sUF(1:4,2) = inv(T_G_UF) * [SV(2,1); SV(2,2); SV(2,3); 1];
    sUF(1:4,3) = inv(T_G_UF) * [SV(3,1); SV(3,2); SV(3,3); 1];

    %screw positions in UF and G CSs
    if k == 1
        sUFi = sUF; %x,y,z in columns
        sSGi = SV';
        T_G_UFi = T_G_UF;   %G-LCS transform at start
    elseif k == 2
        sUFf = sUF;
```

```
        sSGf = SV';
        T_G_UFf = T_G_UF;   %G-LCS transform at end
    end


%% inferior screw positions
    %form coordinate systems for each item
    LF1 = LF(3,:) - LF(2,:);
    LF2 = LF(1,:) - LF(2,:);
    LF3 = cross(LF1,LF2);

    %normalize vectors to form transformation matrix
    LFx = LF1 / norm(LF1);
    LFy = LF2 / norm(LF2);
    LFz = LF3 / norm(LF3);

    %upper fixture in global RF; set origin at middle screw
    T_G_LF = [LFx(1), LFy(1), LFz(1), LF(2,1);...
        LFx(2), LFy(2), LFz(2), LF(2,2);...
        LFx(3), LFy(3), LFz(3), LF(2,3);
        0, 0, 0, 1];

    %P_L = T_LG * P_G (screws in LCS of upper fixture)
    sLF = zeros(4,3);
    sLF(1:4,1) = inv(T_G_LF) * [IV(1,1); IV(1,2); IV(1,3); 1];
    sLF(1:4,2) = inv(T_G_LF) * [IV(2,1); IV(2,2); IV(2,3); 1];
    sLF(1:4,3) = inv(T_G_LF) * [IV(3,1); IV(3,2); IV(3,3); 1];

    %screw positions in LF and G CSs
    if k == 1
        sLFi = sLF;
        sIGi = IV';
        T_G_LFi = T_G_LF;   %G-LCS transform at start
    elseif k == 2
        sLFf = sLF;
        sIGf = IV';
        T_G_LFf = T_G_LF;   %G-LCS transform at end
    end

end

% x,y,z in columns!
sPosUF_if = sUFf(1:3,:) - sUFi(1:3,:);    %difference of screw positions on
superior vertebra in UF LCS
sPosLF_if = sLFf(1:3,:) - sLFi(1:3,:);    %"
inferior "           LF "
sPosSV_if = sSGf - sSGi;    %difference in screw positions on superior
vertebra in GCS
sPosIV_if = sIGf - sIGi;    %"                                  inferior "

% convert changes in LCS back to GCS (goal: displacements aligned w/ global
% axes, which are aligned w/ specimen.  Z-displacement in GCS ~ axial disp.

% check to see if GCS-LCS changes before and after test
```

```
I_check = T_G_UFi * inv(T_G_UFf);   %I_check should be close to I if T_i and
T_f are similar

% align changes w/ GCS - use [R_G_LCS] w/ no translations
sPosGu_if = zeros(3,3);
sPosGu_if(1:3,1) = T_G_UFf(1:3,1:3) * [sPosUF_if(1,1); sPosUF_if(2,1);
sPosUF_if(3,1)];    %superior vert. screws (upper fixture)
sPosGu_if(1:3,2) = T_G_UFf(1:3,1:3) * [sPosUF_if(1,2); sPosUF_if(2,2);
sPosUF_if(3,2)];
sPosGu_if(1:3,3) = T_G_UFf(1:3,1:3) * [sPosUF_if(1,3); sPosUF_if(2,3);
sPosUF_if(3,3)];

sPosGl_if = zeros(3,3);
sPosGl_if(1:3,1) = T_G_LFf(1:3,1:3) * [sPosLF_if(1,1); sPosLF_if(2,1);
sPosLF_if(3,1)];     %inferior vert. screws (upper fixture)
sPosGl_if(1:3,2) = T_G_LFf(1:3,1:3) * [sPosLF_if(1,2); sPosLF_if(2,2);
sPosLF_if(3,2)];
sPosGl_if(1:3,3) = T_G_LFf(1:3,1:3) * [sPosLF_if(1,3); sPosLF_if(2,3);
sPosLF_if(3,3)];

%
%screw 1 is column 1, screw 2 is column 2, screw 3 is column 3

%% Write file
fidstr = ['z:\Ortho Research 3\FergusonLab\Students\Hartman, Robert\ATM
Development\Attachment\022610\faroSP_' state date '.txt'];
fid1 = fopen(fidstr, 'wt');
fprintf(fid1, '%06.4d \t %06.4d \t %06.4d \n', sPosGu_if');
fprintf(fid1, '\n');
fprintf(fid1, '%06.4d \t %06.4d \t %06.4d \n', sPosGl_if');
fprintf(fid1, '\n');
% fprintf(fid1, '%06.4d \t %06.4d \t %06.4d \n', sPosSV_if');
% fprintf(fid1, '\n');
% fprintf(fid1, '%06.4d \t %06.4d \t %06.4d \n', sPosIV_if');
% fprintf(fid1, '\n');
fclose(fid1);
```

B.2.2 Method (b)

This code (1) loads screw-position files before and after a motion captured by the Faro Arm using Rhinocerous 3D, (2) creates local—fixture and anatomic (vertebral)—coordinate systems, (3) forms local-to-global transformations for both LCSs before and after motion, (4) forms anatomic-to-fixture transformations before and after motion, (5) extracts the rotations and

positions from each spatial transformation based on roll-pitch-yaw (RxRyRz), (6) calculates the differences between initial and final angles and positions, and (7) prints the results to a text file.

```
%analyzes .txt files generated from Rhino program using FARO ARM postCrp
date = '021710';
state = '0-0B_';

%need to modify file name as necessary
faroPre = load('z:\Ortho Research 3\FergusonLab\Students\Hartman, Robert\ATM
Development\Attachment\021710\FARO_postCrpB_021710.txt');
faroPost = load('z:\Ortho Research 3\FergusonLab\Students\Hartman, Robert\ATM
Development\Attachment\021710\FARO_postCrpC_021710.txt');

for k = 1:2
    if k == 1
        faro = faroPre;
    elseif k == 2
        faro = faroPost;
    end

    %2/16/10 - order of digitizing: UF>SV>LF>IV
    %2/17 & 2/18 - " : UF>LF>SV>IV
    %teasing out the three points per item
    UF = faro(10:12,:); %upper fixture
    LF = faro(7:9,:); %superior vertebra
    SV = faro(4:6,:); %lower fixture
    IV = faro(1:3,:); %inferior vertebra

    %% superior fixture-specimen transformation
        %form coordinate systems for each item
        %upper fixture
        UF1 = UF(3,:) - UF(2,:);
        UF2 = UF(1,:) - UF(2,:);
        UF3 = cross(UF1,UF2);

        %normalize vectors to form transformation matrix
        UFx = UF1/norm(UF1);
        UFy = UF2/norm(UF2);
        UFz = UF3/norm(UF3);

        %upper fixture in global RF
        T_G_UF = [UFx(1), UFy(1), UFz(1), UF(2,1);...
            UFx(2), UFy(2), UFz(2), UF(2,2);...
            UFx(3), UFy(3), UFz(3), UF(2,3);
            0, 0, 0, 1];

        %superior vertebra
        SV1 = SV(3,:) - SV(2,:);
        SV2 = SV(1,:) - SV(2,:);
        SV3 = cross(SV1,SV2);

        %normalize vectors to form transformation matrix
        SVx = SV1/norm(SV1);
```

```
    SVy = SV2/norm(SV2);
    SVz = SV3/norm(SV3);

    %superior vertebra in global RF
    T_G_SV = [SVx(1), SVy(1), SVz(1), SV(2,1);...
        SVx(2), SVy(2), SVz(2), SV(2,2);...
        SVx(3), SVy(3), SVz(3), SV(2,3);
        0, 0, 0, 1];

    %translation b/w fixture (UF) and specimen (SV)
    if k == 1
        T_UF_SVi = inv(T_G_UF) * T_G_SV;
        T_G_SVi = T_G_SV;
    elseif k == 2
        T_UF_SVf = inv(T_G_UF) * T_G_SV;
        T_G_SVf = T_G_SV;
    end

%% inferior fixture-specimen transformation
    %form coordiate systems for each item
    %lower fixture
    LF1 = LF(3,:) - LF(2,:);
    LF2 = LF(1,:) - LF(2,:);
    LF3 = cross(LF1,LF2);

    %normalize vectors to form tranformation matrix
    LFx = LF1/norm(LF1);
    LFy = LF2/norm(LF2);
    LFz = LF3/norm(LF3);

    %upper fixture in global RF
    T_G_LF = [LFx(1), LFy(1), LFz(1), LF(2,1);...
        LFx(2), LFy(2), LFz(2), LF(2,2);...
        LFx(3), LFy(3), LFz(3), LF(2,3);...
        0, 0, 0, 1];

    %inferior vertebra
    IV1 = IV(3,:) - IV(2,:);
    IV2 = IV(1,:) - IV(2,:);
    IV3 = cross(IV1,IV2);

    %normalize vectors to form tranformation matrix
    IVx = IV1/norm(IV1);
    IVy = IV2/norm(IV2);
    IVz = IV3/norm(IV3);

    %superior vertebra in global RF
    T_G_IV = [IVx(1), IVy(1), IVz(1), IV(2,1);...
        IVx(2), IVy(2), IVz(2), IV(2,2);...
        IVx(3), IVy(3), IVz(3), IV(2,3);...
        0, 0, 0, 1];

    %translation b/w fixture (LF) and specimen (IV)
    if k == 1
        T_LF_IVi = inv(T_G_LF) * T_G_IV;
```

```
            T_G_IVi = T_G_IV;
        elseif k == 2
            T_LF_IVf = inv(T_G_LF) * T_G_IV;
            T_G_IVf = T_G_IV;
        end

end

%upper fixture-superior vertebra
    %superior vertebra relative to upper fixture at initial time: angles and
positions
    angles_svufi = rad2deg(tr2rpy(T_UF_SVi));
    positions_svufi = T_UF_SVi(1:3,4)';

    %superior vertebra relative to upper fixture at initial time: angles and
positions
    angles_svuff = rad2deg(tr2rpy(T_UF_SVf));
    positions_svuff = T_UF_SVf(1:3,4)';

    %difference b/w final and initial position in UFCS: rotations and
displacements
    rotations_svuf = angles_svuff - angles_svufi;
    displacements_svuf = positions_svuff - positions_svufi;

%lower fixture-inferior vertebra
    %superior vertebra relative to upper fixture at initial time: angles and
positions
    angles_ivlfi = rad2deg(tr2rpy(T_LF_IVi));
    positions_ivlfi = T_LF_IVi(1:3,4)';

    %superior vertebra relative to upper fixture at initial time: angles and
positions
    angles_ivlff = rad2deg(tr2rpy(T_LF_IVf));
    positions_ivlff = T_LF_IVf(1:3,4)';

    %difference b/w final and initial position in UFCS: rotations and
displacements
    rotations_ivlf = angles_ivlff - angles_ivlfi;
    displacements_ivlf = positions_ivlff - positions_ivlfi;

%compile differences in larger array
T_off = [rotations_svuf; rotations_ivlf; displacements_svuf;
displacements_ivlf];

%% Write file
fidstring = ['z:\Ortho Research 3\FergusonLab\Students\Hartman, Robert\ATM
Development\Attachment\021710\faroLT_' state date '.txt'];
fid1 = fopen(fidstring, 'wt');
fprintf(fid1, '%06.4d \t %06.4d \t %06.4d \n', T_off');
fprintf(fid1, '\n');
```

APPENDIX C

INTRADISCAL PRESSURE

C.1 PRECONDITIONING PEAK ANALYSIS

This code (1) plots pressure vectors and (2) allows graphical selection of pressure peaks (3) during which the statistics (maximum, minimum, mean, and standard deviation) of selected readings can be calculated.

```
%Rob Hartman, thanks to Bernard Bechara
%25 Jan 2010
%Analysis of cyclic IDP data

%IDP data (time, pressure) needs to be loaded into Matlab (idpDataReadin.m)
%cyclic closed system
x = IDP2_cycWD(:,1);
y = IDP2_cycWD(:,2);
plot(x,y)
title('IDP - extrema analysis')
xlabel('time')
ylabel('IDP (MPa)')
hold on

i=1;
while i <= 10
%code to use rubber box and select a region on the plot
k = waitforbuttonpress;
point1 = get(gca,'CurrentPoint');    % button down detected
finalRect = rbbox;                   % return figure units
point2 = get(gca,'CurrentPoint');    % button up detected
point1 = point1(1,1:2);              % extract x and y
point2 = point2(1,1:2);

% plot selected box on figure
minx=min(point1(1,1),point2(1,1));
miny=min(point1(1,2),point2(1,2));
width=abs(diff([point1(1,1),point2(1,1)]));
height=abs(diff([point1(1,2),point2(1,2)]));
rectangle('Position',[minx, miny,width,height],'LineWidth',3)

% get data within the box and plot in red
f=find(x > minx & x < max(point1(1,1),point2(1,1))...
```

```
    & y > miny & y < max(point1(1,2),point2(1,2)));
plot(x(f),y(f),'r')

% get stats on data within the box
idpMax(i) = max(y(f));
idpMin(i) = min(y(f));
idpAvg(i) = mean(y(f));      % average of y value
idpStd(i) = std(y(f));
timeAvg(i) = mean(x(f));      % average of x value

i=i+1;
end

idpStats = [idpMax; idpMin; idpAvg; idpStd; timeAvg];
%average of average pressures:
idp_meanPeak = mean(idpStats(3,:));
%standard deviations of peaks (average values across peaks)
idp_stdPeak = std(idpStats(3,:));
idpCycPkStats = [idp_meanPeak,idp_stdPeak];
```

C.2 CREEP ANALYSIS

```
% analysis of IDP creep analysis

%IDP data (time, pressure) needs to be loaded into Matlab (idpDataReadin.m)
%cyclic closed system
x = IDP_creepWD(:,1); %IDP2_creepWD(:,1);
y = IDP_creepWD(:,2); %IDP2_creepWD(:,2);

[peakIDP, pkTime] = max(y);
creepPhase = y(pkTime:length(y)); %IDPs after max; during creep phase
idpCreep_range = peakIDP - min(creepPhase); %max IDP value - min IDP value
from creep phase
idpCreep_std = std(creepPhase); %stdev over creep phase
idpCreep_avg = mean(y(pkTime:10000));   %10,000 arbitrary but based on 1100
sec/ 10Hz collection
idpCreep_early = mean(y(pkTime:pkTime+600));   %first minute of creep
idpCreep_mid = mean(y(pkTime+4800:pkTime+6000));    %8-10 minute average
idpCreep_late = mean(y(pkTime+9600:pkTime+10800));  %16-18 minute average
% idpCreep_rms = rms(creepPhase); %rms over creep phase

% get stats
idpCreep_stats = [peakIDP; idpCreep_range; 0; idpCreep_std; idpCreep_avg;
idpCreep_early; idpCreep_mid; idpCreep_late];
% change in creep comes from Excel directly
```

APPENDIX D

THERMAL ANALYSIS

D.1 THERMAL MODEL -EARLY CHAMBER CONCEPT

A simplified thermodynamic model of a well-mixed fluid in a cylindrical chamber was used to observe the effect of tubing size, chamber dimensions, and flow rate and estimate the effect of insulation on temperature within the chamber. While the model was never updated for solid-walled, stainless-steel fixtures, it did predict that smaller tubing inner diameter led to less heat lost across the chamber. It also demonstrated that increasing flow rates from 1 to 40 ml/min caused significant heat loss (>5 ºC) to less than 0.5 ºC lost across the chamber. Using the thermal conductivity of fiberglass insulation and estimated geometry of insulation, the model predicted improved heat retention with fiberglass addition. While the model assumed steady state and no change in temperature along the chamber (well-mixed), these results motivated experimentation.

D.1.1 MATLAB CODE IMPLEMENTING TRANSPORT EQUATION AND STATING ASSUMPTIONS

This basic code was varied to solve for different design parameters. Plots of chamber temperature vs. tubing I.D., chamber I.D., volumetric flow rates, +/- insulation, and varying assumed heat transfer coefficient were generated.

```
%Solves for temperature in tubing of organ culture system
%Assumes: (1) steady-state & (2) well-mixed.  The consequence of (2) is
%that temp. does not vary within the tubing.  Changes can occur from the
%tubing to the chamber based on varying wall conditions.

%This code does not account for the altered thermal conditions of the
%chamber (different walls, size(radius, area), etc)

%clear old variables
clear d D A Q Re

%% determine Reynolds number

%pre-assign volumetric flow matrix
n = 10; %number of Q-guesses
Q = zeros(1,n);

%vary volumetric flow rates
Q(1) = 1.8333*(10^-4) * (.001); %volumetric flow, (L/s)*(m^3/L)
for i=2:n
    Q(i) = Q(i-1) * 2;
end

k = (1) * (10^-6); %kinematic viscosity, (mm^2/s)*(m^2/mm^2) (assmpt:WATER)

%vary diameter
% d = 0.0625:0.01:0.25;  %inches
d = 1.5:.25:2.5;
D = d * (2.54) * (10^-2); %diameter, (in)*(cm/in)*(m/cm)
A = (pi/4) * (D.^2); %pipe cross-sectional area, m^2

for j = 1:n
    for i=1:length(D)
        Re(j,i) = (Q(j) * D(i))/(k * A(i)); %Reynold's number
    end
end

%plot diameter vs. Re for varying flow rates
% for i=1:n
%     hold on
%     plot(d,Re(i,:));
```

```
% end

%% Heat transfer - tube
%variables:
L = 0.5; %length of tubing b/w incubator & chamber, m
R_in = D/2; %tube inner radius, m (ARRAY)
R_out = R_in + .002; %tube outer radius

rho = 10^3; %media density, kg/m^3 (WATER)
c_p = 4180; %media heat capacity, J/(kg K)
% Q_m = 1.1; %volumetric fluid flow, ml/min (1.833 x 10^-5 L/sec)
U_H_in = zeros(1,length(d)); %overall heat transfer coeff, W/(m*K)
h_in = 500 ; %heat transfer coeff (media->wall) (Assmpt: h_water (500-
10,000))
h_out = 10; %heat transfer coeff (wall->air) (Assmpt: h_air (10-100))
k = 0.16; %thermal conductivity, W/(m*K)
A_in = 2*pi*R_in*L; %inner area of tubing
A_out = 2*pi*R_out*L; %outer area of tubing
T_mt = zeros(n,length(d)); %temp. of media, ?K
T_m_in = 37; %temp of media entering the tubing (leaving incubator), C
T_air = 21; %temp of surrounding air

%overall heat transfer coeff needs determined
%based on conduction transport across membrane (h_in, h_out, k, area)
%overall heat transfer is directly proportional to heat transfer
%coefficients (h_in, h_out)
for j=1:n
    for i=1:length(D)
        U_H_in(i) = 1 / ((1 / h_in) + ((R_in(i) * log(R_out(i)/R_in(i))) / k)
+ (A_in(i) / (A_out(i) * h_out)));

    %finds temp. in the media (in the tubing) based on well-mixed assumption
        T_mt(j,i) = (((rho)*(c_p)*(Q(j))*(T_m_in)) +
((U_H_in(i))*(A_in(i))*(T_air))) /...
            (((rho)*(c_p)*(Q(j))) + (U_H_in(i))*(A_in(i)));
    end
end

%% Heat transfer - chamber
%variables:
L = 0.1; %length of tubing b/w incubator & chamber, m
R_in = D/2; %tube inner radius, m (ARRAY)
R_out = R_in + .001; %tube outer radius

rho = 10^3; %media density, kg/m^3 (WATER)
c_p = 4180; %media heat capacity, J/(kg K)
% Q_m = 1.1; %volumetric fluid flow, ml/min (1.833 x 10^-5 L/sec)
U_H_in = zeros(1,length(d)); %overall heat transfer coeff, W/(m*K)
h_in = 500 ; %heat transfer coeff (media->wall) (Assmpt: h_water (500-
10,000))
h_out = 10; %heat transfer coeff (wall->air) (Assmpt: h_air (10-100))
k = 0.16; %thermal conductivity, W/(m*K)
A_in = 2*pi*R_in*L; %inner area of tubing
A_out = 2*pi*R_out*L; %outer area of tubing
T_mc = zeros(n,length(d)); %temp. of media, ?K
% T_m_in = 37; %temp of media entering the tubing (leaving incubator), C
```

```
T_air = 21; %temp of surrounding air

%overall heat transfer coeff needs determined
%based on conduction transport across membrane (h_in, h_out, k, area)
%overall heat transfer is directly proportional to heat transfer
%coefficients (h_in, h_out)
for j=1:n
    for i=1:length(D)
        U_H_in(i) = 1 / ((1 / h_in) + ((R_in(i) * log(R_out(i)/R_in(i))) / k)
+ (A_in(i) / (A_out(i) * h_out)));

    %finds temp. in the media (in the tubing) based on well-mixed assumption
        T_mc(j,i) = (((rho)*(c_p)*(Q(j))*(T_mt(j,i))) +
((U_H_in(i))*(A_in(i))*(T_air))) /...
            (((rho)*(c_p)*(Q(j))) + (U_H_in(i))*(A_in(i)));
    end
end

%plot temp_media_chamber vs. x
for i=1:n
    hold on
    subplot(2,1,1),plot(d,T_mc(i,:));
    title(['Temperature in chamber (well-mixed) for varying flow rates. h_
in, h_ out: ',num2str(h_in),' ',num2str(h_out)])
    xlabel('Diameter (in)');
    ylabel('Temperature in end of tubing (C)');

    subplot(2,1,2),plot(d,T_mt(i,:));
    title(['Temperature in chamber (well-mixed) for varying flow rates. h_
in, h_ out: ',num2str(h_in),' ',num2str(h_out)])
    xlabel('Diameter (in)');
    ylabel('Temperature in end of chamber (C)');

end
```

D.1.2 TEMPERATURE DROP ACROSS THE CHAMBER

Temperature recordings in Figures D.1.2.1 and D.1.2.2 were made at the inlet and outlet of the chamber, respectively.

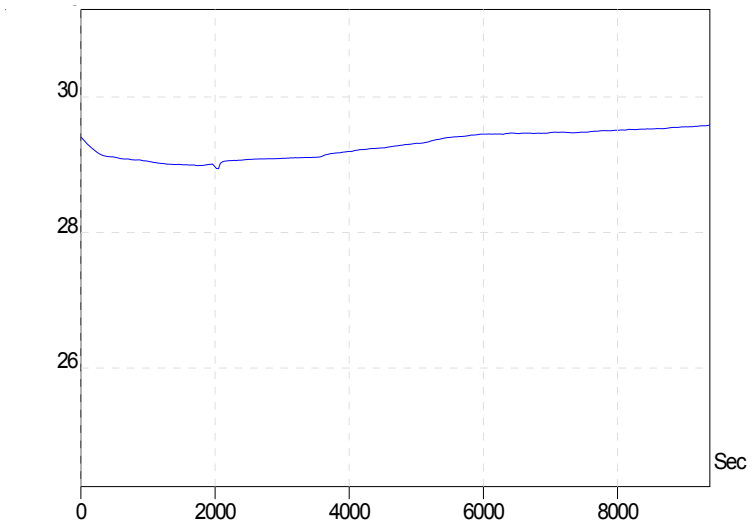

Figure D.1.2.2. Temperature (C °) with RTD in upper fixture

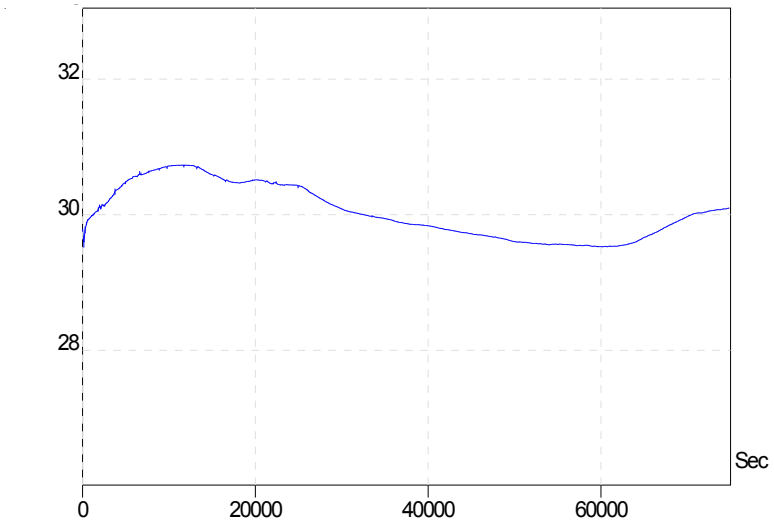

Figure D.1.2.1. Temperature (C °) with RTD in lower fixture

D.1.3 MOVING INSULATED CHAMBER FROM 29ºC TO 25ºC AMBIENT AIR

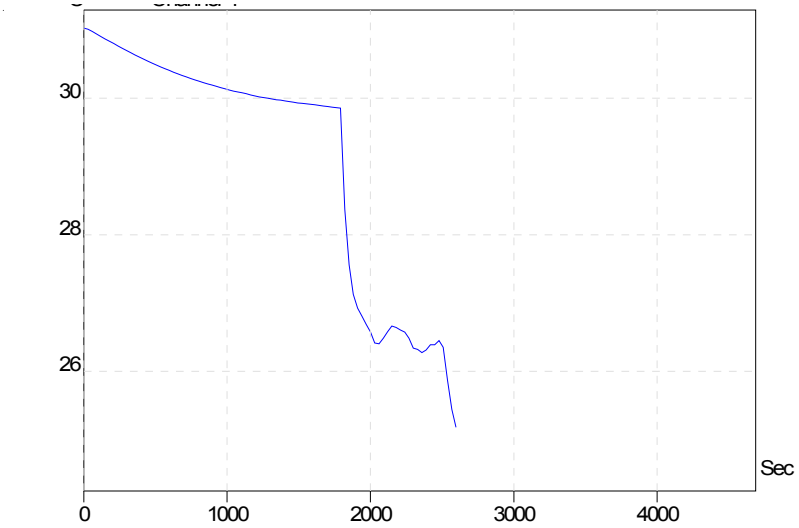

Figure D.1.3. Temperature (C °) within chamber removing it from heated surface to benchtop

D.1.4 EFFECT OF VARYING FLOW RATE ON CHAMBER TEMPERATURES

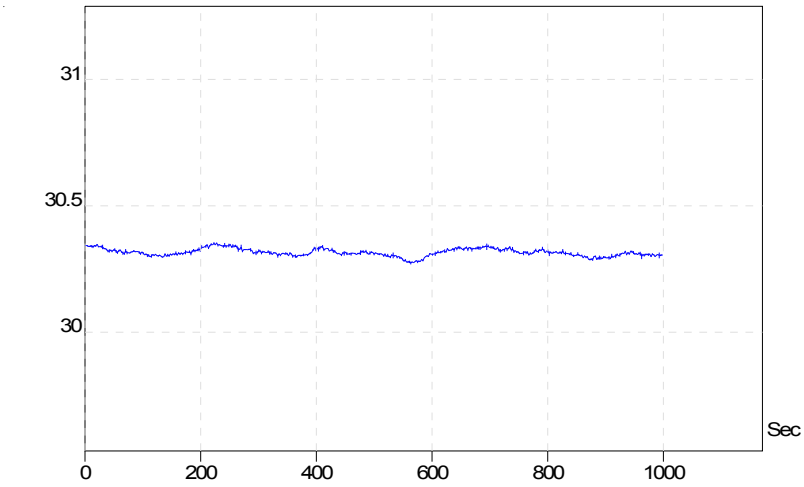

Figure D.1.4.1. Temperature (C °) at flow rate of 5 ml/min

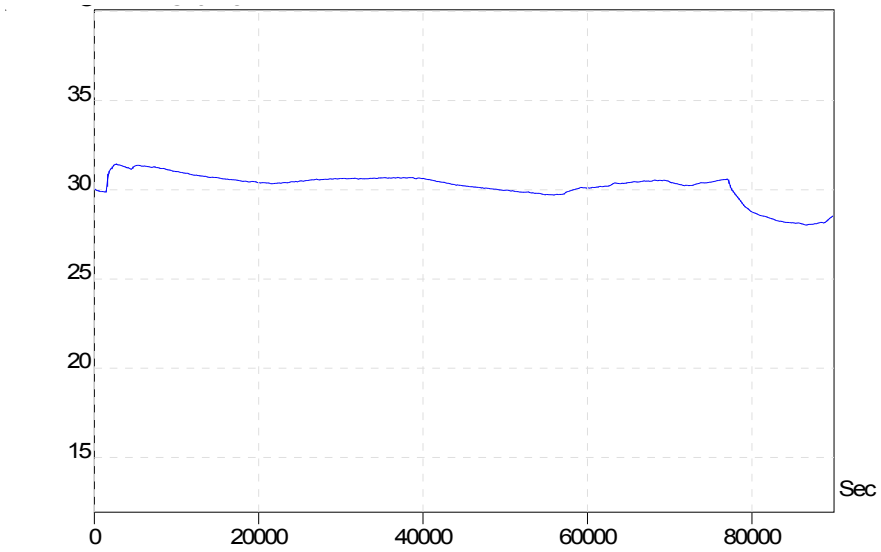

Figure D.1.4.2. Temperature (C °) with flow rate changes. Flow rate increased from 5-10 ml/min at ~1,500 s. Flow rate increased from 10-12.5 ml/min at ~55,000

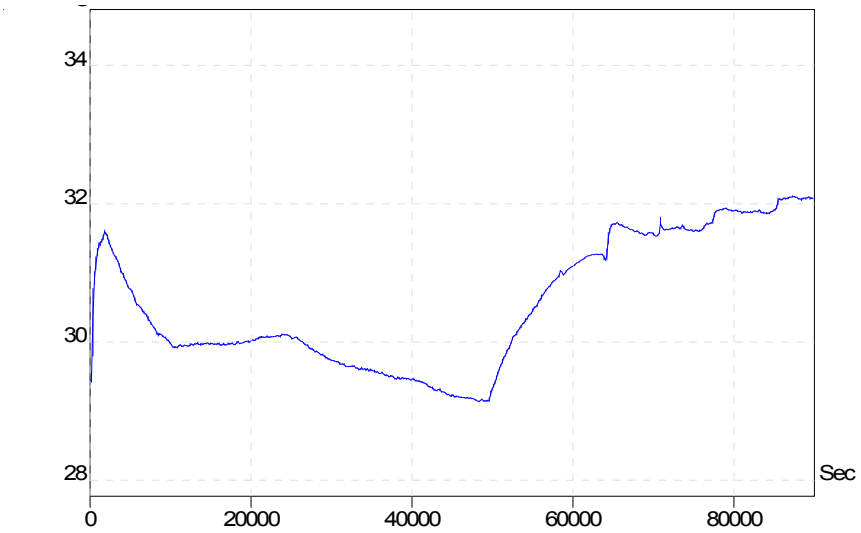

Figure D.1.4.3 Temperature (C °) with flow rate changes. Initial flow rate at 10 ml/min; chamber leak interrupted at ~2,000 s. Increased flow rate to 20 ml/min; chamber leak again at ~26,000 s interrupted temperature increases. Increased flow rate to 30 ml/min at ~49,000 s. Increased flow rate to 35 ml/min at ~64,000 s

APPENDIX E

DISSOLVED OXYGEN ANALYSIS

E.1 USE OF OXYGEN PROBE

E.1.1 CALIBRATION

```
%Rob Hartman - 2/2/2010
%DO calibration ("O and 0's")

%Find equilibrium values for DO collection

%At 21% O2 (DI water equilibrated for 1+ hour)
fn21 = length(DOPV_21_DIH2O_RT); %length of matrix
in21 = round(.5*fn21);  %mid-way of matrix
avgDO21_RT = mean(DOPV_21_DIH2O_RT(in21:fn21,2)); %probe voltage at RT

%At 0% DO - calibration solution (cole-parmer purchased)
fn0 = length(DOPV_0soln_RT); %length of matrix
in0 = round(.5*fn0);  %mid-way of matrix
avgDO0_RT = mean(DOPV_0soln(in0:fn0,2)); %probe voltage at RT

cDOPV = [avgDO0_RT, avgDO21_RT];
cDOPP = [0,21];

lin_coeff = polyfit(cDOPV,cDOPP,1);  %finds coefficients (slope) of linear
polynomial in voltage (x) w/ mass output (p(x))
lin_fit = polyval(lin_coeff,-0.45:.01:0.1); %makes new poly based on
coefficients above
plot(cDOPV,cDOPP,'ro',-0.45:.01:0.1,lin_fit,'b-');
title('Voltage vs. %O2: Linear Fit')
ylabel('% O2')
xlabel('DOP voltage (V)')

%export data to .txt file
calPoly = fopen('dopCalibrationChanging.txt', 'wt'); %opens file in write-
text mode
fprintf(calPoly, '%06.4d \t %06.4d \n', lin_coeff);
fclose(calPoly);
```

E.1.2 CONVERSION FUNCTION

```
function [pDO_37 pDO_25] = DOConvert(DOPVolt)
%must run calibration prior to function
%reads in the coeffcients of the curve fit (intercept, slope)
%dopCalibration012810.txt is set up s.t. the first row corresponds to 37
%degC and the second row corresponds to 25degC (RT).
%[x1 x0] ~ [m b]

FitData = importdata('dopCalibration031510.txt', '\t');
%37 deg
b37 = FitData(1,2);  %y-intercept
m37 = FitData(1,1);   %slope

% 25 deg
b25 = FitData(2,2);  %y-intercept
m25 = FitData(2,1);   %slope

%collecting both b/c fluid warms up over time & might hover b/w the two...
pDO_37 = m37*DOPVolt + b37;  %volt to %O2 @ 37deg C
pDO_25 = m25*DOPVolt + b25;  %volt to %O2 @ 37deg C
```

E.1.3 EXPERIMENTATION COLLECTION TIMER

This timer was integrated with the general control code for the ATM, thus at each time of position and load data acquisition, DOP voltage is recorded.

```
%Timer for DO Probe (DOcollect.m, ...)

i=i+1;

%get DO probe information
[Error DOPvolt ]= ljud_eGet(ljHandle,LJ_ioGET_AIN,2,0,0);
[pDO_37 pDO_25] = DOConvert(DOPvolt);
%time stamp
doTime = toc;

figure(DOfig);
plot(doTime,DOPvolt,'.b');
xlim([0 doTestLength]);
hold on

%time-stamped DOP voltages saved
% DOPV(i,:) = [doTime, DOPvolt];
```

```
DOPVdata(i,:) = [doTime, DOPvolt, pDO_37, pDO_25];

if i > 2
    if doTime > doTestLength
         stopDMCM(port1);
         stop(T_DOP);
    end
end
```

E.2 INITIAL DISSOLVED OXYGEN READINGS (E.G.)

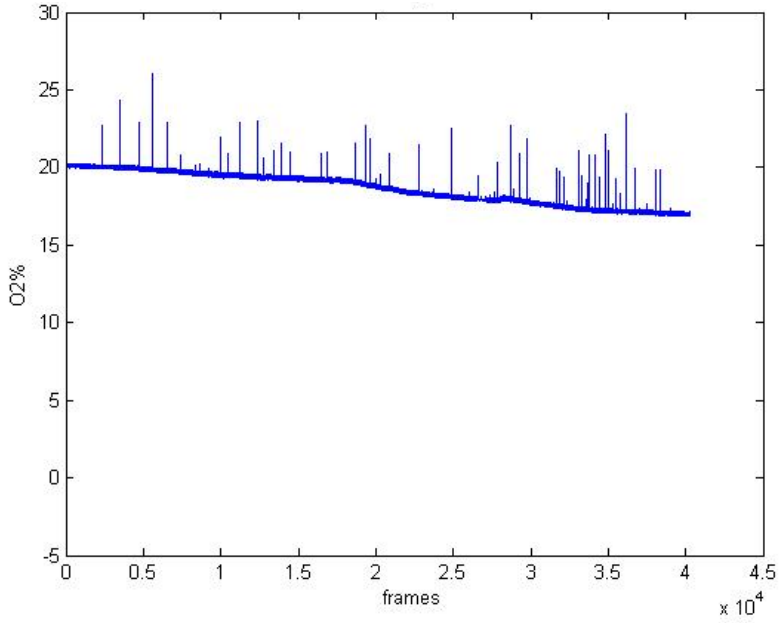

Figure E.2. Dissolved oxygen probe: initial $\%O_2$ readings in chamber fluid

BIBLIOGRAPHY

1. Andersson, G.B., *Epidemiological features of chronic low-back pain.* Lancet, 1999. **354**(9178): p. 581-5.

2. Deyo, R.A. and J.N. Weinstein, *Low back pain.* N Engl J Med, 2001. **344**(5): p. 363-70.

3. Rubin, D.I., *Epidemiology and risk factors for spine pain.* Neurol Clin, 2007. **25**(2): p. 353-71.

4. Chou, R., et al., *Correction: Diagnosis and treatment of low back pain.* Ann Intern Med, 2008. **148**(3): p. 247-8.

5. Choi, B.K., et al., *Exercises for prevention of recurrences of low-back pain.* Cochrane Database Syst Rev, 2010(1): p. CD006555.

6. Smith, C. and K. Grimmer-Somers, *The treatment effect of exercise programmes for chronic low back pain.* J Eval Clin Pract, 2010. **16**(3): p. 484-91.

7. van Middelkoop, M., et al., *Exercise therapy for chronic nonspecific low-back pain.* Best Pract Res Clin Rheumatol, 2010. **24**(2): p. 193-204.

8. Rubinstein, S.M., et al., *A systematic review on the effectiveness of complementary and alternative medicine for chronic non-specific low-back pain.* Eur Spine J, 2010. **19**(8): p. 1213-28.

9. Chou, R., et al., *Surgery for low back pain: a review of the evidence for an American Pain Society Clinical Practice Guideline.* Spine (Phila Pa 1976), 2009. **34**(10): p. 1094-109.

10. Dagenais, S., et al., *Can cost utility evaluations inform decision making about interventions for low back pain?* Spine J, 2009. **9**(11): p. 944-57.

11. Deyo, R.A., et al., *Overtreating chronic back pain: time to back off?* J Am Board Fam Med, 2009. **22**(1): p. 62-8.

12. Deyo, R.A., S.K. Mirza, and B.I. Martin, *Back pain prevalence and visit rates: estimates from U.S. national surveys, 2002.* Spine (Phila Pa 1976), 2006. **31**(23): p. 2724-7.

13. Oesch, P., et al., *Effectiveness of exercise on work disability in patients with non-acute non-specific low back pain: Systematic review and meta-analysis of randomised controlled trials.* J Rehabil Med, 2010. **42**(3): p. 193-205.

14. Deyo, R.A., A.K. Diehl, and M. Rosenthal, *How many days of bed rest for acute low back pain? A randomized clinical trial.* N Engl J Med, 1986. **315**(17): p. 1064-70.

15. Iatridis, J.C., et al., *Effects of mechanical loading on intervertebral disc metabolism in vivo.* J Bone Joint Surg Am, 2006. **88 Suppl 2**: p. 41-6.

16. Hayden, J.A., et al., *What is the prognosis of back pain?* Best Pract Res Clin Rheumatol, 2010. **24**(2): p. 167-79.

17. Roberts, S., et al., *1991 Volvo Award in basic sciences. Collagen types around the cells of the intervertebral disc and cartilage end plate: an immunolocalization study.* Spine (Phila Pa 1976), 1991. **16**(9): p. 1030-8.

18. Clouet, J., et al., *The intervertebral disc: from pathophysiology to tissue engineering.* Joint Bone Spine, 2009. **76**(6): p. 614-8.

19. Brickley-Parsons, D. and M.J. Glimcher, *Is the chemistry of collagen in intervertebral discs an expression of Wolff's Law? A study of the human lumbar spine.* Spine (Phila Pa 1976), 1984. **9**(2): p. 148-63.

20. Setton, L.A. and J. Chen, *Cell mechanics and mechanobiology in the intervertebral disc.* Spine (Phila Pa 1976), 2004. **29**(23): p. 2710-23.

21. Cao, L., F. Guilak, and L.A. Setton, *Three-dimensional morphology of the pericellular matrix of intervertebral disc cells in the rat.* J Anat, 2007. **211**(4): p. 444-52.

22. Sive, J.I., et al., *Expression of chondrocyte markers by cells of normal and degenerate intervertebral discs.* Mol Pathol, 2002. **55**(2): p. 91-7.

23. Clouet, J., et al., *Identification of phenotypic discriminating markers for intervertebral disc cells and articular chondrocytes.* Rheumatology (Oxford), 2009. **48**(11): p. 1447-50.

24. Sowa, G. and S. Agarwal, *Cyclic tensile stress exerts a protective effect on intervertebral disc cells.* Am J Phys Med Rehabil, 2008. **87**(7): p. 537-44.

25. Guilak, F., et al., *Viscoelastic properties of intervertebral disc cells. Identification of two biomechanically distinct cell populations.* Spine (Phila Pa 1976), 1999. **24**(23): p. 2475-83.

26. Hunter, C.J., J.R. Matyas, and N.A. Duncan, *The three-dimensional architecture of the notochordal nucleus pulposus: novel observations on cell structures in the canine intervertebral disc.* J Anat, 2003. **202**(Pt 3): p. 279-91.

27. Trout, J.J., J.A. Buckwalter, and K.C. Moore, *Ultrastructure of the human intervertebral disc: II. Cells of the nucleus pulposus.* Anat Rec, 1982. **204**(4): p. 307-14.

28. Trout, J.J., et al., *Ultrastructure of the human intervertebral disc. I. Changes in notochordal cells with age.* Tissue Cell, 1982. **14**(2): p. 359-69.

29. Baer, A.E., et al., *The micromechanical environment of intervertebral disc cells determined by a finite deformation, anisotropic, and biphasic finite element model.* J Biomech Eng, 2003. **125**(1): p. 1-11.

30. Cao, L., F. Guilak, and L.A. Setton, *Pericellular Matrix Mechanics in the Anulus Fibrosus Predicted by a Three-Dimensional Finite Element Model and In Situ Morphology.* Cell Mol Bioeng, 2009. **2**(3): p. 306-319.

31. Malko, J.A., W.C. Hutton, and W.A. Fajman, *An in vivo magnetic resonance imaging study of changes in the volume (and fluid content) of the lumbar intervertebral discs during a simulated diurnal load cycle.* Spine (Phila Pa 1976), 1999. **24**(10): p. 1015-22.

32. McCarty, N.A. and R.G. O'Neil, *Calcium signaling in cell volume regulation.* Physiol Rev, 1992. **72**(4): p. 1037-61.

33. McMillan, D.W., G. Garbutt, and M.A. Adams, *Effect of sustained loading on the water content of intervertebral discs: implications for disc metabolism.* Ann Rheum Dis, 1996. **55**(12): p. 880-7.

34. Alexopoulos, L.G., et al., *Alterations in the mechanical properties of the human chondrocyte pericellular matrix with osteoarthritis.* J Biomech Eng, 2003. **125**(3): p. 323-33.

35. Alexopoulos, L.G., et al., *Osteoarthritic changes in the biphasic mechanical properties of the chondrocyte pericellular matrix in articular cartilage.* J Biomech, 2005. **38**(3): p. 509-17.

36. Guilak, F., et al., *The deformation behavior and mechanical properties of chondrocytes in articular cartilage.* Osteoarthritis Cartilage, 1999. **7**(1): p. 59-70.

37. Kim, E., F. Guilak, and M.A. Haider, *The dynamic mechanical environment of the chondrocyte: a biphasic finite element model of cell-matrix interactions under cyclic compressive loading.* J Biomech Eng, 2008. **130**(6): p. 061009.

38. Guilak, F.a.M.V.C., *Determination of the mechanical response of the chondrocytes in situ using finite element modeling and confocal microscopy.* ASME Advances in Bioengineering;BED, 1992. **22**: p. 21-24.

39. Ratcliffe, A., J.A. Tyler, and T.E. Hardingham, *Articular cartilage cultured with interleukin 1. Increased release of link protein, hyaluronate-binding region and other proteoglycan fragments.* Biochem J, 1986. **238**(2): p. 571-80.

40. Roberts, S., et al., *Proteoglycan components of the intervertebral disc and cartilage endplate: an immunolocalization study of animal and human tissues.* Histochem J, 1994. **26**(5): p. 402-11.

41. Roughley, P.J., R.J. White, and A.R. Poole, *Identification of a hyaluronic acid-binding protein that interferes with the preparation of high-buoyant-density proteoglycan aggregates from adult human articular cartilage.* Biochem J, 1985. **231**(1): p. 129-38.

42. Tyler, J.A., *Chondrocyte-mediated depletion of articular cartilage proteoglycans in vitro.* Biochem J, 1985. **225**(2): p. 493-507.

43. Cole, T.C., P. Ghosh, and T.K. Taylor, *Variations of the proteoglycans of the canine intervertebral disc with ageing.* Biochim Biophys Acta, 1986. **880**(2-3): p. 209-19.

44. Inerot, S. and I. Axelsson, *Structure and composition of proteoglycans from human annulus fibrosus.* Connect Tissue Res, 1991. **26**(1-2): p. 47-63.

45. Korecki, C.L., et al., *Intervertebral disc cell response to dynamic compression is age and frequency dependent.* J Orthop Res, 2009. **27**(6): p. 800-6.

46. Iatridis, J.C., et al., *Alterations in the mechanical behavior of the human lumbar nucleus pulposus with degeneration and aging.* J Orthop Res, 1997. **15**(2): p. 318-22.

47. Roughley, P.J., *Biology of intervertebral disc aging and degeneration: involvement of the extracellular matrix.* Spine (Phila Pa 1976), 2004. **29**(23): p. 2691-9.

48. Iatridis, J.C., et al., *Degeneration affects the anisotropic and nonlinear behaviors of human anulus fibrosus in compression.* J Biomech, 1998. **31**(6): p. 535-44.

49. Gu, W.Y., et al., *The anisotropic hydraulic permeability of human lumbar anulus fibrosus. Influence of age, degeneration, direction, and water content.* Spine (Phila Pa 1976), 1999. **24**(23): p. 2449-55.

50. Gu, W.Y., et al., *Streaming potential of human lumbar anulus fibrosus is anisotropic and affected by disc degeneration.* J Biomech, 1999. **32**(11): p. 1177-82.

51. Boos, N., et al., *Classification of age-related changes in lumbar intervertebral discs: 2002 Volvo Award in basic science.* Spine (Phila Pa 1976), 2002. **27**(23): p. 2631-44.

52. Nguyen-minh, C., et al., *Measuring diffusion of solutes into intervertebral disks with MR imaging and paramagnetic contrast medium.* AJNR Am J Neuroradiol, 1998. **19**(9): p. 1781-4.

53. Urban, J.P., S. Holm, and A. Maroudas, *Diffusion of small solutes into the intervertebral disc: as in vivo study.* Biorheology, 1978. **15**(3-4): p. 203-21.

54. Urban, J.P. and S. Roberts, *Degeneration of the intervertebral disc.* Arthritis Res Ther, 2003. **5**(3): p. 120-30.

55. Vernon-Roberts, B., R.J. Moore, and R.D. Fraser, *The natural history of age-related disc degeneration: the influence of age and pathology on cell populations in the L4-L5 disc.* Spine (Phila Pa 1976), 2008. **33**(25): p. 2767-73.

56. Gruber, H.E., et al., *Analysis of cell death and vertebral end plate bone mineral density in the annulus of the aging sand rat.* Spine J, 2008. **8**(3): p. 475-81.

57. Horner, H.A. and J.P. Urban, *2001 Volvo Award Winner in Basic Science Studies: Effect of nutrient supply on the viability of cells from the nucleus pulposus of the intervertebral disc.* Spine (Phila Pa 1976), 2001. **26**(23): p. 2543-9.

58. Ishihara, H. and J.P. Urban, *Effects of low oxygen concentrations and metabolic inhibitors on proteoglycan and protein synthesis rates in the intervertebral disc.* J Orthop Res, 1999. **17**(6): p. 829-35.

59. Kitano, T., et al., *Biochemical changes associated with the symptomatic human intervertebral disk.* Clin Orthop Relat Res, 1993(293): p. 372-7.

60. Razaq, S., R.J. Wilkins, and J.P. Urban, *The effect of extracellular pH on matrix turnover by cells of the bovine nucleus pulposus.* Eur Spine J, 2003. **12**(4): p. 341-9.

61. Roberts, S., et al., *Transport properties of the human cartilage endplate in relation to its composition and calcification.* Spine (Phila Pa 1976), 1996. **21**(4): p. 415-20.

62. Haschtmann, D., et al., *Vertebral endplate trauma induces disc cell apoptosis and promotes organ degeneration in vitro.* Eur Spine J, 2008. **17**(2): p. 289-99.

63. MacLean, J.J., J.P. Owen, and J.C. Iatridis, *Role of endplates in contributing to compression behaviors of motion segments and intervertebral discs.* J Biomech, 2007. **40**(1): p. 55-63.

64. Cao, L., F. Guilak, and L.A. Setton, *Three-dimensional finite element modeling of pericellular matrix and cell mechanics in the nucleus pulposus of the intervertebral disk based on in situ morphology.* Biomech Model Mechanobiol, 2010.

65. Iatridis, J.C., et al., *The viscoelastic behavior of the non-degenerate human lumbar nucleus pulposus in shear.* J Biomech, 1997. **30**(10): p. 1005-13.

66. Johannessen, W. and D.M. Elliott, *Effects of degeneration on the biphasic material properties of human nucleus pulposus in confined compression.* Spine (Phila Pa 1976), 2005. **30**(24): p. E724-9.

67. Guehring, T., et al., *Stimulation of gene expression and loss of anular architecture caused by experimental disc degeneration--an in vivo animal study.* Spine (Phila Pa 1976), 2005. **30**(22): p. 2510-5.

68. Lotz, J.C., et al., *Compression-induced degeneration of the intervertebral disc: an in vivo mouse model and finite-element study.* Spine (Phila Pa 1976), 1998. **23**(23): p. 2493-506.

69. Johnson, W.E. and S. Roberts, *'Rumours of my death may have been greatly exaggerated': a brief review of cell death in human intervertebral disc disease and implications for cell transplantation therapy.* Biochem Soc Trans, 2007. **35**(Pt 4): p. 680-2.

70. Gruber, H.E., et al., *Senescence in cells of the aging and degenerating intervertebral disc: immunolocalization of senescence-associated beta-galactosidase in human and sand rat discs.* Spine (Phila Pa 1976), 2007. **32**(3): p. 321-7.

71. Anderson, D.G., et al., *Comparative gene expression profiling of normal and degenerative discs: analysis of a rabbit annular laceration model.* Spine (Phila Pa 1976), 2002. **27**(12): p. 1291-6.

72. Nemoto, O., et al., *Matrix metalloproteinase-3 production by human degenerated intervertebral disc.* J Spinal Disord, 1997. **10**(6): p. 493-8.

73. Omlor, G.W., et al., *Changes in gene expression and protein distribution at different stages of mechanically induced disc degeneration--an in vivo study on the New Zealand white rabbit.* J Orthop Res, 2006. **24**(3): p. 385-92.

74. Sobajima, S., et al., *Quantitative analysis of gene expression in a rabbit model of intervertebral disc degeneration by real-time polymerase chain reaction.* Spine J, 2005. **5**(1): p. 14-23.

75. Antoniou, J., et al., *The human lumbar intervertebral disc: evidence for changes in the biosynthesis and denaturation of the extracellular matrix with growth, maturation, ageing, and degeneration.* J Clin Invest, 1996. **98**(4): p. 996-1003.

76. Nerlich, A.G., E.D. Schleicher, and N. Boos, *1997 Volvo Award winner in basic science studies. Immunohistologic markers for age-related changes of human lumbar intervertebral discs.* Spine (Phila Pa 1976), 1997. **22**(24): p. 2781-95.

77. Sakuma, M., et al., *Effect of chondroitinase ABC on matrix metalloproteinases and inflammatory mediators produced by intervertebral disc of rabbit in vitro.* Spine (Phila Pa 1976), 2002. **27**(6): p. 576-80.

78. Le Maitre, C.L., A.J. Freemont, and J.A. Hoyland, *Localization of degradative enzymes and their inhibitors in the degenerate human intervertebral disc.* J Pathol, 2004. **204**(1): p. 47-54.

79. MacLean, J.J., et al., *The effects of short-term load duration on anabolic and catabolic gene expression in the rat tail intervertebral disc.* J Orthop Res, 2005. **23**(5): p. 1120-7.

80. Kang, J.D., et al., *Toward a biochemical understanding of human intervertebral disc degeneration and herniation. Contributions of nitric oxide, interleukins, prostaglandin E2, and matrix metalloproteinases.* Spine (Phila Pa 1976), 1997. **22**(10): p. 1065-73.

81. Studer, R.K., et al., *p38 MAPK inhibition in nucleus pulposus cells: a potential target for treating intervertebral disc degeneration.* Spine (Phila Pa 1976), 2007. **32**(25): p. 2827-33.

82. Kanemoto, M., et al., *Immunohistochemical study of matrix metalloproteinase-3 and tissue inhibitor of metalloproteinase-1 human intervertebral discs.* Spine (Phila Pa 1976), 1996. **21**(1): p. 1-8.

83. Le Maitre, C.L., et al., *Matrix synthesis and degradation in human intervertebral disc degeneration.* Biochem Soc Trans, 2007. **35**(Pt 4): p. 652-5.

84. Roberts, S., et al., *Matrix metalloproteinases and aggrecanase: their role in disorders of the human intervertebral disc.* Spine (Phila Pa 1976), 2000. **25**(23): p. 3005-13.

85. Podichetty, V.K., *The aging spine: the role of inflammatory mediators in intervertebral disc degeneration.* Cell Mol Biol (Noisy-le-grand), 2007. **53**(5): p. 4-18.

86. Pritchard, S., G.R. Erickson, and F. Guilak, *Hyperosmotically induced volume change and calcium signaling in intervertebral disk cells: the role of the actin cytoskeleton.* Biophys J, 2002. **83**(5): p. 2502-10.

87. Ishihara, H., et al., *Proteoglycan synthesis in the intervertebral disk nucleus: the role of extracellular osmolality.* Am J Physiol, 1997. **272**(5 Pt 1): p. C1499-506.

88. Court, C., et al., *The effect of static in vivo bending on the murine intervertebral disc.* Spine J, 2001. **1**(4): p. 239-45.

89. Chan, W.P., et al., *MRI and histology of collagen template disc implantation and regeneration in rabbit temporomandibular joint: preliminary report.* Transplant Proc, 2004. **36**(5): p. 1610-2.

90. Ohshima, H., J.P. Urban, and D.H. Bergel, *Effect of static load on matrix synthesis rates in the intervertebral disc measured in vitro by a new perfusion technique.* J Orthop Res, 1995. **13**(1): p. 22-9.

91. MacLean, J.J., et al., *Effects of immobilization and dynamic compression on intervertebral disc cell gene expression in vivo.* Spine (Phila Pa 1976), 2003. **28**(10): p. 973-81.

92. Walsh, A.J. and J.C. Lotz, *Biological response of the intervertebral disc to dynamic loading.* J Biomech, 2004. **37**(3): p. 329-37.

93. Sowa, G. *Intervertebral Disc Cells Demonstrate a Threshold Effect in their Response to Mechanical Strain*. in *Association of Academic Physiatrists*. April, 2007. San Juan, PR.

94. Stokes, I.A. and J.C. Iatridis, *Mechanical conditions that accelerate intervertebral disc degeneration: overload versus immobilization.* Spine (Phila Pa 1976), 2004. **29**(23): p. 2724-32.

95. Sowa, G. *Effects of compression on gene expression in nucleus pulposus cells*. in *International Society for the Study of the Lumbar Spine Annual Meeting*. May, 2008. Geneva, Switzerland.

96. Wuertz, K., et al., *Influence of extracellular osmolarity and mechanical stimulation on gene expression of intervertebral disc cells.* J Orthop Res, 2007. **25**(11): p. 1513-22.

97. Maldonado, B.A. and T.R. Oegema, Jr., *Initial characterization of the metabolism of intervertebral disc cells encapsulated in microspheres.* J Orthop Res, 1992. **10**(5): p. 677-90.

98. Sowa, G.A., et al., *Alterations in gene expression in response to compression of nucleus pulposus cells.* Spine J, 2010. [Epub ahead of print].

99. Lotz, J.C., *Animal models of intervertebral disc degeneration: lessons learned.* Spine (Phila Pa 1976), 2004. **29**(23): p. 2742-50.

100. Kroeber, M.W., et al., *New in vivo animal model to create intervertebral disc degeneration and to investigate the effects of therapeutic strategies to stimulate disc regeneration.* Spine (Phila Pa 1976), 2002. **27**(23): p. 2684-90.

101. Ariga, K., et al., *The relationship between apoptosis of endplate chondrocytes and aging and degeneration of the intervertebral disc.* Spine (Phila Pa 1976), 2001. **26**(22): p. 2414-20.

102. Ching, C.T., et al., *The effect of cyclic compression on the mechanical properties of the inter-vertebral disc: an in vivo study in a rat tail model.* Clin Biomech (Bristol, Avon), 2003. **18**(3): p. 182-9.

103. Adams, M.A., et al., *Mechanical initiation of intervertebral disc degeneration.* Spine (Phila Pa 1976), 2000. **25**(13): p. 1625-36.

104. Kim, J., et al., *Cell lysis on a microfluidic CD (compact disc).* Lab Chip, 2004. **4**(5): p. 516-22.

105. Yurube, T., et al., *Matrix metalloproteinase (MMP)-3 gene up-regulation in a rat tail compression loading-induced disc degeneration model.* J Orthop Res, 2010. **28**(8): p. 1026-32.

106. Barbir, A., et al., *Effects of Torsion on Intervertebral Disc Gene Expression and Biomechanics, Using a Rat Tail Model.* Spine (Phila Pa 1976), 2010.

107. Gantenbein, B., et al., *An in vitro organ culturing system for intervertebral disc explants with vertebral endplates: a feasibility study with ovine caudal discs.* Spine (Phila Pa 1976), 2006. **31**(23): p. 2665-73.

108. Haschtmann, D., et al., *Establishment of a novel intervertebral disc/endplate culture model: analysis of an ex vivo in vitro whole-organ rabbit culture system.* Spine (Phila Pa 1976), 2006. **31**(25): p. 2918-25.

109. Korecki, C.L., J.J. MacLean, and J.C. Iatridis, *Characterization of an in vitro intervertebral disc organ culture system.* Eur Spine J, 2007. **16**(7): p. 1029-37.

110. Lee, C.R., et al., *In vitro organ culture of the bovine intervertebral disc: effects of vertebral endplate and potential for mechanobiology studies.* Spine (Phila Pa 1976), 2006. **31**(5): p. 515-22.

111. Lim, T.H., et al., *Rat spinal motion segment in organ culture: a cell viability study.* Spine (Phila Pa 1976), 2006. **31**(12): p. 1291-7; discussion 1298.

112. Wang, D.L., S.D. Jiang, and L.Y. Dai, *Biologic response of the intervertebral disc to static and dynamic compression in vitro.* Spine (Phila Pa 1976), 2007. **32**(23): p. 2521-8.

113. Korecki, C.L., J.J. MacLean, and J.C. Iatridis, *Dynamic compression effects on intervertebral disc mechanics and biology.* Spine (Phila Pa 1976), 2008. **33**(13): p. 1403-9.

114. Junger, S., et al., *Effect of limited nutrition on in situ intervertebral disc cells under simulated-physiological loading.* Spine (Phila Pa 1976), 2009. **34**(12): p. 1264-71.

115. Wang, J., et al., *The expression of Fas ligand on normal and stabbed-disc cells in a rabbit model of intervertebral disc degeneration: a possible pathogenesis.* J Neurosurg Spine, 2007. **6**(5): p. 425-30.

116. Shirazi-Adl, A. and G. Drouin, *Load-bearing role of facets in a lumbar segment under sagittal plane loadings.* J Biomech, 1987. **20**(6): p. 601-13.

117. van der Veen, A.J., et al., *Contribution of vertebral [corrected] bodies, endplates, and intervertebral discs to the compression creep of spinal motion segments.* J Biomech, 2008. **41**(6): p. 1260-8.

118. Beckstein, J.C., et al., *Comparison of animal discs used in disc research to human lumbar disc: axial compression mechanics and glycosaminoglycan content.* Spine (Phila Pa 1976), 2008. **33**(6): p. E166-73.

119. Johannessen, W., et al., *Trans-endplate nucleotomy increases deformation and creep response in axial loading.* Ann Biomed Eng, 2006. **34**(4): p. 687-96.

120. Haschtmann, D., J.V. Stoyanov, and S.J. Ferguson, *Influence of diurnal hyperosmotic loading on the metabolism and matrix gene expression of a whole-organ intervertebral disc model.* J Orthop Res, 2006. **24**(10): p. 1957-66.

121. Selard, E., A. Shirazi-Adl, and J.P. Urban, *Finite element study of nutrient diffusion in the human intervertebral disc.* Spine (Phila Pa 1976), 2003. **28**(17): p. 1945-53; discussion 1953.

122. Erwin, W.M., et al., *The regenerative capacity of the notochordal cell: tissue constructs generated in vitro under hypoxic conditions.* J Neurosurg Spine, 2009. **10**(6): p. 513-21.

123. Guehring, T., et al., *Notochordal intervertebral disc cells: sensitivity to nutrient deprivation.* Arthritis Rheum, 2009. **60**(4): p. 1026-34.

124. Rastogi, A., et al., *Environmental regulation of notochordal gene expression in nucleus pulposus cells.* J Cell Physiol, 2009. **220**(3): p. 698-705.

125. Jung, M., et al., *Increased urinary concentration of collagen type II C-telopeptide fragments in patients with osteoarthritis.* Pathobiology, 2004. **71**(2): p. 70-6.

126. Petersson, I.F., et al., *Cartilage markers in synovial fluid in symptomatic knee osteoarthritis.* Ann Rheum Dis, 1997. **56**(1): p. 64-7.

127. Huebner, J.L. and V.B. Kraus, *Assessment of the utility of biomarkers of osteoarthritis in the guinea pig.* Osteoarthritis Cartilage, 2006. **14**(9): p. 923-30.

128. Ley, C., et al., *Interleukin-6 and tumour necrosis factor in synovial fluid from horses with carpal joint pathology.* J Vet Med A Physiol Pathol Clin Med, 2007. **54**(7): p. 346-51.

129. Nachemson, A.L., *Disc pressure measurements.* Spine (Phila Pa 1976), 1981. **6**(1): p. 93-7.

130. Wilke, H.J., et al., *New in vivo measurements of pressures in the intervertebral disc in daily life.* Spine (Phila Pa 1976), 1999. **24**(8): p. 755-62.

131. Gillespie, K.A. and J.P. Dickey, *Biomechanical role of lumbar spine ligaments in flexion and extension: determination using a parallel linkage robot and a porcine model.* Spine (Phila Pa 1976), 2004. **29**(11): p. 1208-16.

132. Gilbertson L. G., T.C.D., and J. D. Kang, *New methods to study lumbar spine mechanics: delineation of in vitro load-displacement characteristics by using a robotics/UFS testing system with hybrid control.* Oper Tech Orthop, 2001. **10**(4): p. 246-253.

133. Bell K. M., B.Q., R. A. Hartman, and J. D. Kang. *A Robot-Based Approach for Characterizing the Three-Dimensional Mechanical Properties of Rabbit FSU*. in *55th Annual Meeting of the Orthopaedic Research Society (ORS)*. 2009. Las Vegas, NV.

134. Hartman R. A., K.M.B., and J. D. Kang. *Detailed Analyses of the Components of the Posterior Column in a Distractive-Flexion Injury Model*. in *55th Annual Meeting of the Orthopaedic Research Society (ORS)*. 2009. Las Vegas, NV.

135. Adams, M.A., *Mechanical Testing of the Spine - an Appraisal of Methodology, Results, and Conclusions.* Spine, 1995. **20**(19): p. 2151-2156.

136. Goel, V.K. and J.N. Weinstein, *Biomechanics of the spine : clinical and surgical perspective*. 1990, Boca Raton, FL: CRC Press. 295 p.

137. Bell K. M., R.A.H., and J. D. Kang. *In Vitro Spine Testing Control Method Comparison: Displacement Control vs. Hybrid Control*. in *54th Annual Meeting of the Orthopaedic Research Society (ORS)*. 2008. San Fransisco, CA.

138. Stokes, I.A., et al., *Mechanical modulation of vertebral body growth. Implications for scoliosis progression.* Spine (Phila Pa 1976), 1996. **21**(10): p. 1162-7.

139. Csonge, L., et al., *Banking of osteochondral allografts. Part I. Viability assays adapted for osteochondrol and cartilage studies.* Cell Tissue Bank, 2002. **3**(3): p. 151-9.

140. Sowa, G., et al., *Characterization of intervertebral disc aging: longitudinal analysis of a rabbit model by magnetic resonance imaging, histology, and gene expression.* Spine (Phila Pa 1976), 2008. **33**(17): p. 1821-8.

141. Sowa, G., J.P. Coelho, and N. Vo, *Effect of duration and magnitude of tensile loading on gene expression and activity of catabolic mediators of annulus fibrosus cells.* J Orthop Res, 2010 (In revision).

142. Livak, K.J. and T.D. Schmittgen, *Analysis of relative gene expression data using real-time quantitative PCR and the 2(-Delta Delta C(T)) Method.* Methods, 2001. **25**(4): p. 402-8.

143. Sowa, G., et al., *Identification of candidate serum biomarkers for intervertebral disk degeneration in an animal model.* PMR, 2009. **1**(6): p. 536-40.